University of Southern Queensland

Faculty of Engineering and Surveying

System Design of a Hydrogen Induction System as a Retrofit Item Compatible with Existing Internal Combustion Engines

A dissertation submitted by

Mr Kieran Richardson

In fulfilment of the requirements of

Bachelor of Engineering (Honours)

October 2015

ABSTRACT

As the current method of delivering the world's transportation energy demand via fossil fuels becomes increasingly unsustainable, vehicle manufactures and organisations are looking to alternative energy sources for vehicle propulsion such as hydrogen fuel.

This project has been undertaken to establish the feasibility of the *System Design of a Hydrogen Induction System as a Retrofit Item Compatible with Existing Internal Combustion Engines*, by examining the conversion of a Holden 5.0L V8 to accommodate hydrogen combustion. The for the purpose of analysis, a Holden HX GTS sedan has been chosen as a case study vehicle, commonly optioned with the first generation Holden 5.0L V8.

Analysis of urban and extra-urban drive cycles provided theoretical power requirements for the operation of the vehicle for the duration of the cycles. Outputs from the drive cycle analysis were used in an engine simulation model that was modified to accommodate simulation of hydrogen combustion.

Input values for average power and engine speed required to maintain velocity along the drive cycles are supplied to the engine simulation model. The engine simulation model returns a hydrogen fuel consumption of 4.18 kg/100km and 5.34 kg/100km for the extra-urban and urban driving cycles respectively, a gasoline gallon equivalent of 15.4 L/100km and 20.27 L/100km. This provides a theoretical endurance of 133.62 km and 104.14 km from vehicles proposed 5.6 kg of useable hydrogen storage for the cycles respectively.

An extensive literature review is used to identify design modifications that are required to accommodate hydrogen combustion in internal combustion engines. A trade study is used to identify the measures specifically required to adapt the Holden 5.0L case study engine to dual hydrogen/petrol operation modes. The modifications and additional components required were costed where possible, resulting in an estimated minimum cost of AUD $12,664 in parts for the conversion.

TABLE OF CONTENTS

ABSTRACT ..... **II**

TABLE OF CONTENTS ..... **III**

DISCLAIMER PAGE ..... **VII**

CANDIDATES CERTIFICATION ..... **VIII**

ACKNOWLEDGEMENTS ..... **IX**

LIST OF FIGURES ..... **X**

LIST OF TABLES ..... **XII**

NOMENCLATURE AND ACRONYMS ..... **XIII**

1 INTRODUCTION **1**

2 PROJECT OVERVIEW **3**

2.1 PROJECT OBJECTIVES 3

2.2 METHODOLOGY 3

2.3 PROJECT SCOPE 4

2.4 CASE STUDY ENGINE: HOLDEN 5.0L 5

2.5 RESOURCE REQUIREMENTS 6

3 LITERATURE REVIEW **7**

3.1 FUNDAMENTAL CONCEPTS 7

3.1.1 Combustion *7*

3.2 INTERNAL COMBUSTION SYSTEMS 8

3.2.1 Overview of Reciprocating Engines *9*

3.3 SPARK-IGNITION AND COMPRESSION-IGNITION ENGINES 9

3.3.1 Four-Stroke Engine (Otto Cycle) *9*

3.3.2 Diesel Engine (Diesel cycle) *10*

3.3.3 Wankel/Rotary Engine *11*

3.3.4 Carburation *11*

3.3.5 Electronic Fuel Injection (EFI) *14*

3.3.6 Forced Induction (Supercharging) *15*

3.4 HYDROGEN 18

3.4.1 Hydrogen as an Energy Carrier *18*

3.4.2 Hydrogen Production *18*

3.4.3 Hydrogen Storage *20*

3.5 HYDROGEN INTERNAL COMBUSTION ENGINE VEHICLES 25

3.5.1 History *25*

3.5.2 Hydrogen Vehicle Characterisation *26*

3.5.3 Conversion Vehicles *26*
3.5.4 Bi-fuel vehicles *27*
3.5.5 Dedicated Hydrogen Vehicles *29*
3.5.6 Overview of Hydrogen Vehicles *30*
3.6 MEASURES FOR HYDROGEN ENGINE DESIGN OR CONVERSION 30
3.6.1 Spark Plugs *30*
3.6.2 Injection system *30*
3.6.3 Ignition system *31*
3.6.4 Hot spots *31*
3.6.5 Piston rings and crevice volumes *31*
3.6.6 Valve seat and injectors *32*
3.6.7 Lubrication *32*
3.6.8 Crankcase ventilation *33*
3.6.9 Compression ratio *33*
3.6.10 In-cylinder turbulence *33*
3.6.11 Electronic throttle *33*
3.7 HYDROGEN SAFETY 33
3.7.1 Test Apparatus Design *34*
3.7.2 Ventilation *34*
3.7.3 Hydrogen sensors *35*
3.7.4 Flame detectors *35*
3.7.5 Supply system *36*
3.7.6 Vehicular applications *36*
3.8 PRIOR ART 37
3.8.1 Review of Yvon & Lorenzoni *37*
3.8.2 Review of Kahraman, Ozcanli, & Ozerdem *40*
3.8.3 Review of Sopena, Dieguez, Sainz, Urroz, Guelbenzu, Gadina *42*
3.8.4 Review of Babir *45*
3.8.5 Review of Das, Gulati & Gupta *46*
3.8.6 Review of Verhelst & Wallner *49*
3.8.7 Review of Duan, Liu and Sun *56*
4 REQUIREMENTS ANALYSIS 62
4.1 CUSTOMER REQUIREMENTS ANALYSIS 62
4.1.1 Fuel security for classic/historic vehicles in a post-hydrocarbon economy. *62*
4.1.2 Maximise driving range and adequate cruising power *62*
4.1.3 Maintain originality and preserve aesthetics of the vehicle where possible. *62*
4.1.4 Simplicity and owner-maintainable *63*
4.1.5 Minimize cost where possible *63*
4.1.6 Dual-fuel system *63*

4.1.7 Reliability of system ... *63*
4.1.8 Design Specifications ... *63*

5 ENGINE ANALYSIS ... **64**

5.1 DRIVE CYCLE ANALYSIS ... 64
5.1.1 Introduction ... *64*
5.1.2 Method ... *66*
5.1.3 Results ... *69*
5.2 AHRIND MATLAB ENGINE SIMULATION MODEL (AESM) ... 74
5.2.1 Introduction ... *74*
5.2.2 Method ... *75*
5.2.3 Results ... *82*
5.3 DISCUSSION ... 88
5.3.1 Overview of results ... *88*
5.3.2 Drive cycle analysis ... *88*
5.3.3 Engine Analysis ... *90*

6 CONCEPT DESIGN ... **91**

6.1 TRADE STUDY ... 91
6.1.1 Storage and delivery ... *91*
6.1.2 Throttle control ... *92*
6.1.3 Inlet manifold ... *93*
6.1.4 Injectors ... *94*
6.1.5 Engine Control Unit (ECU) ... *95*
6.1.6 Spark Plugs ... *97*
6.1.7 Ignition Coil ... *97*
6.1.8 Engine Modifications ... *97*
6.1.9 Lubrication ... *98*
6.1.10 Crankcase ventilation ... *99*
6.1.11 Safety ... *99*
6.2 COST ... 100

7 CONCLUISONS ... **101**

8 OTHER CONSIDERATIONS AND FURTHER WORK ... **102**

8.1 ETHICAL CONSIDERATIONS ... 102
8.2 FURTHER WORK ... 102

REFERENCES ... **104**

APPENDICIES ... **106**

APPENDIX A – PROJECT SPECIFICATION ... 106
APPENDIX B – RESEARCH RISK ASSESSMENT ... 107

Working with computers *107*
Hardware and peripherals. *107*
Keyboards *107*
Mouse Computer *108*
Monitors *108*
Health effects *108*
APPENDIX C - AHRIND ENGINE SIMULATION SCRIPT FILES – BUTTSWORTH (2007) 110
Appendix C1 – ahrind.m – Engine Simulation (modified) *110*
Appendix C2 – airdata.m – Thermodynamic Properties of Air/combustion Products *111*
Appendix C3 – calcq.m – Calculate Heat Flux *113*
Appendix C4 – ecp.m – Equilibrium Combustion Products *114*
Appendix C5 – farg.m – Mixtures of fuel, air, residual combustion products at low temp *118*
Appendix C6 – plotresults.m – Plot ahrind results *120*
Appendix C7 – RatesComb.m – Combustion Phase derivatives *122*
Appendix C8 – Tadiabatic.m – Calculate Adiabatic flame temp *125*
Appendix C9 – fueldata.m – Thermodynamic properties of fuel (modified) *127*
APPENDIX D - ENGINE SIMULATION SCRIPT FILES – RICHARDSON (2015) 129
Appendix D1 – Drive_Cycle_Anlysis.m – HWFET & UDDS Drive Cycle Analysis *129*
Appendix D2 – Holden_5L_Engine_Anlysis.m *133*
APPENDIX E – DRIVE CYCLE ANALYSIS PLOTS 137
Appendix E1 - Power to maintain speed and power to accelerate over HWFET driving cycle *137*
Appendix E2 - Total power required vs time for the HWFET driving cycle *137*
Appendix E3 - Cumulative fuel consumption vs time for the HWFET driving cycle *138*
Appendix E4 - Power to maintain speed and power to accelerate over the UDDS driving cycle *138*
Appendix E5 - Total power required vs time for the UDDS driving cycle *139*
APPENDIX F - HWFET AESM POWER AND FUEL CONSUMPTION PLOTS 140
Appendix F1 – GGE Surface plot for HWFET driving cycle *140*
Appendix F2 – Specific Fuel consumption surface plot for HWFET driving cycle *140*
APPENDIX G - UDDS AESM POWER AND FUEL CONSUMPTION PLOTS 140
Appendix G1 – GGE Surface plot for UDDS driving cycle *141*
Appendix G2 – Specific Fuel consumption surface plot for UDDS driving cycle *141*

DISCLAIMER PAGE

The Council of the University of Southern Queensland, its Faculty of Health, Engineering & Sciences, and the staff of the University of Southern Queensland, do not accept any responsibility for the truth, accuracy or completeness of material contained within or associated with this dissertation.

Persons using all or any part of this material do so at their own risk, and not at the risk of the Council of the University of Southern Queensland, its Faculty of Health, Engineering & Sciences or the staff of the University of Southern Queensland.

This dissertation reports an educational exercise and has no purpose or validity beyond this exercise. The sole purpose of the course pair entitled "Research Project" is to contribute to the overall education within the student's chosen degree program. This document, the associated hardware, software, drawings, and other material set out in the associated appendices should not be used for any other purpose: if they are so used, it is entirely at the risk of the user.

CANDIDATES CERTIFICATION

I certify that the ideas, designs and experimental work, results, analysis and conclusions set out in this dissertation are entirely my own efforts, except where otherwise indicated and acknowledged.

I further certify that the work is original and has not been previously submitted for assessment in any other course or institution, except where specifically stated

Kieran Richardson

Student Number: 0061033301

Student

Kieran Richardson Signature: _____

Date: _____

ACKNOWLEDGEMENTS

This research was carried out under the principal supervision of Dr Ray Malpress. I would like to personally thank Dr. Malpress for his continued guidance support throughout my project, which has proven invaluable in the preparation of this dissertation.

I would like to express my gratitude to my family, friends, and girlfriend Megan Stark for their continued support.

Appreciation is also due to my brother, Matthew Richardson for his assistance with planning, concept design, and technical assistance.

LIST OF FIGURES

Figure 2.1: Holden 5.0L V8 Engine 6
Figure 2.2: Holden 5.0L specifications, uniquecars&parts, 2015 6
Figure 3.1: 4 strokes of a rotary engine, HSW, 2015 11
Figure 3.2: Simple Carburettor, Judge, 1955. 12
Figure 3.3: Simple downdraft carburettor section, Judge, 1955 12
Figure 3.4: Electrolytic Cell, FCTO, 2015 19
Figure 3.5: Liquid Hydrogen Storage Tank (FCTO, 2015) 22
Figure 3.6: Mazda RX-8 Hydrogen RE engine operation, Mazda, 2003. 27
Figure 3.7: RX-8 Hydrogen RE and Premacy Hydrogen RE hybrid, Mazda, 2003. 28
Figure 3.8: RX-8 Hydrogen RE Hydrogen storage diagram, Mazda, 2003 29
Figure 3.9: Overview of hydrogen ICE vehicles, Verhelst & Wallner, 2009 30
Figure 3.10: Correlation of air-fuel ratio and NOx emissions for homogenous PFI operation, Verhelst & Wallner 54
Figure 3.11: Theoretical power density of a PFI HICE compared to stoichiometric petroleum operation as a function of equivalence ratio and charging strategy, Verhelst & Wallner (Verhelst & Wallner, 2009) 55
Figure 3.12: test instrumentation type and accuracy from Duan, Liu and Sun's experimental apparatus 59
Figure 3.13: 3D CFD simulation model (Duan et al., 2013) 60
Figure 3.14: Simulation results (Duan et al., 2013) 61
Figure 5.1: EPA Highway Fuel Economy Test Driving Schedule (EPA, 2015). 65
Figure 5.2: Caption: EPA Urban Dynamometer Driving Schedule (EPA, 2015). 65
Figure 5.3: Vehicle, fuel, and air properties assumptions 67
Figure 5.4: HX Holden Monaro GTS sedan exterior dimensions 68
Figure 5.5: Command window results display for HWFET driving cycle 69
Figure 5.6: Command window results display for UDDS driving cycle 69
Figure 5.7: Total Power requirement vs time for HWFET cycle 70
Figure 5.8: Total Power requirement vs time for UDDS cycle 70
Figure 5.9: Spread of velocity data points for the HWFET driving cycle 72
Figure 5.10: Spread of total power data points for the HWFET driving cycle 72
Figure 5.11: Spread of velocity data points for the UDDS driving cycle 73
Figure 5.12: Spread of total power data points for the UDDS driving cycle 73

Figure 5.13: The AESM output for in cylinder pressure change over the compression and expansion strokes 74
Figure 5.14: Creation of zeros matrix for desired output in Holden_5L_analysis.m 75
Figure 5.15: Creation of nested loop for induction pressure and fuel-air equivalence ratio in Holden_5L_analysis.m 76
Figure 5.16: Holden 5.0L engine specifications assigned to enginedata.m script file 76
Figure 5.17: Addition of hydrogen polynomial coefficients for species thermodynamic properties to fueldata.m script file to accommodate simulation of hydrogen gas combustion. 77
Figure 5.18: Determining inducted air density via ideal gas law 77
Figure 5.19: Ground speed is calculated as a function of the vehicles effective drive ratio and engine speed 78
Figure 5.20: Surface plot of power output vs equivalence ratio and induction pressure for the average engine speed of the HWFET driving cycle. 82
Figure 5.21: Surface plot of power output vs equivalence ratio and induction pressure for the average engine speed of the UDDS driving cycle 82
Figure 5.22: Surface plot of hydrogen fuel consumption vs equivalence ratio and induction pressure for the average engine speed of the HWFET driving cycle 83
Figure 5.23: Surface plot of hydrogen fuel consumption vs equivalence ratio and induction pressure for the average engine speed of the UDDS driving cycle. 83
Figure 5.24: numerical outputs for wheel power over the fuel-air ratio and induction pressure ranges that have been transcribed into Microsoft Excel for the HWFET driving cycle. 84
Figure 5.25: numerical outputs for fuel consumption over the fuel-air ratio and induction pressure ranges that have been transcribed into Microsoft Excel for the HWFET driving cycle. 84
Figure 5.26: Fuel consumption data for combinations of phi and induction pressure to produce the target power of 20.92 kW for the HWFET driving cycle at 1980 rpm 84
Figure 5.27: Numerical outputs for wheel power over the fuel-air ratio and induction pressure ranges that have been transcribed into Microsoft Excel for the UDDS driving cycle. 85

Figure 5.28: Numerical outputs for fuel consumption over the fuel-air ratio and induction pressure ranges that have been transcribed into Microsoft Excel for the UDDS driving cycle. 85
Figure 5.29: Fuel consumption data for combinations of phi and induction pressure to produce the target power of 9.44 kW for the UDDS driving cycle at 1645 rpm. 85
Figure 5.30: a ‘sectioned’ top view of the wheel power surface plots in Figures 5.18 and 5.19 at 20.92 kW and 9.44 kW. 86
Table 5.1: Summary of key results from sections 5.1.3 and 5.2.3 88
Figure 6.1: Compressed H2 storage tank details 92
Figure 6.2: Harrop inlet manifold stock list photograph 93
Figure 6.3: Quantum Technologies Hydrogen and CNG injectors 95
Figure 6.4: MoteC M84 ECU 96
Figure 6.5: NGK BP6FS Holden 5.0L spark plug stock image. 97
Table 6.1: Minimum component cost estimate 100

LIST OF TABLES

Table 5.1: Summary of key results from sections 5.1.3 and 5.2.3 88
Table 6.1: Minimum component cost estimate 100

NOMENCLATURE AND ACRONYMS

The following abbreviations have been used throughout the text and bibliography:

AESM	Ahrind Engine Simulation Model
BDC	Bottom Dead Centre
BTE	Brake Thermal Efficiency
BMEP	Brake Mean Effective Pressure
BSFC	Brake Specific Fuel Consumption
CA	Crankshaft Angle
CCD	Charged Coupled Device
CI	Compression Ignition
CFD	Computational Fluid Dynamics
CNG	Compressed Natural gas
CO	Carbon Monoxide
CO2	Carbon Dioxide
DI	Direct Injection
ECU	Engine Control Unit
EERE	Energy Efficiency and Renewable Energy, (office of)
EFI	Electronic Fuel Injection
EGR	Exhaust Gas Recirculation
EV	Electric Vehicle
FEA	Finite Element Analysis
FCV	Fuel Cell Vehicle
HICE	Hydrogen Internal Combustion Engine
HICEV	Hydrogen Internal Combustion Engine Vehicle
IC	Internal Combustion
ICE	Internal Combustion Engine

IMEP	Indicated Mean Effective Pressure
LNG	Liquefied Natural Gas
LPG	Liquefied Petroleum Gas
MEP	Mean Effective Pressure
NOx	Nitrogen Oxides
OEM	Original Equipment Manufacturer
PEM	Polymer Electrolyte Membrane
PFI	Port Fuel Injection
PID	Proportional-Integral-Derivative
RE	Rotary Engine
SFC	Specific Fuel Consumption
SI	Spark Ignition
SULEV	Super Ultra Low Emission Vehicle
STP	Standard Temperature & Pressure
TBI	Throttle Body Injection
TDC	Top Dead Centre
TMI	Timed Manifold Injection
ULEV	Ultra Low Emission Vehicle
WOT	Wide Open Throttle

1 INTRODUCTION

The current method of delivering the world's energy demand, based primarily on fossil fuel, is becoming increasingly unsustainable as once abundant fossil fuel reserves are now clearly exhaustible. Global warming and local pollution hotspots associated with fossil fuel usage are further significant environmental and societal problems. These are strong drivers for research, development and demonstration of alternative energy sources, carriers, and for transportation sectors, and powertrains (Verhelst & Wallner, 2009).

Vehicles are identified as a major source of air pollutants such as carbon monoxide, nitric oxides, and hydrocarbons, as well as the greenhouse gas carbon monoxide. Thus there is a growing shift within the transportation industry from traditional petroleum based fuels such as petrol and diesel fuel to cleaner burning alternative fuels such as natural gas, alcohols or alcohol blends, LPG, and hydrogen and hydrogen enriched fuels (Çengel & Boles 2001).

However, vehicle manufacturer Mazda suggest that over 95% of the world currently uses petrol and diesel internal combustion engines, and even by 2020 90% still will be, leaving just 10% using these alternatives (Mazda, 2015). It is implied that to see a substantial and immediate reduction of vehicle emissions, manufacturers must adapt renewable technology to vehicles used globally right now. The use of hydrogen as an energy carrier has been investigated as part of most governmental strategic plans for sustainable energy systems, and is subject to continued research into its use as a combustion fuel.

Verhelst & Wallner highlight that the attractiveness of hydrogen lies in the versatile methods by which it can be produced; the long-term viability of a number of methods; the various methods to produce energy from hydrogen; the virtually zero harmful emissions and potential efficiency from its use. Compared to other alternative energy carriers, hydrogen is advantageous in terms of volumetric and gravimetric energy storage density. However, there exist serious challenges that need to be overcome when hydrogen is used as an energy carrier. Hydrogens low density implies low energy density compared to currently available fuels, even when compressed or liquefied, both of which incur substantial energy losses. Bulk storage, distribution, and on board vehicle storage are heavily compromised as a result. Further, Verhelst & Wallner suggest that in the case of hydrogen-fuelled vehicles, we must ensure that the well-to-wheel greenhouse emission reduction compared to the production of hydrocarbon fuels is positive. However, the

potential advantages and desirable combustion properties of hydrogen are substantial enough to warrant investigation and further research (Verhelst & Wallner, 2009).

This project aims to establish the feasibility of the **System Design of a Hydrogen Induction System as a Retrofit Item Compatible with Existing Internal Combustion Engines**, by examining the conversion of a Holden 5.0L V8 to accommodate hydrogen combustion.

2 PROJECT OVERVIEW

This chapter outlines the objectives and scope of this research, and details the project execution.

2.1 Project Objectives

The objectives of this research project were defined as follows:

1. Design a hydrogen induction system capable of retro-fitment to an existing internal combustion engine using a Holden 5.0L V8 as a case study.
2. Perform extensive literature review surrounding hydrogen internal combustion phenomena.
3. Identify from literature review all measures for design and modification required to achieve reliable operation of case study engine.
4. Identify customer requirements, from which concept design specifications can be established.
5. Create concept design comprising of any modifications and new componentry selection required for engine operation, as identified.
6. Use a trade study to aid in optimisation of design for specific case study engine: compare suitability of off-the-shelf componentry options based on satisfaction of design specifications.
7. Modify the ahrind MATLAB combustion model to accommodate hydrogen combustion analysis and perform engine analysis to determine performance and emission characteristics of the engine concept for hydrogen vs petroleum operation.
8. Perform cost analysis of the concept design (estimations of cost, market uptake, safety, and other factors concerning implementation of the technology into the automotive market).

2.2 Methodology

The following section details the methodologies employed to achieve project objectives.

Appeal exists in maintaining iconic vehicles of the past. Although suitable fuels for such vehicles are likely to remain available for some time, an investigation into the use of alternative fuels seems justifiable (Barbir, undated). This investigation examines the conversion of a Holden 5.0L V8 to accommodate hydrogen combustion.

Analysis of urban and extra-urban drive cycles provided theoretical power requirements for the operation of the vehicle for the duration of the cycles. Outputs from the drive cycle analysis were used in an engine simulation model that was modified to accommodate simulation of hydrogen combustion.

An initial review of available literature was conducted surrounding combustion of fuels, conventionally fuelled internal combustion engines, hydrogen as a potential energy carrier, as well as its production and methods of storage. This led into hydrogen specific internal combustion literature, where phenomena unique to hydrogen internal combustion was investigated as well as prior art. From the literature review, all key design measures for hydrogen engine conversion were identified. All component replacement, addition and design modification requirements were established and a trade study performed.

From here, to identify what the concept design should be, an examination of key customer requirements was conducted. From the customer requirements a series of quantitative and qualitative specifications was established.

A trade study was used to compare available technologies against the design specifications to optimise component selection and modifications. Areas for design or modification included storage/refuelling, fuel delivery, induction, ignition, combustion, exhaust, lubrication and cooling, and safety categories. Ethical and environmental considerations were also investigated.

2.3 Project Scope

Significant progress in hydrogen-fuelled internal combustion engines has been made in recent times in terms of achievable power density, efficiencies and emissions. However, there are still many challenges to the widespread adoption of hydrogen technology and this investigation did not provide answers to them. This section outlines the limitations set on the scope of works for this investigation.

The following investigation:

- Did not provide solutions to challenges involved in on-board hydrogen storage. Rather this investigation evaluated current on-board hydrogen storage technology to establish which option was optimal for the concept design.
- Did not provide innovative solutions for the power density challenges that exist for hydrogen internal combustion engines. This investigation evaluated currently

available technologies for hydrogen induction that are compatible with the case study engine.

- Did not involve the redesign or evaluation of existing components except where modification or installation of extra equipment was required. Equipment that is common to both hydrogen and petroleum operation was not examined (ie transmission, differential, passenger compartment, etc).
- Did not focus on developing new MATLAB models for hydrogen combustion. The investigation involved the adaption of existing ahrind MATLAB models to produce performance and emissions characteristics for the case study engine for hydrogen and petroleum operation.

These limitations were set to limit the depth of the investigation to reflect an undergraduate thesis report. The limitations also reduced the likelihood of over-constraining the design.

2.4 Case Study Engine: Holden 5.0L

The Holden V8 is an overhead valve pushrod engine that was produced by General Motors Holden between 1969 and 2000. The V8 was initially offered in 253 and 308 cui variants until 1985 when the 253 cui variant was dropped. In 1985, the engine capacity of the 308 was reduced to 304 cui to slip beneath the 5000 cc engine capacity ceiling for Group A touring cars. The 304 retained the 308 basic engine block, while crank, cylinder heads, and other engine changes were made to accommodate fuel injection and improved efficiency.

Due to its long production run, replacement parts, aftermarket induction manifolds, cylinder heads, supercharger kits, injection systems and a host of other parts are available for the Holden 5.0L, both OEM and aftermarket. This makes it an ideal engine for a hydrogen case study, its versatility allowing for numerous induction combinations. The Holden 5.0L has been selected as the subject of the case study for this project due to the

large volume of historic and classic vehicles that utilise the power plant and the availability of parts and equipment, Figure 2.1.

Figure 2.1: Holden 5.0L V8 Engine

The engine specifications for cylinder bore, stroke, compression ratio, and maximum power output (Figure 2.2) were used for inputs and reference for; thermodynamic analysis; hydrogen combustion simulation in MATLAB to determine performance characteristics; and to identify measures for engine modification to accommodate hydrogen combustion.

2.5 Resource Requirements

This section details the resource requirements for the project. Due to the theoretical nature of the investigation, the majority of these resources were the access to software and computer programs.

Microsoft word was used extensively for all word processing tasks within the project.

Figure 2.2: Holden 5.0L specifications, uniquecars&parts, 2015

This program was selected due to its widespread availability, ease of use, and familiarity and experience with the software.

The reference management software Endnote X7 has been used to manage and collate references and the material cited in this dissertation. The software was selected for its ease of use, the added convenience it brings to the management of a large number of references, and its integration of both Microsoft Word and with databases such as Science Direct and Scopus.

The spreadsheet application Microsoft Excel has also been used extensively. The program is very useful for graphical display of information, tabulation and data analysis, decision

matrix design, and numerous other applications. Familiarity with the program and its widespread use and accessibility were contributing factors for its selection as a computational aid in this project.

MATLAB was selected as the main numerical computing environment for basic to complex calculations, combustion modelling, data and numerical analysis in this project. A portion of the combustion analysis within this project has come from the adoption of existing rudimentary combustion MATLAB models, necessitating its use. Familiarity with the program and its powerful computing power were also strong motivations for its selection for the project.

Access to the internet has become a mandatory requisite for any research project. Access to the USQ library and databases such as Science Direct and Scopus have also been greatly utilized in the review of available literature relating to the investigation.

3 LITERATURE REVIEW

This chapter concerns the review of literature surrounding hydrogen internal combustion.

3.1 Fundamental Concepts

In order to understand the development of models established within this project, a comprehension of the fundamental thermodynamics, fluid mechanics, numerical analysis and dynamics concepts upon which these models are built is required. The following sections provide a brief outline of these concepts.

Please note that the outlined concepts are far from comprehensive, and the cited material should be referred to if more detailed explanations of any phenomena are required. For a description of the terms and symbols used in Equations in this section, refer to the nomenclature and acronyms page.

3.1.1 Combustion

This section focuses on a particular type of chemical reaction, known as combustion, due to its fundamental importance to the workings in this document.

Fuels and oxidisers

Any material that can be burned to release thermal energy is called a fuel. Most familiar fuels consist primarily of hydrogen and carbon. Known as hydrocarbon fuels, they are

denoted by the general formula C_nH_m. Hydrocarbon fuels exist in all phases. Some well-known hydrocarbons are coal, petroleum and natural gas (Çengel & Boles, 2001).

A chemical reaction during which fuel is oxidised releasing a large quantity of energy is called combustion. As it is free and readily available, the oxidiser most commonly used in combustion is air. On a mole or volume basis, dry air is composed of 20.9% oxygen, 78.1% nitrogen, 0.9% argon, and in small amounts of helium, carbon dioxide, neon and hydrogen. In the combustion reactions considered in this document, the argon is treated as nitrogen, and the trace amounts of other gases are disregarded. Dry air is then approximated as 21% oxygen and 79% nitrogen. Thus, each mole of oxygen in a combustion reaction is accompanied by 0.79/0.21 = 3.76 moles of nitrogen (Çengel & Boles, 2001).

During combustion nitrogen behaves as an inert gas and thus does not react with other elements, other than forming trace amounts of nitric oxides. However, the presence of nitrogen greatly affects the outcome of a combustion process. Nitrogen typically enters a combustion chamber in large quantities at a low temperature then exits at considerably higher temperatures, absorbing a large quantity of the energy released during combustion (Çengel & Boles, 2001). For the sake of simplicity, nitrogen was considered to act completely inert in the Equations used within this document. It is worth noting however that in reality, the high temperatures encountered in an internal combustion engine would cause a small fraction of nitrogen to form hazardous gases such as nitric oxide.

Reactants

Predicting the composition of the products of a combustion reaction is relatively easy when the process is assumed to be complete and the exact amounts of products are known. All that is required is to apply the mass balance to each element that appears in the Equation, without taking any measurements. In an actual combustion process, it is not as simple. Actual combustion processes are hardly ever complete, even in the presence of excess air. Thus, it is impossible to predict the composition based on mass balance application alone. The only alternative is to measure the amount of each component in the products directly (Çengel & Boles, 2001).

3.2 Internal Combustion Systems

In order to understand the explanations and justifications supplied in this document, some basic knowledge of internal combustion systems is required. In this section, several different types of internal combustion systems are introduced and explained.

3.2.1 Overview of Reciprocating Engines

The reciprocating engine has proved to be a versatile invention with wide and varied applications since its invention. In a reciprocating engine the piston reciprocates in the cylinder between two fixed positions, namely top dead centre (TDC) – the position of the piston when it forms the smallest volume in the cylinder – and bottom dead centre (BDC), when it forms the largest volume in the cylinder (Çengel & Boles, 2001).

The distance between TDC and BDC is the largest distance the piston can travel and is termed the stroke of the engine. The diameter of the cylinder is called the bore. The air-fuel mixture is drawn into the cylinder via the intake-valve, and combustion products are expelled from the cylinder via the exhaust valve (Çengel & Boles, 2001).

The clearance volume is the volume formed in the cylinder by the piston at TDC. The displacement is the volume displaced by the piston as it moves between the two points. The ratio of the displacement to the clearance volume is known as the compression ratio R of the engine (Çengel & Boles, 2001).

$$R = \frac{V_{max}}{V_{min}} = \frac{V_{BDC}}{V_{TDC}} \qquad \text{Equation 3.1}$$

3.3 Spark-Ignition and Compression-Ignition Engines

Reciprocating engines are classified as either spark ignition (SI) engines or compression-ignition (CI) engines, depending on how combustion is initiated within the cylinder. In SI engines, a spark plug delivers a charge to the cylinder and ignites the compressed air-fuel mixture. In CI engines, the air-fuel mixture is compressed above its self-ignition temperature and self-ignites as a result (Çengel & Boles, 2001).

3.3.1 Four-Stroke Engine (Otto Cycle)

The Otto cycle is the ideal cycle for SI reciprocating combustion engines. It was named after German engineer Nikolas Otto for his application of Beau de Rochas' engine cycle in the creation of the world's first successful four-stroke engine. In most SI engines, the piston completes four strokes and two crankshaft revolutions per thermodynamic cycle.

These are called four-stroke engines, with the strokes namely; intake, compression, power, and exhaust (Çengel & Boles, 2001).

Initially both the intake and exhaust valves are closed with the piston at TDC. During the intake stroke the piston moves down the cylinder, creating a vacuum that draws in an air-fuel mixture via the intake valve. Once the piston reaches BDC, the intake valve closes sealing the volume within the cylinder. The piston then makes its way back up the cylinder, compressing the air-fuel mixture in what is called the compression stroke. Shortly before the piston reaches TDC the sparkplug delivers a spark and the compressed air-fuel mixture ignites, increasing the temperature and pressure within the combustion chamber. The increased pressures of combustion force the piston back down the cylinder, producing usable work output during the power stroke via connection of the piston to the crankshaft via a connecting rod. At the end of the stroke, the piston reaches BDC marking the completion of the first mechanical stroke. At this point the cylinder is filled with the products of combustion. The piston moves back up the cylinder, expelling the exhaust gasses from the system via the exhaust valve (Çengel & Boles, 2001).

3.3.2 Diesel Engine (Diesel cycle)

The diesel engine, first proposed by Rudolph Diesel in the 1890s, is very similar to the four-stroke engine discussed in the previous section, the main difference being the ignition method. As previously mentioned, in four-stroke SI cycle engines the air-fuel mixture is compressed to a temperature below the fuels auto-ignition temperature, and combustion is initiated by the firing of the spark plug. In a CI engine, the air is compressed to a temperature above the auto-ignition temperature of the fuel, and combustion is initiated upon contact as the fuel is injected into the cylinder (Çengel & Boles, 2001).

In SI engines, compression ratios are limited by the onset of auto-ignition. However, in CI engines, diesel is injected into the cylinder which contains only compressed air, eliminating the chance of auto-ignition. CI engines are then able to operate at much higher compression ratios, typically between 12 and 24.

3.3.3 Wankel/Rotary Engine

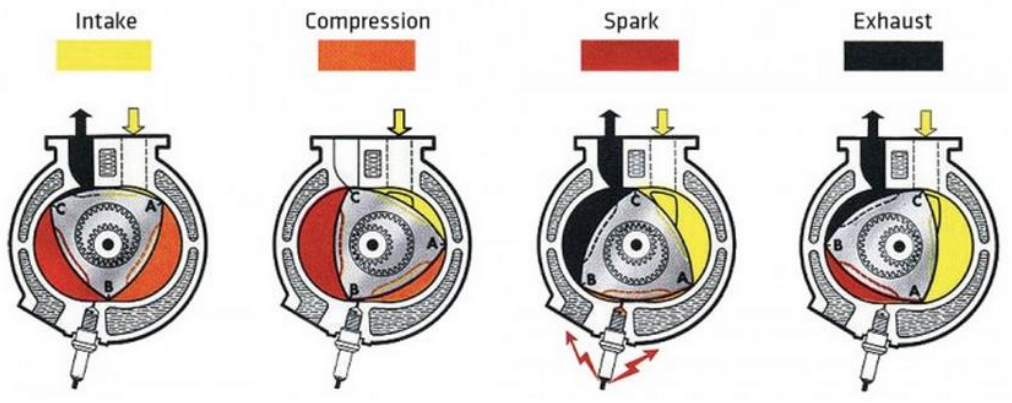

Figure 3.1: 4 strokes of a rotary engine, HSW, 2015

Like a reciprocating piston engine, the rotary engine converts the pressure created from the combustion of a compressed air-fuel mixture into a useable rotational force. In a rotary engine, a triangular rotor follows an oval-like epitrochoid shape, keeping the apexes of the rotor in contact with the housing to create three separate sealed volumes within the housing. As the rotor moves around the chamber, each of the three volumes of gas alternately expand and contract, drawing the air-fuel mixture into the engine, compressing it, and harnessing the pressure change due to combustion and expansion of gases before expelling the products of combustion out the exhaust port (HSW, 2015b). Figure 3.1 depicts the path of the rotor within the housing.

3.3.4 Carburation

In early model vehicles, small outdoor power equipment, and small displacement vehicles, a carburettor is used to deliver the air-fuel charge to the engine. The purpose of a carburettor is to supply the required proportions of air and fuel to the engine, namely, weaker in fuel for economy, and richer for power. Figure 3.2 depicts a simple downdraft carburettor, (Judge, 1955).

An elementary carburettor consists of a fuel reservoir, known as the float chamber, in which the level of fuel is kept constant by a float-actuated needle valve. The fuel from this chamber supplies a small orifice jet which is situated in the narrowest part, or throat, of a venturi or choke tube. The main air supply is drawn through the vertical tube from below, and passes through the venturi and thus takes up the fuel, the mixture passing upwards to the engine. The throttle valve controls the amount of the mixture delivered to

the engine, providing power output control. The principle of the simple carburettor is illustrated in Figure 3.3, (Judge, 1955).

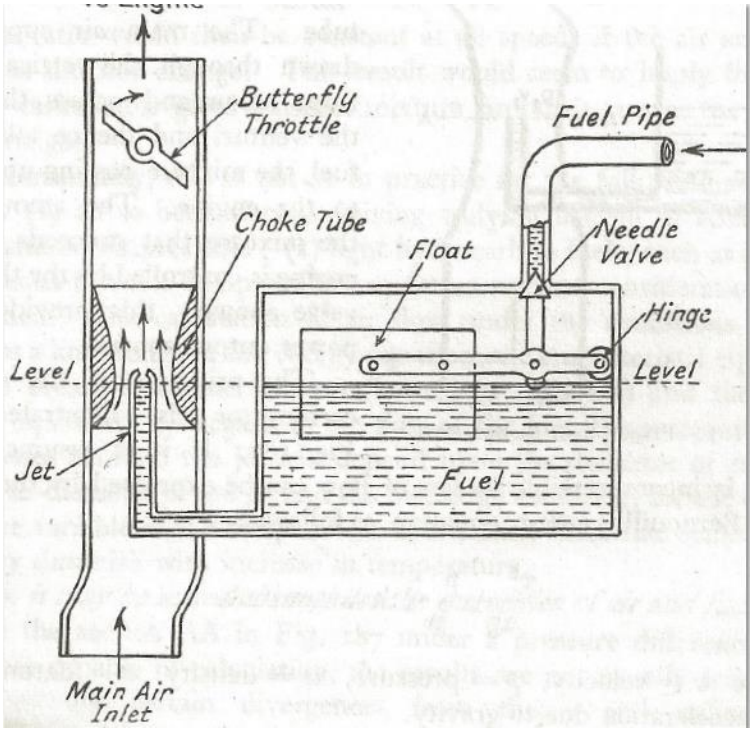

Figure 3.3: Simple downdraft carburettor section, Judge, 1955

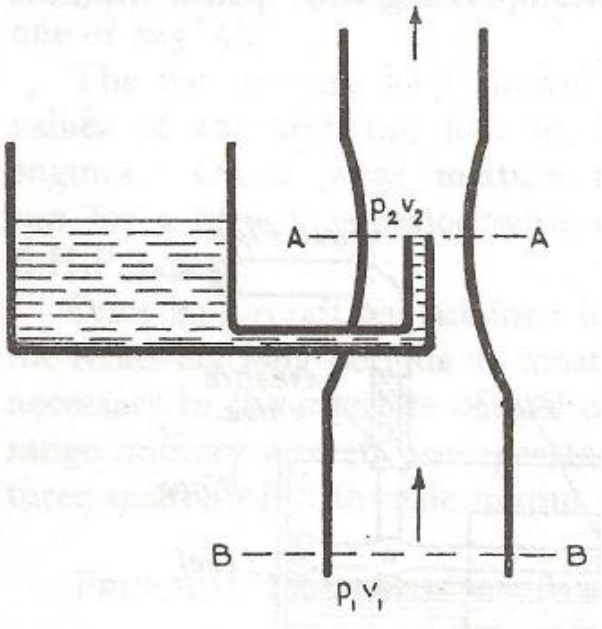

Figure 3.2: Simple Carburettor, Judge, 1955.

If the air is assumed incompressible, its law of flow can be approximated by Bernoulli's Equation, shown in Equation 3.2.

$$\frac{v^2}{2g} + \frac{p}{w} + h = \text{constant}$$ Equation 3.2

Where v is velocity, p is pressure, w density, h is datum head, and g is acceleration due to gravity. Then, if v_1 is the velocity at B and v_2 the velocity at A, p_1 and p_2 the pressures at B and A respectively, then Equation 3.2 can be expressed as Equation 3.3.

$$\frac{v_1^2}{2g} + \frac{p_1}{w} = \frac{v_2^2}{2g} + \frac{p_2}{w}$$ Equation 3.3

From this relationship it is apparent that as the velocity increases from v_1 to v_2, due to the reduction in cross-section, the pressure drops from atmospheric pressure p_o, corresponding to $v_1 = 0$ to a value p_2 below atmospheric pressure. Since the pressure on the fuel in the float chamber is atmospheric, the fuel flows out of the jet at a pressure equal to (p_o-p_2). The quantity of fuel flowing in per second would be proportional to $\sqrt{d(p_o - p_2)}$ where d is the density of the fuel (Judge, 1955).

Similarly, the quantity of air is proportional to $\sqrt{w(p_o - p_2)}$. Therefore, if both the air and fuel were assumed incompressible and viscosity was assumed negligible, the mass ratio of fuel to air is expressed as shown in Equation 3.4.

$$\frac{W_{Air}}{W_{Fuel}} = \frac{\sqrt{w(p_o - p_2)}}{\sqrt{d(p_o - p_2)}} = \sqrt{\frac{w}{d}}$$ Equation 3.4

The ratio would be constant at all engine speeds if the air and fuel densities did not change, implying carburettors supply constant mixture proportions over the speed range. In practice, this is not the case, for the following reasons, namely (1) air is both viscous – giving eddying instead of laminar flow – and is compressible; (2) light hydrocarbon fuels are viscous but not compressible. The calculation of airflow under the above conditions requires a knowledge of the energy balance Equation, the characteristic Equation for the pressure – volume relation (known or assumed), and the continuity Equation. The flow of fuel that actually passes through the jet depends on the ratio of length to diameter of the jet, and the discharge coefficient for the outlet. Other variables include fuel temperature as the density and viscosity lessen with temperature increase (Judge, 1955).

Therefore, while the quantities of air and fuel that pass through section AA in Figure 3.3 under a pressure potential of p_1-p_2 can be calculated, the results are not usually reliable due to divergence from theory and unknown variables (Judge, 1955).

The demise of the carburettor

As vehicles evolved and became less rudimentary, so too did the carburettor to accommodate the various operating requirements and emission laws. To handle some of these tasks, late model vehicles had carburettors that had five circuits:

- Main circuit: provides the correct amount of fuel for efficient cruising.
- Idle Circuit: supplies low fuel level for idle operation.
- Accelerator pump: provides extra bursts of fuel when the accelerator is depressed, reducing delay in throttle response.
- Power enrichment circuit: supplies additional fuel when the car is under load (uphill, towing operations).
- Choke: provides additional fuel on cold start.

Although the carburettor was used as the primary method of fuel delivery for much of the existence of the internal combustion engine, and for other applications such as lawnmowers and chainsaws – it still is, the carburettor has long since been replaced by fuel injection in automotive applications (HSW, 2015a).

3.3.5 Electronic Fuel Injection (EFI)

Throttle Body Injection (TBI).

Carburettors were initially superseded by TBI systems (single port or central fuel injection) incorporating electronically controlled fuel injector valves into a throttle body. As these systems were almost a bolt-on replacement for carburetted engines, only minor changes to engine design were required for their implementation (HSW, 2015a).

One or two injectors mounted in the throttle body, spray fuel into the intake manifold. An electric fuel pump (commonly mounted in or near the fuel tank) creates fuel pressure, which is controlled by a regulator mounted on the throttle body. When the injectors are energised, fuel is sprayed into the manifold in a rapid series of bursts (rather than a continuous stream).

Fuel distribution issues that affect carburetted induction are also present in TBI, however TBI systems benefit from superior cold-start characteristics through better atomisation of fuel and no troublesome choke mechanism. TBI was implemented only briefly in the United States during the 1980s before tougher emission laws necessitated a change to PFI.

Port Fuel Injection (PFI).

For PFI or multiport injection, each cylinder has its own injector which supplies fuel directly into the intake port. As only air flows through the intake manifold, the manifold remains dry and there are no issues with fuel puddling on cold-start or fuel separation causing uneven fuel mixtures in the central and end cylinders. This allows greater uniformity in fuel delivery to each cylinder resulting in better fuel economy, reduced emissions, and higher performance.

Direct Injection (DI)

For direct injection, each cylinder has its own injector which supplies fuel directly into the combustion chamber. Direct injection rapidly becoming the preferred method of injection for vehicle manufacturers, delivering greater efficiency and control of combustion.

3.3.6 Forced Induction (Supercharging)

During the intake stroke of a four-stroke engine, the rapid descent of the piston causes a vacuum in the cylinder, inducting a charge of air from the inlet manifold. The fuel is either added to the combustion chamber via PFI, DI, or is already present having been mixed with the inducted air via carburation. The charge is compressed and ignited. The rapid expansion of gases due to combustion of the charge drives the piston back down the cylinder, and the force of this vertical displacement is harnessed through the rotation of the crankshaft (HSW, 2015c).

The power harnessed is limited by a number of factors including the volume of fuel available for combustion. Increasing the fuel available is not sufficient to increase power output in itself, as the fuel requires a certain volume of air for efficient combustion (14 parts air to 1 part fuel for typical combustion), meaning more air is required. Increasing the amount of inducted air can be achieved by means of forced induction such as supercharging. A supercharger increases the intake pressure by compressing air to above atmospheric pressure, without creating a vacuum, forcing more air into the engine, and thus more fuel can be added to the charge, resulting in power increase (HSW, 2015c).

Supercharger function

A supercharger is any device that pressurises the intake air to above atmospheric pressure, providing ‘boost’. Both superchargers and turbochargers achieve this; the latter is in fact a shortened term for ‘turbo-supercharger’, its official name. The main difference between the two is the source of energy by which they are driven; turbochargers are driven by the mass-flow of exhaust gasses driving a turbine, while superchargers are powered mechanically by belt or chain-drive from the engine’s crankshaft.

Unlike turbochargers that use the mass-flow of exhaust gases created by combustion to power the compressor, a supercharger draws its power from the crankshaft, via an accessory belt. Supercharger rotors come in various shapes and sizes, though their function of compressing air prior to induction is common to all (HSW, 2015c).

To compress the air, the supercharger must spin rapidly – faster than that of the engine crank, resulting in a smaller compressor gear or pulley than is found on the crankshaft. Superchargers can spin at speeds as high as 50,000 to 65,000 rpm. A compressor spinning at 50,000 rpm corresponds to a boost of approximately 40-60 kPa over atmospheric pressure. At a typical atmospheric pressure of 101.3 kPa, this is a 40-60% increase in the amount of air inducted (HSW, 2015c).

As the air is compressed, the air temperature increases and loses density. The air cannot expand as much upon combustion and lowers its potential power advantages as a result.

The following concerns the work of Jegs Automotive from their online publication “Everything you want to know about superchargers”. Jegs Automotive are a performance auto parts stockist based in the United States, born out of a necessity for quality performance parts required by the Founders racing team in the 1950s. Jegs Automotive are a large retailer of performance parts including superchargers, turbochargers and fuel injection systems for V8 engines.

Supercharger types

Currently there are three basic types of superchargers sold in the performance market; namely roots type, centrifugal type and screw type superchargers.

Centrifugal type

A centrifugal supercharger is similar to a turbo-supercharger with the primary difference being that the former is driven by the crankshaft via a belt, and the turbo-supercharger receives drive from the force of the exhausting combustion gases. These superchargers

operate at extremely high speeds, achieved through an additional step up inside the casing. For a centrifugal design, the boost is proportional to the impeller speed, and as a result typically does not produce high levels of boost at lower engine speeds.

Screw type

The screw type supercharger is similar in appearance to a roots type supercharger, but the internals differ significantly. In a screw type supercharger, the rotors interleave one another, progressively compressing the air inside the casing as it is inducted. Screw type rotors are manufactured to extremely high tolerances, making them more expensive than a roots type.

Roots type

The roots type is the simplest and least expensive of the superchargers. Acting as an air pump, the roots type compresses the charge within the manifold and cylinders rather than in the supercharger casing. The centrifugal types are termed 'internal compression' superchargers to reflect compression of air inside the supercharger casing, while a roots type is termed an 'external compression' supercharger as air compression takes place outside the supercharger. The roots supercharger has been utilised in automotive applications since the 1930s, and development over this time has resulted in a highly refined product from a number of manufacturers.

If a cylinder were completely filled with air in the induction stroke, the engine would be said to have a 100% volumetric efficiency. Due to airflow restrictions caused by induction design (aircleaner, cylinder head, cam timing, etc.) an engine is not able to induct a full charge of air. A supercharger increases the volumetric efficiency of an engine by mitigating these restrictions. The amount of air and fuel that can be inducted into a supercharged engine exceeds the 100% volumetric efficiency of a highly efficient naturally aspirated engine.

Boost

Boost is the air pressure created by the supercharger, and is a function of engine displacement, supercharger displacement, and supercharger impeller speed. Boost can be increased by increasing supercharger impeller speed relative to the engine speed (overdriving), and reduced by decreasing the relative impeller speed (underdriving). If the size of the supercharger remains the same, and the displacement of the engine is reduced, the boost increases.

3.4 Hydrogen

3.4.1 Hydrogen as an Energy Carrier

The attractiveness of using hydrogen as an energy carrier lies in the long term viability of some of the production techniques. Hydrogen can be sourced from fossil fuels; from renewable energy such as biomass, wind, solar, and nuclear power. Hydrogen is also clean burning; there virtually no harmful emissions; and potentially high efficiency at the point of its use. However, there are serious challenges to overcome when hydrogen is to be used as an energy carrier. Thus, the distribution, bulk storage and on-board vehicle storage are heavily compromised. However, the advantages offered by hydrogen are deemed significant enough to warrant further exploration (Verhelst & Wallner, 2009).

3.4.2 Hydrogen Production

Hydrogen can store and deliver usable energy, but it does not typically exist in its elemental form in nature and must be produced from compounds that contain it. Hydrogen can be produced from a variety of resources, including fossil fuels such as natural gas, coal (with carbon capture), nuclear energy; and other renewable energy sources such as biomass, wind, solar, geothermal and hydroelectric power, using a diverse range of processes (FCTO, 2015). This section focuses on the production of hydrogen from natural gas reforming, and via electrolysis.

Natural Gas and Other Fossil Fuels

Natural gas reforming is an advanced and widely used process by which hydrogen is derived from Methane. 95% of the hydrogen produced in the USA is obtained by natural gas reforming. The EERE view this as an important technology for the near-term production of hydrogen (FCTO, 2015).

Most hydrogen produced in the United States is a product of steam-methane reforming, a process by which high-temperature steam (700°C-1000°C) is used to produce hydrogen from a methane source, namely natural gas. The methane reacts with steam under pressure in the presence of a catalyst to produce hydrogen, carbon monoxide, and small concentrations of carbon dioxide. The process is endothermic and thus requires the addition of heat (FCTO, 2015). Equation 3.2 depicts this reaction:

$$CH_4 + H_2O \rightarrow CO + 3H_2 \qquad \text{Equation 3.2}$$

A subsequent reaction, termed the water-gas shift reaction, reacts steam and carbon monoxide with a catalyst to produce more hydrogen and carbon dioxide. Equation 3.3 depicts this endothermic reaction:

$$CO + H_2O \rightarrow CO_2 + H_2 \qquad \text{Equation 3.3}$$

In a final step termed 'pressure-swing adsorption', carbon dioxide and other impurities are removed from the gas stream, leaving high purity hydrogen. Steam reforming can use other fuels such as ethanol, propane and petroleum to produce hydrogen (FCTO, 2015).

Re-forming is a low-cost method of producing commercial volumes of hydrogen to facilitate the growth in hydrogen powered vehicles in the near term. It is expected that hydrogen production from natural gas will be supplemented by production from renewable resources and other low-carbon energy resources (FCTO, 2015).

Electrolysis

Electrolysis is a promising option for the renewable and clean production of hydrogen. Electrolysis is the process of splitting water molecules into their elemental components using electricity, Figure 3.4. The reaction takes place in an electrolyser, which like fuel cells, consists of an anode and a cathode, separated by an electrolyte. Electrolysers can vary greatly in size from small appliance-sized suited for small scale distribution, to large-scale central production facilities (FCTO, 2015).

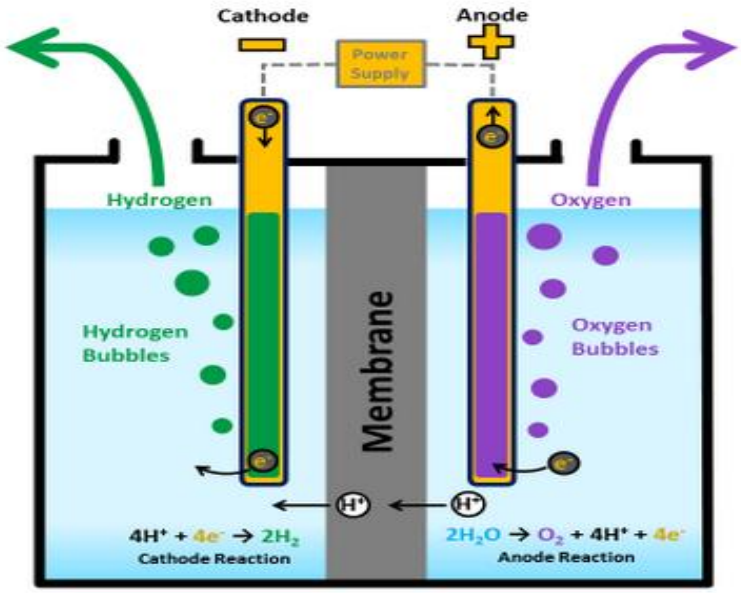

Figure 3.4: Electrolytic Cell, FCTO, 2015

In a polymer electrolyte membrane (PEM) electrolyser, the electrolyte is a solid specialty plastic material. Water reacts at the anode to form oxygen and hydrogen cat-ions. Equation 3.4 depicts the anode reaction:

$$H_20 \rightarrow O_2 + 4H^+ + 4e^- \qquad \text{Equation 3.4}$$

The disassociated electrons flow through an external circuit and the hydrogen ions selectively move across the PEM to the cathode. At the cathode, the hydrogen ions combine with electrons from the external circuit to form hydrogen gas. Equation 3.5 depicts the cathode reaction:

$$4H^+ + 4e^- \rightarrow 2H_2 \qquad \text{Equation 3.5}$$

(FCTO, 2015)

Hydrogen produced via electrolysis has potential opportunities for synergy with viable power generation from renewable energy sources. This would greatly reduce the well-to-wheel ecological footprint of hydrogen-powered vehicles.

3.4.3 Hydrogen Storage

On-board storage of hydrogen for transportation applications remains as one of the most technically challenging barriers to the widespread commercialisation of hydrogen-fuelled vehicles (FCTO, 2015). The EERE hydrogen storage activity primarily focuses on the applied research and development of low-pressure, materials-based technologies that facilitate a driving range of more than 500km while meeting safety, cost, packaging and performance requirements to be competitive in the current car market. While some automotive firms have prototypes that have achieved this, the driving range must be achievable across different models without compromising on the above criteria. Hydrogen storage is required for other vehicle applications, for stationary plant and equipment, hydrogen delivery, and hydrogen refuelling infrastructure (FCTO, 2015).

Storing enough hydrogen on-board a vehicle to achieve a driving range of more than 500km represents a significant challenge. Hydrogen has nearly three times the energy content of petrol on a weight basis (120MJ/litre for hydrogen, 44MJ/kg for petrol). However, on a volumetric basis the trend reverses (8MJ/litre for liquid hydrogen, 32MJ/litre for petrol). For hydrogen vehicles to be competitive against hydrocarbon-fuelled vehicles, a comparable driving range must be achieved (FCTO, 2015).

Hydrogen can be stored physically as either liquid or gas. Gas storage requires high-pressure tanks (5,000-10,000 psi), and liquid storage requires cryogenic temperatures because the boiling point temperature at one atmosphere is -252.8^{o}C (FCTO, 2015).

Hydrogen can also be stored by adsorption on the surface of a solid or by absorption within a solid. In absorption, hydrogen is disassociated into hydrogen atoms which are then incorporated into the solid lattice framework – this method may allow for storage of larger quantities of hydrogen in smaller volumes, at a lower pressure and at temperatures close to room temperature. It is also possible to achieve volumetric storage densities comparable or superior to that of liquid hydrogen as the hydrogen molecule disassociates into atomic hydrogen within the metal hydride lattice (FCTO, 2015).

Compressed Hydrogen

The energy density of hydrogen gas can be increased by storing hydrogen at higher pressures. These higher pressures necessitate material and design improvements in order to ensure tank safety and integrity. To reduce the cost of producing high pressure hydrogen requires advances in compression technologies (FCTO, 2015).

Carbon fibre reinforced 5,000psi and 10,000psi compressed hydrogen tanks are under development by Quantum Technologies and other manufacturers, and are already used in several prototype hydrogen powered vehicles. The tank lining is a high-molecular-weight polymer, which serves as a hydrogen gas permeation barrier. The gas pressure load-bearing component of the tank encapsulates the permeation barrier. An outer shell is placed on the tank for impact and damage resistance (FCTO, 2015).

The driving range of a hydrogen powered vehicle with compressed hydrogen tanks is dependent on vehicle type, application, the amount of hydrogen stored, and at what pressure. The driving range can be increased at the expense of cost and cargo space within the vehicle. Volumetric capacity, high pressure and cost then are the key challenges for compressed hydrogen tanks. Refuelling times, compression energy penalties and the management of heat during compression also need to be considered as the mass and pressure of on-board hydrogen increases (FCTO, 2015).

Issues with compressed gas tanks centre on high pressure, weight, volume, conformability and cost. The cost of high-pressure compressed tanks is essentially governed by the cost of carbon fibre that is required for light-weight structural reinforcement. Investigations are under way to identify lower cost carbon fibre that can meet the safety specifications

and high pressure requirements for hydrogen gas tanks. The lower cost carbon fibre must still be capable of meeting tank thickness constraints to meet volumetric capacity requirements. Therefore, lowering cost without compromising weight and volume is a key challenge for compressed hydrogen tanks (FCTO, 2015).

Two approaches currently under investigation in the pursuit of increased gravimetric and volumetric storage capacities of compressed hydrogen are cryo-compressed tanks, and the other conformable tanks. Cryo-compressed tanks exploit the increased volumetric tank capacity as the tank temperature decreases, at a fixed volume and pressure. Thus, in cooling a tank from room temperature to 77K (the temperature of liquid nitrogen), its volumetric capacity increases by a factor of four, however, system volumetric capacity is less than this due to the increased volume required for the cooling system (FCTO, 2015). Present liquid petrol tanks in vehicles are highly conformable, in order to take maximum advantage of available space. Conformable hydrogen tank structures are based on the location of structural supports. For greater degrees of conformability, internal cellular-type load bearing structures may also be a possibility (FCTO, 2015).

Liquid Hydrogen

The energy density of hydrogen can be increased by storing hydrogen in a liquid state. However, liquid hydrogen tanks have issues including hydrogen boil-off, the energy required for hydrogen liquefaction, volume, weight, and tank cost. The energy requirements for hydrogen liquefaction is typically 30% of the heating value of hydrogen.

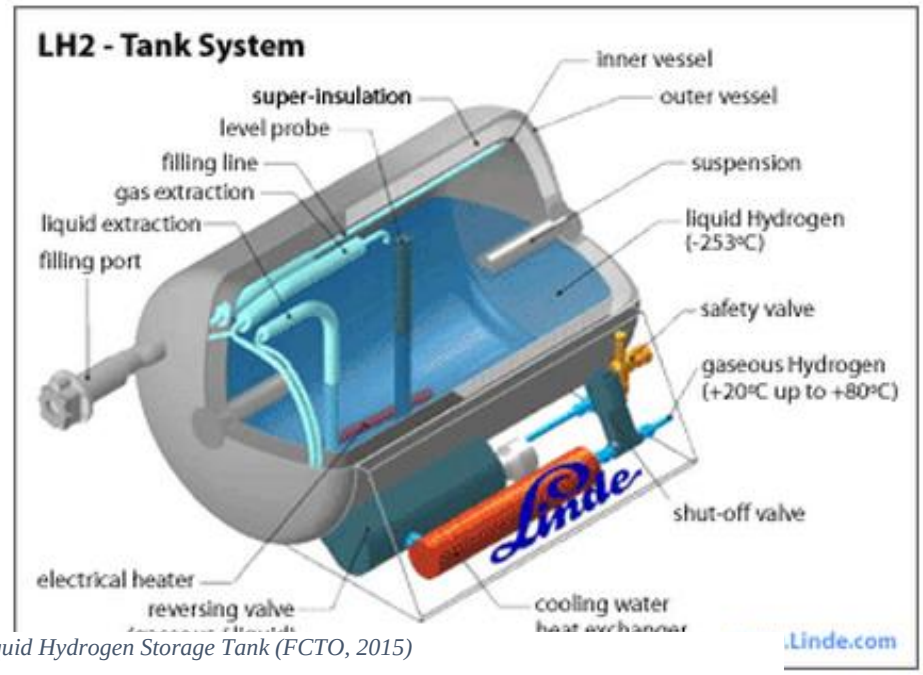

Figure 3.5: Liquid Hydrogen Storage Tank (FCTO, 2015)

New approaches are needed to lower these energy requirements and thus the cost of liquefaction. Hydrogen boil-off must be mitigated or eliminated entirely for cost, efficiency and vehicle range, as well as for safety considerations when vehicles are parked in confined spaces. Insulation requirements lower the gravimetric and volumetric capacity of liquid hydrogen tanks. Figure 3.5 depicts a sectional view of a LH_2 tank system (FCTO, 2015).

Liquid hydrogen tanks can store greater amounts of hydrogen in a given volume than compressed gas tanks. The volumetric capacities of liquid hydrogen and compressed hydrogen at 10,000 psi is 0.070 kg/L and 0.030 kg/L, respectively (FCTO, 2015).

Solid storage:

At present, there are three generic mechanisms known for storing hydrogen in materials, namely absorption, adsorption, and chemical reaction. In absorptive hydrogen storage, hydrogen is absorbed directly into the bulk of the material. In simple crystalline metal hydrides, this absorption occurs by incorporating atomic hydrogen into interstitial sites in the crystallographic lattice structure (FCTO, 2015).

Adsorption is divided into physisorpiton and chemisorption based energetics of the mechanism. Physisorbed hydrogen is comparatively weakly and energetically bond to the material than to chemisorbed hydrogen. Sorptive processes usually require highly porous materials to maximise the surface area available for hydrogen sorption to occur, allowing for easy uptake and release of hydrogen from the material (FCTO, 2015).

The chemical reaction method for hydrogen storage requires displacive chemical reactions for hydrogen generation and storage. For on-board reversible reactions, hydrogen generation and storage take place by the simple reversal of the chemical reaction as a product of modest changes in temperature and pressure. The hydrogen generation reaction is not reversible under modest temperature/pressure changes in many cases. Thus, getting hydrogen back into the starting material must be done off-board, even though hydrogen can be generated on-board the vehicle (FCTO, 2015).

Metal Hydrides

Metal hydrides provide potential for reversible on-board hydrogen storage and release at low temperatures and pressures. Hydrogen can form metal hydrides with some metals and alloys. Elements with unfilled valence shells or subshells are suitable hydriding substances. During the formation of a metal hydride, hydrogen molecules are split and

hydrogen atoms form chemical compounds by sharing their electrons with the unfilled valence shells of the metal atom and the K shells of the hydrogen atoms (Barbir, undated).

The formation of a hydride is an exothermic process, meaning heat is generated. This means that in order to release the hydrogen from a metal hydride, heat must be supplied. These processes are depicted in the reversible chemical reaction shown in Equation 3.6 below (Barbir, undated).

Charging/ discharging absorption of hydrogen:

$$M + \mathrm{x}H_2 \rightleftharpoons \mathrm{MH_{2x}} + heat \qquad \text{Equation 3.6}$$

Where M represents the hydriding substance: a metal, element or alloy. The rate of these reactions increase with an increase in surface area. Thus, usually, the hydriding substances are in powdered form to increase reaction speed (Barbir, undated).

In this way effective storage is created that is comparable to the density of liquid hydrogen. However, if the mass of the metal is considered, then the metal hydride gravimetric storage density is comparable to the storage of pressurised hydrogen. The best gravimetric storage density achievable is approximately 0.07kg of hydrogen gas per kilogram of Magnesium alloy (Barbir, undated).

A primary advantage of solid storage of hydrogen in a hydriding substance is safety. If a hydride tank were to sustain serious damage, such as in a vehicle collision, the tank would not pose a fire hazard as the hydrogen would remain in the metal structure, effectively inert (Barbir, undated).

Chemical Hydrogen Storage

Storage technologies in which hydrogen is generated through a chemical reaction are termed ‘chemical hydrogen storage’ methods. Common reactions involve reacting chemical hydrides with water or alcohols. However, these reactions are not easily reversed on board a vehicle, and thus the spent fuel and/or by-products must be removed from the vehicle and regenerated off the vehicle (FCTO, 2015).

Hydrolysis reactions

Hydrolysis reactions are characterised by the oxidation reaction of chemical hydrides with water to produce hydrogen. The most studied example to date is the reaction of sodium Borohydride, its reaction is depicted in Equation 3.7.

$$NaBH_4 + 2H_2O \rightarrow NaBO_2 + 4H_2$$ Equation 3.7

In this form, the mixture of inert stabilizing liquid protects the hydride from contact with moisture, and allows the hydride to be pumped. At the point of use, water is added and mixed, producing high-purity hydrogen (FCTO, 2015).

The reaction is controllable in an aqueous solution via pH and a catalyst. Despite the high material hydrogen capacity and fast release kinetics, the borohydride regeneration requires off-board access. The cost, energy requirements, and life impacts of regeneration are key areas of current investigation (FCTO, 2015).

3.5 Hydrogen Internal Combustion engine vehicles

Hydrogen ICEs for transport applications are currently under development and are intended to provide an equivalent driving experience in terms of drivability, range, and safety as conventional fuels. Current HICEVs have a reduced driving range and luggage capacity compared to conventionally fuelled vehicles, primarily due to challenges with on-board hydrogen storage. However, due to the availability of hydrogen, its potential to be a zero emission fuel, the extensive knowledge surrounding engine design, manufacture, durability and maintenance, as well as the capacity of combustion engines to run on both hydrogen and conventional fuels, they are considered a bridging technology towards a widespread hydrogen economy. Numerous hydrogen engine-powered vehicles have been designed ranging from motorcycles, passenger cars, pickup trucks to buses and off-road equipment (Verhelst & Wallner, 2009).

3.5.1 History

Verhelst & Wallner comment that the idea of running an internal combustion engine on hydrogen fuel is almost as old as the concept of the ICE itself. In 1807, Swiss scientist Francois Issac de Rivas invented a combustion engine that used a mixture of hydrogen and air for fuel, and designed a car for the engine, creating the first internal combustion engine vehicle, though he was ultimately unsuccessful. The first successful internal combustion hydrogen vehicle was patented in 1860 by Jean Joseph Etienne Lenoir, a two-stroke gas-driven engine with a horizontal arrangement, supplied with hydrogen via electrolysis. In 1933 Norsk Hydro operated a HICEV supplied with hydrogen from on-board reformation of ammonia. In the same year, Erren Engineering Company proposed the first hydrogen DI by injecting pressurised hydrogen into air or oxygen inside the combustion chamber, rather than via carburetion which commonly resulted in backfire.

The patented system required special fuel injection, and control mechanisms, however left other engine characteristics intact. Using hydrogen as a booster, the design eliminated backfire and achieved significantly more complete combustion of hydrocarbons, higher output and lower SFC. In 1974 the Musashi Institute of Technology introduced the first Japanese HICE; the Musashi 1, using a 4 stroke engine and high pressure on-board storage. The Musashi 1 was superseded in 1975 by the Musashi 2, sporting fuel injection and liquid storage. The Musashi 3 was released in 1977 and was powered by a SI 2-stroke engine with DI. A joint venture between BMW and the German aerospace centre saw the release of their first hydrogen vehicle in 1979 (Verhelst & Wallner, 2009).

3.5.2 Hydrogen Vehicle Characterisation

Verhelst & Wallner advise that HICEVs can be characterised as either conversion or dedicated vehicles, with conversion vehicles adapted for hydrogen combustion either by the manufacturer or an aftermarket supplier, and dedicated hydrogen vehicles are designed and manufactured for hydrogen operation by OEM. Both dedicated hydrogen fuel and dual fuel engines that accommodate hydrogen or another hydrocarbon fuel have been produced. Classified by on-board storage method, H2 vehicles can be categorised as compressed hydrogen and cryogenic liquid hydrogen vehicles. The following sections provide a brief overview of selected hydrogen vehicles. Hydrogen combustion enhancement vehicles are not considered (Verhelst & Wallner, 2009).

3.5.3 Conversion Vehicles

Electric Transportation Engineering Corporation produced a conversion truck based on the Chevrolet/CMC Silverado/Sierra 1500HD. The ETEC HICE Truck uses compressed hydrogen to fuel its 6.0L V8 engine with hydrogen port-fuel injection. The engine has induction forced via a belt driven supercharger with intercooler to increase the power output of the engine. Hydrogen is stored in three 150L, Type 3 aluminium lined, carbon-fibre reinforced tanks at up to 350 bar, supplying up to 10.5kg of usable hydrogen. The truck has an estimated curb weight of 3,000 kg. A performance and emissions characteristics analysis of this vehicle for operations between $0.35 < \Phi < 0.5$ showed fuel consumption numbers between 4.1 and 4.5kg of hydrogen per 100km, an energy equivalent of 15.5-17L per hundred of petroleum at emission levels in the ULEV and SULEV ranges. About 20 ETEC HICE Truck Conversion vehicles have been built so far (Verhelst & Wallner, 2009).

3.5.4 Bi-fuel vehicles

BMW have introduced six generations of hydrogen ICEVs since 1979, the latest version is the BMW Hydrogen 7, a bi-fuel luxury sedan powered by a 6.0 L V12 engine. BMW claim that the H7 has successfully completed the process of series development, meaning that all components have undergone the same design, manufacturing and quality control process as other BMW production vehicles. The H7 is built in parallel to the BMW 5, 6 & 7 series vehicles in BMW's Dingolfing Plant, with the power plant coming from the production plant in Munich, like all BMW twelve cylinder engines. The engine has two separate fuel systems, allowing the vehicle to run on hydrogen as well as petroleum. The hydrogen utilises PFI, supplied by a cryogenic hydrogen tank in the storage compartment of the vehicle, and holds approximately 8kg of liquid hydrogen, providing a driving range of 200 km under hydrogen operation, and an additional 480 km on petroleum. About 100 units have been produced. Mazda have developed several generations of hydrogen powered rotary vehicles since 1991, culminating in the Mazda RX-8 Hydrogen RE in 2003 (Verhelst & Wallner, 2009).

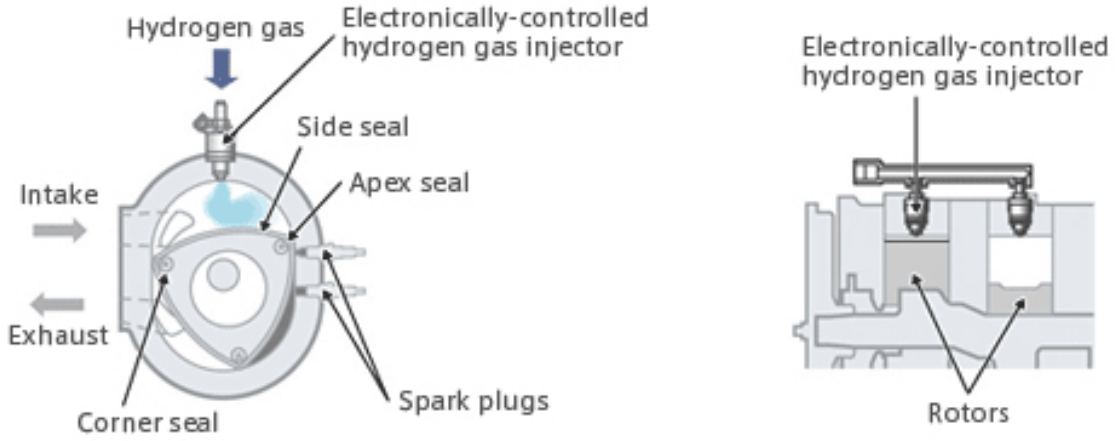

Figure 3.6: Mazda RX-8 Hydrogen RE engine operation, Mazda, 2003.

Mazda have successfully converted their RENSIS Wankle rotary engine to run on both hydrogen and petrol, claiming that the few modifications to the existing RE platform have allowed them to develop the RENSIS hydrogen rotary at low cost. The RENSIS engine employs the direct injection of hydrogen via an electronically controlled gas injector. The system draws air in from a side port and injects hydrogen directly into the intake chamber via the injector installed on the top of the housing. Figure 3.6 depicts Mazda's Hydrogen RE engine concept (Mazda, 2015).

Mazda claim the unique structure of the RE greatly reduces the occurrence of abnormal combustion (backfiring) due to the absence of intake/exhaust valves, and the separation of low and high temperature intake and combustion chambers respectively. Further, Mazda suggest that the comparatively long duration of the intake process compared with that of traditional reciprocating engines encourages thorough mixing of hydrogen and air prior to combustion (Mazda, 2015).

The utilisation of direct injection aims to achieve high output under hydrogen combustion conditions. The direct injection system is applied by installing an electronically-controlled hydrogen gas injector at the top of the rotor housing. Mazda claim the RE is well suited to direct injection due to considerable structural freedom of injector layout. Another gas injector is installed on the intake pipe for premixing and direct injection, depending on driving conditions, allowing for better optimisation of hydrogen combustion. When operating on petrol, the fuel is supplied from the same petrol injector found in the standard petrol engine (Mazda, 2015).

Mazda employ lean burn at low engine speeds and EGR and three-way catalyst at high engine speeds to reduce NOx emissions. Mazda claim that optimal and appropriate use of lean burn and EGR satisfies both high output and low emissions criteria. The technology has been packaged in both the Mazda RX-8 Hydrogen RE and the Mazda Premacy Hydrogen RE Hybrid. Figure 3.7Figure 3.7 displays Mazda's two hydrogen

platforms.

Since the latter uses the combustion of hydrogen to power electric motors, we are only concerned with the RX-8 Hydrogen RE. However, it is worth noting that the Premacy produces approximately 40% more power than the RX-8 Hydrogen RE, resulting in higher acceleration, and improved fuel economy. Mazda attribute the performance gains

Figure 3.7: RX-8 Hydrogen RE and Premacy Hydrogen RE hybrid, Mazda, 2003.

to switching the rotary engine from a longitudinal to a transverse layout in the Premacy, reducing intake and exhaust resistance, improving combustion. The Premacy has a Driving range of 200 km on hydrogen fuel (Mazda, 2015).

Figure 3.8 depicts the RX-8 Hydrogen RE vehicle layout.

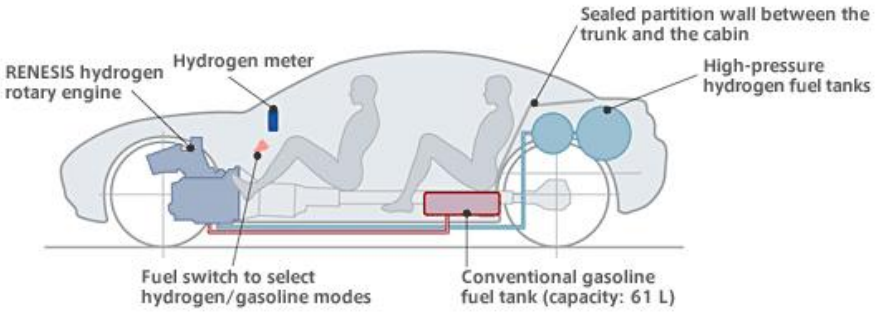

Figure 3.8: RX-8 Hydrogen RE Hydrogen storage diagram, Mazda, 2003.

The seating capacity of the RX-8 remains unchanged from the petrol model. However, with two hydrogen tanks installed in the cargo area, practicality is significantly hindered. The tanks contain pressurised hydrogen at 35MPa, the current national standard for hydrogen fuelling stations (Mazda, 2015). While the RX-8 delivers similar power and torque outputs to base model while running on petrol, outputs shrink from 154kW and 222Nm to just 80kW and 140Nm on hydrogen. Combined with its driving range of just 100km on hydrogen, the performance is limiting to say the least (GoAuto, 2009).

In Japan, the vehicle is offered only for lease to domestic governments and enterprises since 2006, and participation in the Norwegian hydrogen highway project, HyNor. S. Barkker et al suggested that the main reason for Mazda's commitment to internal combustion hydrogen engines, next to the lower cost of ICEs compared to FCVs, is its proprietary rotary engine. The engine design allows for greater control of the hydrogen combustion than in conventional reciprocating engines. To compensate for lower fuel efficiency, Mazda have chosen bivalent engines. Mazda's prototypes have never reached driving ranges in excess of 230km without refuelling (Bakker, van Lente, & Meeus, 2012).

3.5.5 Dedicated Hydrogen Vehicles

The BMW H7 Mono-Fuel demonstration vehicle, based on the H7 bi-fuel, was built to showcase potential emissions reduction from a dedicated hydrogen vehicle. The removal of petrol delivery lines, injectors and rail, associated EGR, and two high pressure fuel pumps (causing significant parasitic drag) form the most significant changes.

Performance and emission characteristics analysis found NOx and CO levels to be at just a fraction of the SULEV standard. For non-methane hydrocarbon emissions, the results showed emissions averaged 0g/km, which required the car to actively reduce emissions compared to ambient concentrations. The fuel consumption results showed 3.7 kg/100km (13.8 L/100km petroleum equivalent) for the FTP-75 test cycle, and 2.1 kg/100km (7.8 L/100km petroleum equivalent) for the highway cycle (Verhelst & Wallner, 2009).

3.5.6 Overview of Hydrogen Vehicles

Figure 3.9 below is a summary from Verhelst & Wallner of the above described hydrogen vehicles.

Name	Year	Engine	Tank	Capacity	Range	Units made
Rivaz	1807	1-cyl	Compressed			Prototype
Lenoir	1860	1-cyl	Water electrolysis			Prototype
Norsk Hydro	1933		Ammonia reforming			Prototype
Musashi 1	1974		Compressed	7 Nm^3		Prototype
Musashi 2	1975		Cryo	230 L		Prototype
Musashi 3	1977	2-stroke	Cryo	65 L		Prototype
BMW	1979	3.5 L	Cryo		300 km	
Ford P2000	2001	2.0 L I4	Compressed	1.5 kg	100 km	
BMW Hydrogen 7	2003	6.0 L V12	Cryo	8 kg	200 + 480 km	~100
Mazda RX-8 Hydrogen RE	2003	2 × 654 cc	Compressed	2.4 kg	100 + 550 km	>30
Ford Shuttle Bus	2004	6.8 L V10	Compressed	29.6 kg	240–320 km	
ETEC Silverado	2004	6.0 L V8	Compressed	10.5 kg	up to 335 km	~20
Quantum Prius	2005	1.5 L I4	Compressed	1.6 kg (reg.)/2.4 kg (ext.)	100–130 km	>30

Figure 3.9: Overview of hydrogen ICE vehicles, Verhelst & Wallner, 2009

(Verhelst & Wallner, 2009)

3.6 Measures for Hydrogen Engine Design or Conversion

The following discusses measures identified by Verhelst & Wallner for engine design or conversion to accommodate hydrogen combustion. The abnormal combustion problems previously identified, or rather how to mitigate or prevent their occurrence, has led to most of the countermeasures put forward in early work on HICEs.

3.6.1 Spark Plugs

Cold-rated plugs are recommended to avoid the temperature of the spark plug electrode exceeding the auto-ignition temperature limit of hydrogen, resulting in backfire. Non platinum tipped electrode spark plugs are to be used, as platinum is a catalyst for hydrogen oxidation (Verhelst & Wallner, 2009).

3.6.2 Injection system

It is clear from the previous section that timed injection is a prerequisite. One option is the utilisation of PFI and program timing such that an air cooling period is created in the initial phase of the inlet stroke, and all hydrogen is inducted leaving none remaining in

the manifold once the intake valve is shut. This may not be required as work has been published reporting no correlation between injection timing and backfire. The other option is DI during charge compression. For DI high flow rate injectors with instantaneous flows of around 4-6 g/s at 100 bar supply are required. For PFI arrangements, the need for high flow requirements can be replaced with multiple injectors. Further, timed injection lessens the volume of unburnt fuel in the intake manifold at any point, mitigating the severity of any potential backfire (Verhelst & Wallner, 2009).

3.6.3 Ignition system

To avoid residual ignition energy causing uncontrolled ignition, the system should be adequately grounded or the resistances of the ignition cable changed. Induction ignition in adjacent ignition cables should be avoided, i.e. by adopting a coil on plug system. Counterintuitively, a high voltage output ignition system should be used, as the ignition of hydrogen mixtures requires an increased secondary ignition voltage (likely a result of lower ion concentration of a hydrogen flame compared to that of a hydrocarbon). Multi-coil or coil on plug systems also satisfy this condition. Alternatively, the spark plug gap can be reduced to lower the ignition voltage – not an issue for hydrogen engines as there is almost no deposit formation, however not suitable for dual fuel applications (Verhelst & Wallner, 2009).

3.6.4 Hot spots

Hotspots within the combustion chamber have potential to cause surface ignition or backfire, and should be mitigated or eliminated where practicable. Mitigation methods include cooled exhaust valves; multivalve engine heads to further lower exhaust valve temperature; adequate oil control; additional coolant passages around areas of high thermal loads; the previously mentioned delayed injection to create a cooling period at the beginning of the intake stroke; proper scavenging (i.e. variable valve timing) to decrease residual gas temperature (Verhelst & Wallner, 2009).

3.6.5 Piston rings and crevice volumes

Verhelst & Wallner cite experiments in which careful cleaning of the engine, enhanced oil control or even non-lubricated operation, scavenging of residual gases, cold rated spark plugs and/or cooled exhaust valves have been utilised to eliminate hot spots, and backfire has still occurred. Verhelst & Wallner suggest that the small quenching distance

of hydrogen and its wide flammability limits allowing combustion in the piston top land, (the crevice volume above the top piston ring), is being overlooked by investigators. Hydrogen engines have demonstrated operating on stoichiometric mixtures without backfire, by careful selection of piston rings and crevice volumes, without any requirement for timed injection or cooled exhaust valves. Thus propagating hydrogen flames into top land can be prevented by reducing piston top land clearance. Verhelst & Wallner cite Swain et al's use of 0.152mm to quench hydrogen flame. Other researchers have changed crevice volumes and/or piston rings aiming to reduce the reflow of unburned mixture from the second land (crevice volume between first and second piston rings) to the top land, preventing the fuelling of a top land flame during intake or exhaust. The smaller quenching distance of a hydrogen flame corresponds to an increased thermal load for the piston top. Verhelst & Wallner cite Berger et al in suggesting a special coating to the top piston ring groove may be applied to account for this (Verhelst & Wallner, 2009).

3.6.6 Valve seat and injectors

A suitable valve seat material is required to be selected to account for the lack of upper cylinder lubrication from the combustion of hydrogen compared to petroleum, and the injectors designed accordingly. This is the case for any dry gaseous fuel, however it can be more critical for hydrogen as some gases (i.e. CNG) contain trace amounts of oil from the oil mist in the compressor used to compress the fuel. Hydrogen compressors are normally built to higher tolerances to reduce the leakage rate (Verhelst & Wallner, 2009).

3.6.7 Lubrication

A high water concentration compatible engine lubrication oil must be chosen, namely a demulsifying oil or a synthetic oil which forms a solution with water. An ashless oil is recommended to avoid formation of deposits. Verhelst & Wallner cite a high percentage of hydrogen (+5 vol%) was measured in the composition of hydrogen in the crankcase, resulting from blowby. Blowby rates for hydrogen combustion can be expected to be relatively high due to rapid pressure rise caused by the high burn rate of hydrogen as a result of its high flame speed properties. An investigation into the composition of the lubricating oil compared to that of unused oil found that the properties had significantly changed, notably a strong decrease of lubricating qualities. The best solution, though currently unavailable, is the use of an engine oil specifically developed for hydrogen

combustion. For safety, it is recommended that a forced crankcase ventilation system be mounted to the engine to ensure hydrogen concentration is below the lower flammability limit (Verhelst & Wallner, 2009).

3.6.8 Crankcase ventilation

Positive crankcase ventilation is recommended for non-throttled operation (high manifold pressures), to decrease hydrogen concentrations from blowby in the crankcase. As WOT operation is adopted where possible to increase efficiency, high manifold pressures result. Thus the pressure difference between the crankcase and the manifold is insufficient and cannot be used as a driving force for crankcase ventilation as is used in throttled engines. This can be resolved by the placement of a venturi in the intake (Verhelst & Wallner, 2009).

3.6.9 Compression ratio

The ideal compression ratio should be as high as possible to increase efficiency, limited by increased heat loss or the onset of abnormal combustion (surface ignition for hydrogen combustion). The selection of compression ratio is dependent on the application, as optimum compression ratio for highest efficiency may be different from optimum ratio for maximum power output. HICE compression ratios range from 7.5:1 to 14.5:1.

3.6.10 In-cylinder turbulence

Low turbulence combustion chambers such as pancake/disk chamber and axially aligned intake port can be used due to hydrogen's high flame speed. This increases efficiency due to increasing volumetric efficiency and decreasing heat loss. Verhelst & Wallner suggest they may be necessary to avoid excessive rates of pressure rise at stoichiometric operation, where high in-cylinder turbulence has potential to cause very fast flames, leading to knocking combustion (Verhelst & Wallner, 2009).

3.6.11 Electronic throttle

Hydrogen engines should be run under WOT conditions where practical, though throttling may be required at low load to maintain stable combustion and reduce unburned hydrogen emissions. At medium-high loads, throttling may be required to limit NOx emissions. This can only be achieved where electrically controlled throttle position replaces mechanically controlled throttle via accelerator (Verhelst & Wallner, 2009).

3.7 Hydrogen Safety

The unique physio-chemical properties of hydrogen necessitates an adapted approach in developing a safety concept for both static test engines and in vehicular applications. The low density and gaseous state of hydrogen at atmospheric conditions, in addition to the wide flammability limits and invisibility of the gas and its flames require measures to guarantee a level of safety equivalent to operation of conventional hydrocarbon fuelled vehicles. When suitable safeguards are implemented to account for these unique properties by facility designers, engineers and operators, hydrogen operation can be as safe as, if not safer than, conventional fuels (Verhelst & Wallner, 2009).

3.7.1 Test Apparatus Design

For hydrogen combustion to occur, Verhelst & Wallner advise that both an ignitable hydrogen-air mixture and source of ignition must be present. Verhelst & Wallner suggest it is practically impossible to eliminate all sources of ignition when a hydrogen ICE is operated in an enclosed space. However, the number of sources, especially sources close to areas typically associated with hydrogen accumulation, should be minimised. It is best practice to de-energize electrical equipment in proximity to the testing area. As these sources of ignition cannot be fully eliminated, ventilation should also be employed (Verhelst & Wallner, 2009).

3.7.2 Ventilation

Testing facilities for hydrogen ICEs are generally designed to be much larger than those for conventional fuel ICEs. For hydrogen testing, enclosed test cells and an open test cell in a high bay are the two scenarios considered for ventilation purposes. Verhelst & Wallner suggest that as a rule of thumb, 1-2 full air exchanges per minute has been established for ventilation of closed cell testing. In order to effectively remove heat and hydrogen leakage from the test engine, cross ventilation is widely used for enclosed tests. Fume hoods are used extensively in both enclosed and high bay testing. Crankcase ventilation in hydrogen ICEs requires additional consideration since concentrations of hydrogen have been shown to be in excess of 5 Vol%. Possible solutions for both static testing and vehicular applications suggest venting the crankcase to the atmosphere, routing ventilation to testing extractors/flumes, as well as variations of combining forced crankcase ventilation with an oil separator with or without a catalyst for the formation of water from available hydrogen, after which normal EGR route gases to the inlet manifold (Verhelst & Wallner, 2009).

3.7.3 Hydrogen sensors

Several off-the-shelf items are available commercially for hydrogen detection including electrochemical, catalytic, thermal conductivity, semiconductor-based and microelectromechanical sensors. Verhelst & Wallner recommend placement of sensors at locations where hydrogen leakage or spills are possible, hydrogen connections, where hydrogen has the potential to cause accumulation as well as in intake and exhaust ports. When designing a detection system for hydrogen one should consider detector response time, detection range, durability/longevity, maintenance and calibration required. A concentration of 1 Vol% is a commonly used and accepted alarm activation threshold for hydrogen in air, which is equivalent to 25% of the lower flammability limit. In addition to permanent/static hydrogen sensors, most testing facilities employ portable sensors for personal protection and leak investigation (Verhelst & Wallner, 2009).

3.7.4 Flame detectors

A hydrogen-air flame is invisible to the human eye, and any visibility is caused by the presence of impurities, though at reduced pressures a pale blue or purple flame may be present. Hydrogen detection systems varying in sophistication have been used to protect operating personnel from the severe burns that would occur if exposed to hydrogen flame. Verhelst & Wallner classify hydrogen flame detectors into the following groups:

- Thermal fire detectors: detectors classified as rate-of-temperature rise and overheat detectors are a reliable option and have been available for many years. Thermal detectors must be located at or close proximity to a flame (Verhelst & Wallner, 2009).
- Optical sensors: are used to detect hydrogen flame in Ultraviolet (UV) and Infrared (IR) spectral regions. UV systems are extremely sensitive though, are prone to false indications, and can be blind in foggy conditions. IR systems are not overly sensitive to hydrogen fires, being designed for hydrocarbon fires (Verhelst & Wallner, 2009).
- Imaging systems: detect flames primarily in the thermal IR region, and cannot provide continuous monitoring with alarms. User input or advanced programming is required to determine if the image displayed is a hydrogen flame. UV imaging systems are very expensive, requiring special optics. Systems that use lowlight silicon charge coupled device (CCD) video technology with filters focused on the

940-nm and 1100-nm emissions peak are a low cost option, and have been used at various facilities (Verhelst & Wallner, 2009).

- Brooms: such as dry corn straw or sage grass brooms have been used to detect small hydrogen fires as the material easily ignites as it passes through a flame. A dry fire extinguisher or dust thrown into the air also causes a hydrogen flame to emit visible radiation.

3.7.5 Supply system

In both static testing and vehicular scenarios, hydrogen is stored in cryogenic liquid form or as a compressed gas. Typical storage pressure ranges from 138 bar to 414 bar for compressed hydrogen scenarios. Liquid hydrogen is stored at a temperature of -253°C generally in heavily insulated passive storage systems, meaning no further active cooling is provided to the vessel. Despite high levels of insulation, heating causes liquid hydrogen to evaporate, resulting in increased pressure build up and eventually a blowoff of hydrogen. For purging and safe leak check operations, high-pressure helium is generally used, connected in tandem to the hydrogen supply line.

For most scenarios, hydrogen or helium passes through manual shut off valves and valve checks then is supplied to a pressure regulator. Once the hydrogen is regulated to the desired delivery pressure, the hydrogen is fed to the testing apparatus via several manual and solenoid-operated safety valves. A fast-acting, remotely operated, normally closed three-way valve is used in close proximity to the test engine. If the engine does not rotate/start, a hydrogen leak is detected and the fast-acting three-way valve automatically closes. For long-term shutdowns or for when maintenance is required, the hydrogen supply lines are usually purged to the atmosphere and purged with compressed helium (Verhelst & Wallner, 2009).

Accurate metering of the volume of fuel consumed is crucial for performance analysis of any ICE testing and provides the basis for calculation of research development-relevant characteristics such as engine efficiency. Automated or manual monitoring of fuel consumption can also be used to detect leaks, significantly increasing the safety of hydrogen testing (Verhelst & Wallner, 2009).

3.7.6 Vehicular applications

There exists even less control over ignition sources in vehicular applications than in test cell design. Strategies combining hydrogen leak detection and development of diluted

concentration hydrogen with lower ignition limits have been implemented to provide a level of safety for hydrogen vehicles comparable to conventionally fuelled vehicles. During operation, critically placed hydrogen sensors monitor hydrogen concentration throughout the vehicle and actions are taken based on the severity of the leak. Mitigation methods include driver warnings, active forced ventilation, and executive measures such as disabling the starter relay or hydrogen supply(Verhelst & Wallner, 2009). Verhelst & Wallner suggests hydrogen sensors are critical in the engine compartment, hydrogen storage area, and passenger compartment to ensure the highest level of safety and the early detection of any leaks. Due to the complexity of a car's ventilation system, CFD simulations with elaborate hydrogen release detection tests have been performed to determine the most efficient location for hydrogen sensors. In the event of malfunction or accident/collision, both cryogenic and compressed hydrogen storage systems have the potential to allow the build-up of pressure. Extensive safety testing including crash tests and exposure to fire tests have been performed to establish the risks in collision scenarios. Verhelst & Wallner suggest that if properly designed, a hydrogen storage system releases pressure with vents critically positioned in the vehicle. The implementation of hydrogen vehicles will also require adequate training for operators as well as potential rescue personnel (Verhelst & Wallner, 2009).

3.8 Prior Art

The concept of using existing internal combustion technology as a platform for hydrogen combustion is not a new idea. Several concepts have been developed by individuals and corporations in the past, with some vehicle manufacturers implementing the technology in concept vehicles and prototypes, and even hinting at mass production for public use. In this section, several similar engines are investigated.

3.8.1 Review of Yvon & Lorenzoni

The following concerns the work of K. Yvon and J. Lorenzoni from the 2006 publication "*Hydrogen-powered lawn mower: 14 years of operation*" in the International Journal of Hydrogen Energy. This paper was closely looked at in preliminary research, and is credited with providing partial inspiration for the investigation undertaken in this document.

In 1993 Lorenzoni and Yvon presented a hydrogen-powered lawn mower, adapted from a commercial model. The commercial petrol engine was adapted to hydrogen by making

small adjustments to the carburettor and the fitment of a hydrogen reservoir containing a metal hydride powder (Yvon & Lorenzoni, 2006). The initial project aimed to demonstrate the ease with which a well-known and relatively polluting device running on hydrocarbon fuels can be converted to a less polluting device running on hydrogen (Yvon & Lorenzoni, 2006). The device was put into operation in 1991, and by publication of the mower's performance in 2006, the prototype was claimed to have been operated without major interruption since it was commissioned. Lorenzoni and Yvon claim the only maintenance work performed during the evaluation was changing the lubrication oil annually, one replacement spark plug and hydrogen regulating valve, and one reactivation of the hydrogen tank due to accidental air contamination (Yvon & Lorenzoni, 2006).

The lawn mower's power unit was a single cylinder four-stroke ICE with spark ignition and 80cm^3 cylinder capacity. The commercially available unit received modification to the carburettor and petrol reservoir. The carburettor was adapted by replacing the fuel float and principle fuel jet with a hydrogen injection nozzle. The nozzle was connected via needle valve to the metal hydride storage tank mounted above the engine. The power of the engine was regulated by the hydrogen supply value and the carburettor choke. The hydrogen reservoir was a commercially available model containing 1 litre of hydrogen sponge, composed of an alloy powder of titanium, vanadium, chromium and manganese (Yvon & Lorenzoni, 2006). The hydrogen used in combustion was obtained by the desorbing of the metallic powder at ambient temperature. The hydrogen tank was rechargeable at a hydrogen pressure of approximately 30bar within less than an hour. The tank added approximately 12kg to the mowers weight and stored a hydrogen volume of 1 Nm^3. Hydrogen pressures of 3-25bar were achieved, depending on the temperature and filling state of the tank. During hydrogen desorption the reservoir cooled by approximately 15^{o}C, resulting in a progressively decreasing hydrogen pressure (Yvon & Lorenzoni, 2006).

Lorenzoni and Yvon claim the performance of the hydrogen fuel was comparable to the petrol-powered model, with a power loss of approximately 20% at full power (3,000rpm). In practice, the engine was said to be regulated to run at a reduced power level (2,000rpm), with full power required for limited conditions namely wet or lengthy grass. One charge of hydrogen was said to last for 40mins of operation, which correlates to about 800m^2 of cut lawn.

Analysis of exhaust gases found water vapour, small quantities of nitric oxide (0.3 ppm) and nitrogen dioxide (1.6 ppm) (Yvon & Lorenzoni, 2006). Interestingly, Lorenzoni and Yvon also found a significant reduction in operational noise compared with that of the petrol powered model. Backfiring occurred only under certain circumstances, including humid air or in insufficient air inlet to the IC engine. In practice, the carburettor choke remained on the full inlet position (Yvon & Lorenzoni, 2006).

The installation of the hydrogen fuel tank added around 12kg to the mass of the mower, a considerable increase, which in turn made non-tractive mowers more difficult to push. This of course could be attenuated by opting for a self-tractive model, but this comes at the expense of engine power and higher hydrogen consumption (Yvon & Lorenzoni, 2006).

Another inconvenience was the difficulty of recharging the hydrogen tank. At the time of publication, Yvon and Lorenzoni remark that hardly any infrastructure for doing this existed, meaning that recharges would require external service or interim storage of pressurised hydrogen, requiring additional investment (Yvon & Lorenzoni, 2006).

A further inconvenience was costs. The costs for adapting the existing petrol ICEs to hydrogen were relatively minor, but those of installation of a metal hydride reservoir were important. Hydrogen is considerably more expensive than petrol at equal energy content, especially if high purity hydrogen is used. This was not a major issue however, due to the relatively low fuel requirements of this application (Yvon & Lorenzoni, 2006).

Finally, the operation of the hydrogen model saw a clearly reduced duration time (30-40 mins) compared to that of the petrol model (2-3 hours). This drawback was further aggravated by the decrease of hydrogen supply during operation. During prolonged operation, Lorenzoni and Yvon noticed that the hydrogen pressure above the metal hydride storage bed decreased due to cooling of the reservoir (positive hydrogen desorption enthalpy) (Yvon & Lorenzoni, 2006). The implications of this suggested that during long mowing operations work may need to discontinue for about 20 minutes in order to allow the temperature of the storage bed to increase, and thus increase the pressure to rise again to operational level.

For economic evaluation Lorenzoni and Yvon considered both costs and marketing. The following currency conversions were correct at the time of writing, and refer to the price at the time of publication of Lorenzoni and Yvon's work in 2006. Additional costs are

obviously incurred and modifications are required in the conversion of a commercial petrol motor to hydrogen fuel. As lawnmowers tend to run at a constant rpm, the necessary modifications are minor and can be performed by a skilled technician in a matter of hours. For this just a few additional parts are required, namely hydrogen tubes and connections, and a needle valve. At the time of publication Lorenzoni and Yvon suggested that these modifications would amount to an estimated €200 - $285 AUD (Yvon & Lorenzoni, 2006). However, the installation of the metal hydride storage tank required a considerable investment. The model chosen by Lorenzoni and Yvon was no longer in production, with a tank of comparable specifications selling for a price of €900 ($1,287 AUD), and another €100 ($143 AUD) in flexible hydrogen transfer line, doubling the price of the corresponding petrol model (Yvon & Lorenzoni, 2006). Operation costs are dependent on the price of the hydrogen and its distribution. Lorenzoni and Yvon commented that in Switzerland, industrial hydrogen of 99.95% purity in pressurised vessels (50L at 200Bar) was sold for 150SFr/bottle ($208 AUD), which puts 1 charge = $1m^3$ of hydrogen at €5 ($7.15 AUD) (Yvon & Lorenzoni, 2006). Lorenzoni and Yvon suggested that due to their robust prototype requiring minimal maintenance, the average operating costs amounted to €20/season ($28.6 AUD). Lorenzoni and Yvon cited the UK New and Renewables Energy Programme which states that the European lawn mower market in 1997 was worth $1billion, with internal combustion claiming 59% share, electric 35%, battery 3%, and hand operated taking 2%. Lorenzoni and Yvon indicated that in view of their increased weight and reduced autonomy compared to petrol powered models, hydrogen-powered lawn mowers were expected to compete with battery operated models for market share. Lorenzoni and Yvon suggested that while the two products' ecological advantages were similar, hydrogen-powered models had practical advantages. Lorenzoni and Yvon estimated a market share of 5%, representing a total market value of $50 million/year.

3.8.2 Review of Kahraman, Ozcanli, & Ozerdem

The following concerns the work of Kahraman, Ozcanli, & Ozerdem from the 2006 publication "*An experimental study on performance and emission characteristics of a hydrogen fuelled spark ignition engine*" in the International Journal of Hydrogen Energy. This paper was closely investigated due to its similarity to the investigation undertaken within this document.

Kahraman et al.'s investigation aimed to establish the suitability of using an existing petroleum ICE for hydrogen combustion in automotive applications by comparing the

performance and emission characteristics of the engine under petroleum and hydrogen operation experimentally. Variations in torque, power, BTE, BMEP, exhaust temperature, and emissions (NOx, CO, CO2, HC and O2) vs engine speed were compared for both petroleum and hydrogen. Comparison energy analysis was undertaken. In addition engine design modifications necessarily made to accommodate hydrogen induction and operation without changing basic characteristics of the existing engine were discussed (Kahraman et al, 2006). Testing found reduced power at low speed operation, less heat loss, and 10 times lower NOx emissions for hydrogen combustion when compared to that of petroleum.

Kahraman et al. highlighted the benefits of hydrogen as an internal combustion fuel, noting that hydrogen does not cause combustion problems such as vapour lock, cold wall quenching, inadequate vaporization or poor mixing, and does not produce toxic products. Hydrogen has a high heating value on a mass basis, and low on a volume basis. Combined with other thermo-physical properties, Kahraman et al. suggested that hydrogen has unique and desirable heat transfer characteristics for internal combustion (Kahraman et al, 2006).

The testing apparatus consisted of a dynamometer, exhaust emission analyser, fuel metering device, and auxiliary equipment coupled to the test engine. The engine driveshaft was connected to the dynamometer, the ambient pressure and temperature, engine speed, and torque values were read from gauges. Compressed hydrogen (20MPa) was supplied from 50L steel gas tanks, the first stage pressure regulator was installed on the tank, the second stage regulator was installed above the engine's radiator. Two pressure regulators reduced hydrogen pressure first to 300 kPa and then to atmospheric pressure. A Sun MGA 1200 gas analyser was used to measure CO, CO_2, O_2, and HC composition in exhaust gases as well as engine speed, exhaust gas temperature, and air fuel ratio. MRU Vario D52 was used for NOx exhaust emission levels (Kahraman et al, 2006).

The test engine used was a Fiat licensed Tofas 1.2L 4cyl naturally aspirated SI engine, fed by a 2bbl Solex carburettor. The engine produces 60Hp (DIN) at 5,600 rpm and 89Nm at 3,400rpm from an 8.8:1 compression ratio. The engine bore and stroke are 73mm and 71.5mm respectively. *A conversion kit was used for Hydrogen feeding* and the addition of spray nozzles for water was essential to provide backfire free operation. Spray nozzles were installed 40mm from the inlet valves. Ignition timing was statically set at 10^{o}C.

Testing ranged from 2,600-4,000rpm – engine speeds lower than 2,600rpm experience severe backfiring, and 4,000rpm is the rpm ceiling of the engine. In order to avoid temperature and pressure variations, hydrogen testing followed immediately after petroleum testing when the engine was already at operating temperature (Kahraman et al, 2006).

The testing found that at 3,100rpm under hydrogen operation, the petroleum torque specifications were matched, and exceeded at higher speeds; a result expected by Kahraman et al. due to hydrogen's fast burning characteristics. Kahraman et al. suggested that lower speed operation increased mechanical losses, and proposed that this may be overcome via forced induction. The brake power output data showed a power reduction under hydrogen operation, especially at lower engine speeds. (Kahraman et al, 2006) attributed this power loss to the lower volumetric specific energy content of the fuel. The results showed hydrogen providing greater brake thermal efficiency, even at lower engine loads. Kahraman et al. claimed a 31% increase in brake thermal efficiency under hydrogen operation compared to that of petroleum .

3.8.3 Review of Sopena, Dieguez, Sainz, Urroz, Guelbenzu, Gadina

The following concerns the work of Sopena, Dieguez, Sainz, Urroz, Guelbenzu & Gadina from the 2009 publication "*Conversion of a commercial spark ignition engine to run on hydrogen: a performance comparison using hydrogen and gasoline*" in the International Journal of Hydrogen Energy. This paper was investigated due to its relevance to the topic.

Sopena et al performed modifications to a commercially available Volkswagen Polo 1.4L engine to operate on hydrogen fuel. Changes were made primarily to the inlet manifold, gaseous fuel injectors, oil radiator and to the electronic management unit (ECU). Injection and advanced timing maps were produced for lean charge mixtures of equivalence ratios λ =1.6-3.0. The engine control parameters provided safe hydrogen operation free from abnormal combustion symptoms of backfire and pre-ignition. Low NOx emissions were also observed. Under hydrogen operation the engine achieved a maximum brake torque of 63 Nm at 3,800 rpm and maximum brake power output of 32kw at 5,000 rpm. Generally, hydrogen operation achieved a greater BTE than that of petroleum operation, except under lean burn (λ=2.5) conditions and engine speeds exceeding 4,000rpm.

Sopena et al predicted a maximum speed of 140km/h for hydrogen operation (Sopena et al., 2010).

Hydrogen is termed a clean burning alternative fuel as neither carbon-based pollutants nor greenhouse gases would be emitted when hydrogen is produced from renewable sources. With significant interest developing within the automotive industry in hydrogen as a fuel, it is important to ensure hydrogen is produced cost-effectively from renewable energy sources resulting in a positive move to hydrogen. While there is little doubt that global fleet numbers of hydrogen vehicles will increase in the near future, it is doubtful whether hydrogen FCVs or ICEs will be the prevailing solution, with both options having unique advantages and drawbacks. Sopena et al suggested that most vehicle manufacturers are focusing their hydrogen vehicle development on FCVs, however the likes of Mazda and BMW have committed to ICE hydrogen vehicles. The engine used in testing was a naturally aspirated SI engine from a Volkswagen Polo. The 1.4L in line 4 cylinder engine had a compression ratio of 10.5:1, and the fuel was fed via port injection, producing 59kW at 5,000 rpm and 132Nm at 3,800 rpm (Sopena et al., 2010).

Sopena et al suggested that the well-known thermo-physical properties of hydrogen make it a desirable combustion fuel. Low ignition energies, wide flammability limits, high flame speed properties, combined with 'clean' emissions are advantageous or SI engines at low loads when lean burn and WOT conditions are employed. These same characteristics give rise to limitations in the form of abnormal combustion, namely backfiring, pre-ignition and knock, resulting in increased NOx emissions. Supercharging, EGR, and direct injection are methods proposed to mitigate or overcome these phenomena. Sopena et al employed fuel feeding control through PFI and changes to the ECU to retain the original engine platform (Sopena et al., 2010).

The original plastic inlet manifold was replaced with a cast manifold to increase reliability should backfire occur. The petroleum injectors were substituted for hydrogen injectors (quantum technologies), and hydrogen leakage due to vibration was prevented by firmly fixing the injectors to the manifold by means of a supporting rail. A low pressure gas collector was installed to ensure a constant pressure feed was maintained to the injectors. The OEM ECU was replaced by a programmable MoteC M 400 unit. Most of the OEM sensors and actuators were retained with the exception of the O2 sensor replaced with a wideband Bosch LSU 4.9 unit, and a new oil temperature sensor was fitted. The sensors and actuators were connected to the MoteC unit and calibrated. Injection and ignition

timing maps were produced. Other modifications included a water-oil heat exchanger installed on the oil filter to maintain constant oil temperature, increased diameter of crankcase ventilation piping to prevent hydrogen accumulation, and the removal of the three-way catalyst as it was not required due to low NOx combustion products (Sopena et al., 2010).

The gas supply system consisted of two lines, hydrogen and nitrogen. Nitrogen was used to purge the hydrogen line prior to start up. Both lines were fed by two 50L gas cylinders at 200 bar. Two hydrogen sensors were placed on the apparatus to detect hydrogen leakage at rates well below lower ignition level of the hydrogen air mix, connected to a control unit indicating hydrogen concentration in the room. The apparatus was programmed such that if the sensors detected unsafe levels of hydrogen concentration, the supply of hydrogen would automatically be stopped, and the system purged with nitrogen (Sopena et al., 2010).

Sopena et al found that the injection timing had a strong influence on the engine performance at low load and engine speeds, and could be adjusted to avoid backfire. Injection maps were created by employing a strategy of operating between 1.6-3 ranges for values of lambda at all loads while varying torque via throttling. Values of lambda lower than 3 were selected to avoid incomplete combustion, and higher than 1.6 to avoid engine knock at high load and engine speed. The start of the injection remained constant at the point where the exhaust valve closed to ensure no hydrogen leakage to the exhaust manifold, and the valve cooled somewhat with the inlet air reducing the likelihood of pre-ignition. Injection was completed before closing of the inlet valve, and in most cases, before the piston reached TDC (Sopena et al., 2010).

Ignition timing maps were developed allowing maximum brake torque with the lowest NOx emissions. A conservative approach or retarding ignition advance to valves was adopted. In contrast to petroleum ICEs, Sopena et al found the optimum spark advance for maximum brake torque under hydrogen operation depended essentially on lambda, except for low loads and engine speeds (Sopena et al., 2010).

The performance of hydrogen operation was evaluated in terms of BMEP, brake power, brake SFC, and emissions characteristics compared to petroleum operation. The BMEP as a function of engine speed for λ values of 1.6, 2, and 2.5 at WOT was compared for hydrogen and petroleum operation. Maximum BMEP for hydrogen was achieved at the

same engine speed as petroleum operation, though considerably lower for hydrogen due to the low density of the fuel. Maximum brake power was limited by the maximum engine speed of the engine at 5,000 rpm. Under hydrogen operation 32kW was achieved at $\lambda = 1.6$ for WOT conditions, compared to 59kW for petroleum operation at the same speed. A comparison of SFC petroleum equivalent for λ values of 1.6, 2, and 2.5 at WOT against petroleum SFC showed a higher thermal efficiency for hydrogen operation. Sopena et al attributed this to the faster combustion and closer to constant volume process, and thus more efficient thermodynamic cycle than that of gasoline. This was termed a 'remarkable result' by Sopena et al commenting on the higher lambda values for hydrogen operation. Further, it is noted the highest lambda value corresponded to the highest thermal efficiency for the HICE (Sopena et al., 2010).

Under hydrogen operation, CO and HC emissions due to EGR were extremely low. The most important emissions were NOx, which increased with λ as expected. For λ values of higher than 1.8, low NOx emissions of 50-75 ppm were observed, and between 350-550 ppm for $\lambda = 1.6$ depending on engine speed. Although significant, these values were well below the 1,000-2,500 ppm range typically seen for hydrogen operation (Sopena et al., 2010).

3.8.4 Review of Babir

The following concerns the work of F. Babir from the 1996 publication "*Review of hydrogen conversion technologies*" from the Clean Energy Research Institute. This paper was investigated due to its relevance to the topic investigated in this document.

This paper reviewed hydrogen conversion technologies including combustion in ICEs.

HICEs are on average 20% more efficient than comparable petroleum engines. Thermal efficiency is a function of compression ratio and ratio of specific heats Cp and Cv. By increasing the compression ratio or the specific heat ratio, the thermal efficiency can be increased. In HICEs, both ratios are higher than that of petroleum due to hydrogen's lower self-ignition temperature and lean burn capability. However, a power loss is observed due to hydrogen's lower energy content in stoichiometric mixtures. A stoichiometric petroleum-air mixture pre-mixed externally occupies 30% of cylinder volume vs 2% for that of a hydrogen-air mixture. Under these conditions the energy use of the hydrogen mixture is only 85% of the hydrogen mixture, thus resulting in a 15% reduction in power. Fuel injection can be used to improve power output (Barbir, undated).

One of the more important advantages of hydrogen ICEs, Babir suggested, is the lower emission of pollutants than that of a petroleum ICE. Hydrogen has a wide flammability range of 5-75% vol, allowing high excess air to be used to lower NOx emissions. NOx emissions can also be reduced via cooling of the combustion environment, including water injection, EGR, or using liquid hydrogen. NOx emissions from HICEs are typically 1 order of magnitude lower than that of petroleum combustion. Small amounts of CO2 and Co emissions have been detected in hydrogen engines due to lubrication oil (Barbir, undated).

Low ignition energy and fast flame propagation of hydrogen has induced abnormal combustion in HICEs. These problems have been overcome by the addition of hydrogen to the combustion charge at the point where and when the conditions for pre-ignition are reduced, such as separate delivery of hydrogen and air to the combustion chamber. Water injection and EGR techniques are also employed to control pre-ignition. Babir noted that research surrounding hydrogen internal combustion often surrounds modification of existing petroleum ICEs, and suggested that a redesign of the combustion chamber and coolant systems to accommodate hydrogen's unique combustion properties has potential to be the most effective method of solving abnormal combustion problems (Barbir, undated).

Despite the already developed and demonstrated hydrogen conversions available, and their clear advantage over existing technologies, hydrogen is not being used as a fuel on a large scale (except in the space industry). The reasons for this are varied and complex, and include technical, economic and political aspects (Barbir, undated).

Hydrogen fuel must be considered in a frame of the entire energy system, Babir suggested. Hydrogen technology implementation must be accompanied by equally viable technologies for production, storage, transportation, and distribution (Barbir, undated).

3.8.5 Review of Das, Gulati & Gupta

The following concerns the work of Das, Gulati & Gupta from the 2000 publication "*A comparative evaluation of the performance characteristics of a spark ignition engine using hydrogen and compressed natural gas as alternative fuels*" in the International Journal of Hydrogen Energy. This paper was investigated due to its relevance to the topic investigated in this document.

The purpose of the investigation by Das et al was to evaluate the potential of hydrogen combustion in small horsepower spark ignition engines as a clean burning fuel alternative. The performance of hydrogen was compared against CNG, a readily available alternative fuel. The engine was run separately with either hydrogen or CNG by the use of electronically controlled injection system. A performance analysis of combustion characteristics was performed for each fuel.

Das et al proposed that the depletion of fossil fuel reserves and subsequent increases in noxious emissions have prompted a review of the role of the ICE. It was predicted that in view of the ICE's versatility, they will continue to dominate transport propulsion systems for some time to come. Despite conversion losses, the power to weight ratio of an ICE exceeds that of the battery powered of FC vehicles when considering power storage. Das et al suggested that this mandates the integration of environmentally friendly technology with existing internal combustion technology to ensure the safe survival of existing ICE technology.

Various alternative fuels are being investigated globally to reduce the impact of vehicle emissions. Hydrocarbons currently used release about the same amount of CO2 per amount of heat released from their combustion, with higher hydrogen content hydrocarbons displaying little improvement. Hydrogen presents as a practically acceptable, carbon-free combustion fuel. The work of Das et all did not discuss the characteristics of other alternative fuels such as methanol, ethanol, EVs, LPG, biogas or vegetable oils.

Das et al highlighted that the difference between CNG and petroleum ICE operation arises from the chemical and physical properties of the fuel. Petroleum fuels are liquids at room temperature, while CNG remains in a gas state above temperatures of -161°C. CNG has a lower density than gasoline, though its physio-chemical properties make CNG an excellent combustion fuel. CNG has a higher octane number compared to that of gasoline, allowing for a higher compression ratio to be utilised without onset of abnormal combustion. The higher self-ignition temperature of CNG lends itself to lower risk of ignition in the event of leakage when compared to that of petroleum. The combustion of CNG requires an altogether different induction mechanism at normal temperatures and pressures as it is a gas. CNG has been widely used in SI engines in various applications, predominantly conversions are allowed for both petroleum and CNG operation. The paper investigated dual CNG/hydrogen operation.

Hydrogen combustion does not experience vapour lock, cold wall quenching, inadequate vaporisation, poor mixing and other typical problems associated with liquid fuels. Hydrogen is a “clean-burning” fuel producing only water vapour from combustion with air. Hydrogen combustion does not produce toxic combustion products such as hydrocarbons, oxides of sulphur or carbon dioxide. Some oxides of nitrogen are produced, and experimentation by Das et al showed that this value can be drastically reduced by monitoring engine operation. Like CNG, hydrogen also requires modified induction from a typical liquid fuel ICE. Das et al developed a common system for the fuel injection of both forms of gaseous fuel as part of their work.

15 years of research and development related to hydrogen operated engines in IIT, Delhi, have observed that the mode of fuel induction greatly influences performance and emission characteristics for SI HICEs. Das et al noted similar observations during testing of the CNG operation. Abnormal combustion problems including backfire and rapid pressure rise rate are greatly influenced by the fuel formulation technique, particularly in context of system development for hydrogen operation. Various fuel induction methods such as carburation, continued manifold injection, timed manifold injection, and low pressure direct injection were evaluated under both CNG and hydrogen operation. Carburation and continuous manifold injection were observed to result in backfiring for CNG operation under certain conditions. The frequency and severity of backfire was substantially lower under CNG operation, and uncontrollable for hydrogen fuelling. The high thermal energy causing backfiring was found to be either spark plug, exhaust valve or some deposits acting as hot spots within the combustion chamber. Timed manifold injection proved a reliable method of induction, particular for hydrogen operation. Das et al were unable to eliminate abnormal combustion in carburettor inducted hydrogen operation. The hydraulic operated and cam actuated injection proved to be an effective mechanism for induction of hydrogen and CNG while eliminating abnormal combustion.

TMI and cam actuated injection systems described above were developed, the details of their development are not related to this investigation. Experimentation activities were performed on a single cylinder, 4 stroke, SI engine with the injection system installed. A dynamometer was fitted, and safety devices such as flame traps, pressure regulators and non-return valves were incorporated where required. The engine was tested first over 2,000, 2,200, 2,400, and 2,600 rpm ranges under petroleum operation to obtain reference data, being a petroleum ICE. Hydrogen testing was performed under WOT conditions,

with flow regulated through hydrogen gas supply system. Performance tests for hydrogen operation were performed under the following conditions: spark advanced to 25° before TDC; supply pressure = 0.1 MPa; Injection Duration = 290° crank angle; injection timing 20° after TDC. Compression ratio of 8.0:1 remained constant. These conditions provided optimum hydrogen operation with minimal undesirable combustion phenomena, smooth engine operation, and accurate injector response. The same tests were applied to CNG operation, with injector timing set at TDC. The performance characteristics of the engine were determined and relevant performance parameters graphed. Throughout testing there were no symptoms of abnormal combustion for hydrogen operation, though its performance was limited due to speed and load conditions. Maximum engine speed for hydrogen was 300prm, vs 4,000rpm under CNG operation.

The results showed that hydrogen operation achieved a higher BTE than that of CNG over the entire engine speed range. Hydrogen's wide range of flammability allowed for controlling engine power via regulation of fuel rate without throttling air intake. Optimum performance was observed at 2,000rpm for the injection system. Das et al also found BSFC was low for the hydrogen operation.

Das et al concluded from their results that an appropriately designed solenoid-actuated electronically controlled injection system can be used to adapt a petroleum ICE to reliably operate on both CNG and hydrogen. It was also suggested that additional safety features are necessarily required for hydrogen operation due to the low minimum ignition energy and high flame speed of the fuel. Das et al observed a reduction in brake SFC and BTE improved under hydrogen operation compared to that of CNG operation. A BTE of up to 31.19% and 27.59% was achieved for hydrogen and CNG operation respectively.

3.8.6 Review of Verhelst & Wallner

The following concerns the work of Verhelst & Wallner from the 2009 publication "*Hydrogen-fuelled internal combustion engines*" in the International Journal of Hydrogen Energy. This paper was investigated due to its relevance to the topic investigated in this document.

The threat posed by climate change and the striving for energy security have prompted governments to implement strategic plans to decrease primary energy use, remove carbon fuels and facilitate modal shifts. Hydrogen as a future energy carrier has taken a

prominent place in these strategic plans. A number of vehicle manufacturers are now leasing demonstration hydrogen fuelled vehicles with ICEs and FCVs. Developing countries are pushing HICE technology as an affordable medium term solution to decrease local pollution. Verhelst & Wallner's article provides a comprehensive overview of HICEs including hydrogen combustion fundamentals; mixture formation strategies and their associated emissions characteristics; measures to convert existing vehicles; dedicated hydrogen engine features; a state of the art on increasing power output and efficiency while controlling emissions and modelling.

Verhelst & Wallner stated that the current method of delivering the world's energy demand based primarily on fossil fuel, is becoming increasingly unsustainable. Once abundant fossil fuel reserves are now clearly exhaustible. Global warming and local pollution hotspots associated with fossil fuel usage are further significant environmental and societal problems. These are strong drivers for research, development and demonstration of alternative energy sources, carriers, and for transportation sectors, powertrains. The use of hydrogen as an energy carrier has been investigated as part of most governmental strategic plans for sustainable energy systems.

Verhelst & Wallner highlighted that the attractiveness of hydrogen lies in the versatile methods by which it can be produced; the long-term viability of a number of methods; the various methods to produce energy from hydrogen; the virtually zero harmful emissions and potential efficiency from its use. Compared to other alternative energy carriers, hydrogen is advantageous in terms of volumetric and gravimetric energy storage density, however, there exist serious challenges that need to be overcome when hydrogen is used as an energy carrier. Hydrogen's low density implies low energy density compared to currently available fuels, even when compressed to 700 bar or liquefied, both of which incur substantial energy losses. Bulk storage, distribution, and on board vehicle storage are heavily compromised as a result. Further, Verhelst & Wallner suggested that in the case of hydrogen-fuelled vehicles, we must ensure that the well-to-wheel greenhouse emission reduction compared to the production of hydrocarbon fuels is positive. However, the potential advantages and desirable combustion properties of hydrogen are substantial enough to warrant investigation and further research.

There are a wide array of works and opinions published as to what determines the 'best' fuel carrier for internal combustion: heavily optimised ICE hydrocarbon fuels, biofuels, electricity, hydrogen, etc. There are a host of aspects to take into consideration, ranging

from lifecycle energy use, greenhouse emissions, tailpipe emissions, cost, practicality, customer acceptance/market uptake, etc., which are not so easily scored and ranked to establish a clear winner, Verhelst & Wallner suggested.

The following information discusses the efforts undertaken to model and analyse regular combustion of hydrogen in ICEs, i.e. where spark initiated combustion develops a turbulent flame and propagates throughout the combustion chamber, consuming the available fuel-air mixture.

Mixture formation and load control strategies

Hydrogen engines can be operated at extremely lean air-fuel ratios compared to conventional fuels due to the wide ignition limits of hydrogen. Quantitative, qualitative and combined strategies for part-load operation of hydrogen engines have been proposed in literature. Quantitative control refers to strategies that limit the volume of fresh charge available for combustion to limit power output while maintaining a constant air fuel ratio. Qualitative control refers to strategies that adjust the air-fuel ratio by adjusting the amount of fuel introduced to the engine while allowing maximum air flow (Verhelst & Wallner, 2009).

The classification based on part-load operation is closely associated with the air-fuel ratio employed. Work has been published on hydrogen engines operated at stoichiometric as well as lean air-fuel ratios. Stoichiometric operation provides significant power output compared to lean burn operation, with NOx reduction via conventional after treatment systems. Lean burn strategies however result in significant increases in achievable engine efficiencies. Recent literature suggests the adoption of both lean burn and stoichiometric operation (Verhelst & Wallner, 2009).

Verhelst & Wallner inform that supercharged operation has been put forward in works as a promising solution for mitigating reduced power output related to hydrogen operation with external mixture formation. For optimum efficiency, turbocharging is the preferred option; though reduced throttle response and a reduction in exhaust energy compared to conventional fuelled ICEs may pose a challenge for the implementation of a turbocharged hydrogen ICE (Verhelst & Wallner, 2009).

Proper mixture formation process design is critical for achieving high engine efficiency, Verhelst & Wallner suggested, whilst meeting increasingly stringent emission reduction targets. Not unlike conventional fuelled ICEs, hydrogen engines have undergone similar

continuous improvement and refinements of mixture formation strategies. Mixture formation strategies are classified based on the location of mixture formation or the location of hydrogen admission. External mixture formation refers to concepts which hydrogen and air are mixed outside of the combustion chamber, and internal mixing refers to concepts where combustion reactants are introduced directly into the combustion chamber. Combinations of external and internal mixing strategies have been put forward by some researchers. The mixture formation strategy has a significant impact on the theoretical power output of the engine. This power discrepancy between strategies is caused by the low density of hydrogen, resulting in a significant decrease in the density of the mixture with external mixing applications (Verhelst & Wallner, 2009).

Verhelst & Wallner implied that it is possible to differentiate systems that utilise carburation, mechanically controlled injection or electronically controlled injection using a timing control/quantity of fuel based classification. Modern hydrogen ICEs almost exclusively utilize EFI systems, though the requirements and specifications vary greatly depending on location or injection and the temperature of injected hydrogen. Generally, lower pressures (2-8 bar) are used for external mixing injection systems, compared to that of direct injection (5-250 bar). Exposure of injector to in cylinder temperatures is an area requiring further development to reach industry reliability standards (Verhelst & Wallner, 2009).

The two most prevalent mixture formation strategies for HICEs are PFI and DI modes. PFI is currently being used in engine research as well as in manufacturer demonstrator vehicles, while DI mode HICEs are still in a research and prototyping stage. The following section summarised from Verhelst & Wallner describes the most typical characteristics and variations between and within these specific mixture formation concepts. However, it is appropriate to reflect on the energy cost of supplying low and high pressure hydrogen for PFI and DI applications respectively(Verhelst & Wallner, 2009).

Hydrogen induction for use in either PFI or DI applications requires a certain delivery pressure. The most efficient method of delivering the hydrogen at the required pressure is dependent on the type of on-board storage and the pressure required for injection. Low pressure hydrogen injection is achievable with compressed hydrogen storage at 700 bar, and even high pressure injection at pressures exceeding 100 bar. However, without an auxiliary compressor, the full amount of stored hydrogen is not available for use. If an

on-board storage system comprising of compressed hydrogen at 700 bar feeds a 100 bar injector, only 6/7 of the mass of stored hydrogen can be utilised before the pressure inside the storage vessel drops below the delivery pressure. The energy required to compress hydrogen, on or off board, is significant. Even under ideal conditions, the energy required to compress hydrogen from 1 bar to 1000 bar requires greater than 7% of the heating value of the hydrogen. If stored on-board in cryogenic form, liquid hydrogen compression can be achieved more efficiently in the liquid state. This reduces the work required for compression by a factor of 5-6 compared to compression from a gaseous state. However, Verhelst & Wallner implied that there remain several questions in the construction and material selection of cryogenic pumps. Further, the method currently employed for the large scale liquefaction of hydrogen requires approximately 30% of the energy content of hydrogen (Verhelst & Wallner, 2009).

Port Fuel Injection

Hydrogen PFI is currently the prevailing hydrogen mixture formation strategy, and is already being implemented in a variety of applications that differ in several aspects including part-load control, air-fuel ratio and charging strategy. Prior to comparison of these strategies, Verhelst & Wallner suggested an understanding of the principle correlation between the air-fuel ratio and formation of NOx emissions as a function of the equivalence ratio that is applicable for homogenous mixture formation concepts is required (Verhelst & Wallner, 2009).

Figure 3.10 from Verhelst & Wallner depicts a typical trace of NOx emissions as a function of equivalence ratio for homogenous PFI operation.

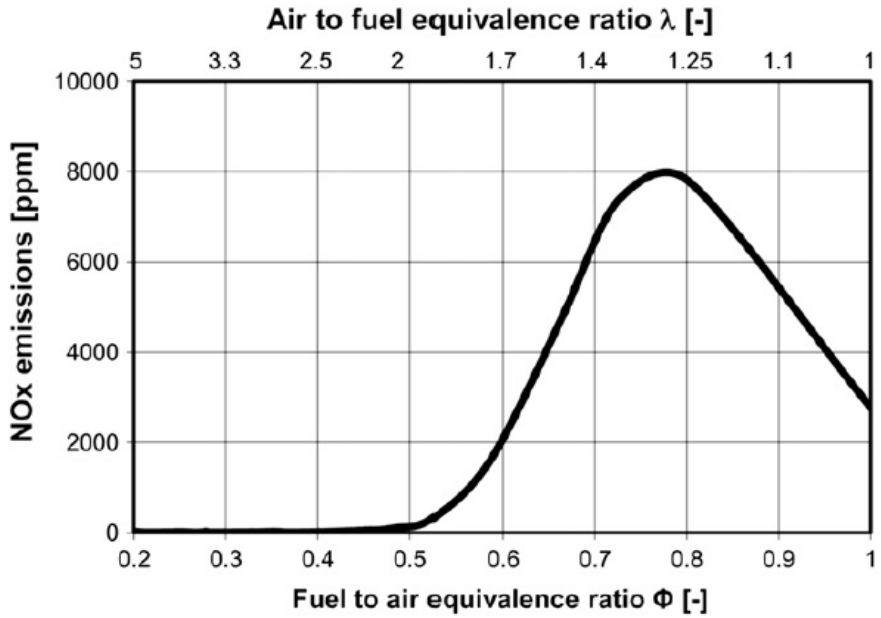

Figure 3.10: Correlation of air-fuel ratio and NOx emissions for homogenous PFI operation, Verhelst & Wallner

The combustion of lean hydrogen-air mixtures with equivalence ratios less than 0.5 ($\lambda > 2$) results in extremely low amounts of NOx emissions. The combustion temperatures do not exceed the NOx critical value of ~1800K due to the excess available air in the combustion chamber. Exceeding the NOx critical equivalence ratio is marked by an exponential increase in NOx emissions, peaking at the approximate fuel-air equivalence ratio of 0.75 ($\lambda \sim 1.3$). For stoichiometric combustion, the NOx emissions are approximately 1/3 of the peak value. The highest temperatures of combustion are observed at a fuel-air equivalence ratio approaching 1.1, although at this ratio, the oxygen concentration is low and as a result this is not the point at which NOx emissions peak (Verhelst & Wallner, 2009).

Due to NOx emissions being a function of the fuel air ratio, numerous operating strategies have been developed to achieve adequate power densities whilst avoiding excessive NOx emissions. Conventional petroleum ICEs converted to hydrogen operation have been operated by employing a lean constant air-fuel ratio strategy. Using conventional throttle and replacing the petroleum fuel system with hydrogen injectors, Verhelst & Wallner suggested that one can easily implement this strategy. Selection of an equivalence ratio below the critical limit of NOx emissions results in extremely low emission characteristics without the use of after treatment systems. Abnormal combustion is also avoided using this strategy as the low temperatures of combustion results in a reduced thermal load of the engine and an increased demand in ignition energy for lean hydrogen air mixtures. Abnormal combustion is also avoided for lean operating strategy due to relatively low temperature of combustion, the reduced thermal load of the engine, and an increased demand in ignition energy for lean hydrogen-air mixtures. However, employing a lean burn strategy results in a further significant loss in power density than for stoichiometric operation. A constant fuel-air equivalence ratio of 0.5 results in a theoretical maximum power output of the hydrogen engine that is only 50% of a

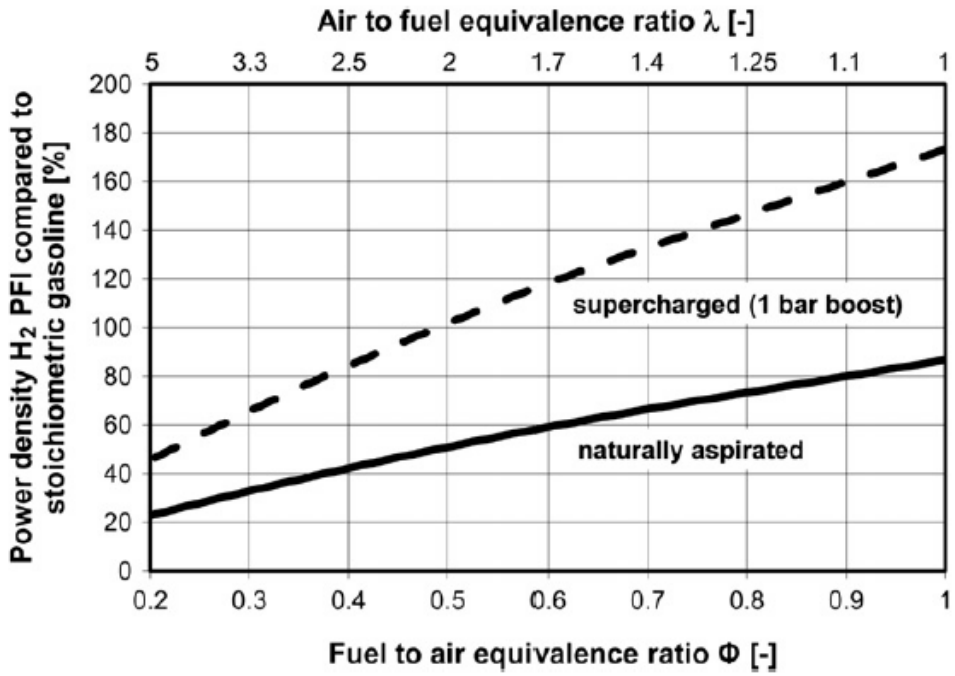

Figure 3.11: Theoretical power density of a PFI HICE compared to stoichiometric petroleum operation as a function of equivalence ratio and charging strategy, Verhelst & Wallner (Verhelst & Wallner, 2009)

conventional petroleum engine in stoichiometric operation. Investigations into the

implementation of supercharging technology to offset power loss from lean air-fuel ratio operation has been performed by several researchers (Verhelst & Wallner, 2009).

As mentioned earlier, employing a lean burn strategy can greatly increase engine efficiency compared to that of petroleum. Acceptable power output is achieved through setting the air-fuel ratio as high as practicable while meeting emissions targets. Reducing the equivalence ratio further improves engine efficiencies, peaking at approximately 0.3. The peak is a local minimum of losses due to longer burn duration, and heat transfer and more favourable properties of the working fluid. A sharp decrease in efficiency was observed at equivalence ratios lower than 0.22, attributed to unburned hydrogen and slower burn rate (Verhelst & Wallner, 2009).

Subsequently an operating strategy was evaluated for both naturally aspirated and supercharged engine vehicles using a variable equivalence ratio as a function of engine load. Implemented over a range of $0.2 < \Phi < 0.5$ on a GM Chevrolet 454 'big block' SI PFI engine, resulted in a 20% increase in engine power compared to a carburetted version, without increasing likelihood of backfire (Verhelst & Wallner, 2009).

The study also concluded that as a result of the wide range of applied mixture composition, the ignition timing range is also wide. Injection timing was observed to have significant influence in the low load and speed region, and found to not be critical in the high load and speed region (Verhelst & Wallner, 2009).

Supercharging combined with a variable equivalence ratio strategy can provide another significant increase in power density. Verhelst & Wallner informed that drive-cycle simulation based on steady-state engine efficiency and emission maps of a 2.3L supercharged hydrogen engine indicated a 3% increase in fuel economy from employing a variable equivalence ratio strategy compared to a constant value of $\Phi = 0.5$ (Verhelst & Wallner, 2009).

3.8.7 Review of Duan, Liu and Sun

The following concerns the work of Duan, Liu and Sun from the 2013 publication "*Backfire control and power enhancement of a hydrogen internal combustion engine*" in the International Journal of Hydrogen Energy. This paper was investigated due to its relevance to the topic investigated in this document.

The frequent occurrence of backfire in PFI hydrogen ICEs for equivalence fuel-air ratios exceeding 0.56 limits further power enhancement of engine power. Inlet PFI testing and

computational fluid dynamics models were established to explore factors that cause backfire under high loads. The fuel-air mixture concentration and temperature are some essential factors governing the occurrence of backfire. Timing optimisation and induction pressure of the hydrogen reduces concentration distribution of the intake mixture and the temperature of the high-concentration mixture through the inlet valve, controlling backfire. The control of backfire allows for the operation of hydrogen engines at high equivalence-fuel air ratios (greater than 1.0). Significant enhancement of power output can be obtained through optimised hydrogen injection timing and pressures (Duan et al., 2013).

As petroleum resources become more depleted, researchers are beginning to focus more on alternative fuels for vehicles. Hydrogen, a clean burning, highly combustible and abundant fuel is an ideal alternative fuel for transportation. Fuel cells and internal combustion engine hydrogen vehicles are two primary areas of investigation for hydrogen vehicle applications. Several key technologies stand in the way of taking full advantage of the potentially high efficiencies of hydrogen fuel cell vehicles, thus they remain costly and cannot be used extensively in the short term. Existing internal combustion engines can be converted to hydrogen operation at relatively low cost, making them the most foreseeable application for the near future (Duan et al., 2013)

Hydrogen has a lower ignition energy and wider ignition range than that of petroleum, meaning the backfire and other abnormal combustion processes occur more easily in HICEs, especially under high loading conditions. Literature demonstrates that maintaining normal operation, or further enhancing power output of HICEs is limited by intense backfire for mixture equivalence ratios exceeding 0.56. The research areas of backfire control and power enhancement are important to the advancement of HICE technology (Duan et al., 2013).

Backflow of high-temperature combustion gases from the exhaust are predicted to be the lead cause of backfire in HICEs, resulting in spontaneous combustion in the inlet manifold. Thus, any reduction of the temperature of a high concentration mixture inside the inlet is an effective backfire mitigation strategy. Researchers have investigated the effect of water addition to the inlet mixture to reduce temperature, and thus backfire, though this strategy has resulted in the destruction of the lubrication film of the cylinder wall, increasing wear and reducing efficiency (Duan et al., 2013).

Backflow of high temperature gases can be reduced by increasing inlet pressure, enabling backfire control. This also increases volumetric efficiency and power output. Decreasing overlapping inlet and exhaust valve angles further reduces backflow quantity of high-temperature exhausting combustion gases, facilitating high fuel-air equivalence ratios. Both measures necessitate the use of a pressurised induction system or variable valve timing system, and are both costly (Duan et al., 2013).

For non-supercharged ICEs, the optimisation of hydrogen injection timing to allow the hydrogen-air mixture to enter the cylinder initially to cool down the residual exhaust gas is a proven effective method for control of backfire phenomena. In Duan, Liu and Sun's investigation, 3D simulation of PFI of hydrogen and a hydrogen engine test system were established to investigate the influences of injection timing and pressure on backfire. Duan, Liu and Sun discovered an optimised strategy for hydrogen injection timing and pressure. It is claimed that the strategy facilitates hydrogen operation free from backfire and with increased power output, even when fuel-air equivalence ratios exceed stoichiometric levels (Duan et al., 2013).

Duan, Liu and Sun converted a 2.0L naturally aspirated four-cylinder (86mm x 86mm x 4) petroleum engine to a PFI hydrogen ICE. The engine has a compression ratio of 10:1, with inlet valve opening and closing angles of 348 º, 608 º CA and exhaust valve opening and closing angles of 136º, 368º CA. The injection and control systems were also redesigned. The opening and closing times of the intake and exhaust valves were fixed .(Duan et al., 2013)

The original packet ignition system had one igniter for every two cylinders and two ignitions in each working cycle and in each cylinder; one in the power stroke and one in the intake stroke during which backfire can occur. The ignition system was replaced with an independent ignition system whereby one igniter was supplied for each cylinder, and one ignition in the power stroke is supplied, eliminating the effect of ignition system on backfire. The sparkplug was replaced with a cold-rated one, avoiding backfire caused by high temperature of the electrode. The intake valve opens at an angle of 348º CA, and the exhaust valve closing angle 368º CA, an overlap of 20º CA (Duan et al., 2013).

The hydrogen was stored in steel bottles at 20MPa and supplied to the injection rail at 0.2-0.6MPa. An electronically controlled hydrogen injection valve was installed on the

injection rail, and hydrogen injected into the port when the valve was open. Due to the large volume of hydrogen in the injection rail, variations in injection pressure were kept smooth during operation. By adjusting the second stage pressure reducing valve, the amount of hydrogen supplied was manually modified (Duan et al., 2013).

A Dw160 electric eddy current dynamometer absorbed the output torque and power of the test engine to maintain stable operation of the engine. The system collected data on power, torque, speed, and temperature, and other data sets. Cooling water and lubricant thermostat systems ensured cooling and lubrication respectively during the operation of the engine, ensuring accuracy of the test (Duan et al., 2013).

During the experiment, Duan, Liu and Sun's self-developed electronic control unit allowed for adjustment of hydrogen injection timing, ignition timing and other control

Table 2 – Accuracies of test instruments.

Test instrument	Type	Accuracy
Electric eddy current dynamometer	DW160	1%
Internal combustion engine test and control system	FC2000	–
Hydrogen mass flowmeter	Coriolis mass flowmeter	0.5%
Air mass flowmeter	Hotline mass flowmeter	0.5%
Crankshaft sensor	Kistler2613B	0.1° CA
Cylinder pressure sensor	Kistler6117B	0.001 MPa

Figure 3.12: test instrumentation type and accuracy from Duan, Liu and Sun's experimental apparatus

parameters. An electronic throttle control was used to adjust airflow, maintaining a fuel-air equivalence ratio of 0.2 at low load conditions through adjusting throttle from 0-100%. A fuel-air equivalence ratio between 0.2 and 1.0 was maintained under high load conditions through increased hydrogen injection time by operating at WOT. Instantaneous pressure data for backfire detection was installed in the inlet port. A temperature sender installed at the exhaust pipe and a crankshaft sensor installed on the end of the crankshaft provided temperature and engine speed data respectively. A Coriolis mass flowmeter and hotline mass flowmeter measured hydrogen and air mass flows respectively, allowing the fuel-air ratio to be calculated, and thus the efficiency of the engine (Duan et al., 2013). A table of the test instruments used by Duan, Liu and Sun and their accuracy is provided in Figure 3.13.

Duan, Liu and Sun suggested that difficulty in using existing test equipment to measure temperature, concentration distribution, and variation inside the inlet port and the cylinder led to the development of a 3D CFD simulation model. In Duan, Liu and Sun's study a 3D mesh model including inlet pipe, manifold, inlet port, hydraulic injection valve, and cylinder was developed to investigate the temperature, concentration distribution in the inlet port and cylinder. Duan, Liu and Sun assumed that analysis of a single cylinder is sufficient representation of the four, and that any variations between cylinders can largely be ignored as a full analysis would greatly increase simulation time and would not significantly increase the quality of results. Symmetries of the cylinders and inlets were also assumed to simplify modelling. Therefore, the model has only half of the inlet pipe, port and cylinder. The total mesh is greater than 170,000, and is depicted in Figure 3.14.

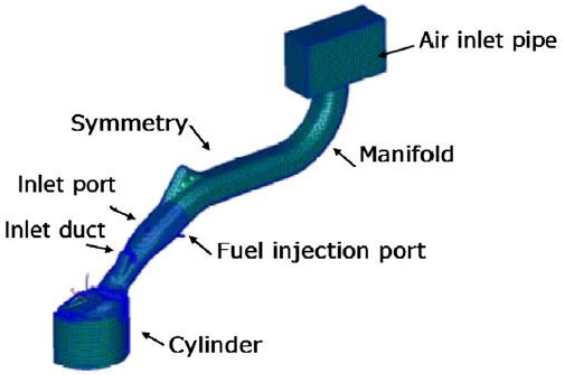

Fig. 2 – 3D mesh model of HICE.

Figure 3.13: 3D CFD simulation model (Duan et al., 2013)

Duan, Liu and Sun used AVL-Fire V8.31 simulation software in their study. Extended Coherent Flame Model (ECFM) combustion model and K-ε turbulence model were adopted to calculate mixture and combustion process. The ECFM model simulates the combustion process based on laminar flame speed and turbulent intensity. When mixture and combustion progress of HICE are simulated, mass and heat transportation, spray, and combustion models are active. Duan, Liu and Sun set boundary and initial conditions prior to simulation, with the air inlet boundary set as the total pressure, the hydrogen inlet boundary set as mass flow. Other boundaries are set as fixed wall or symmetry wall (where heat transfer is considered). Based on experience, Duan, Liu and Sun set the initial temperature of the fixed or symmetry wall from 300 to 600K. The initial pressure of the inlet pipe and cylinder were set to 98.1 kPa and 100 kPa, the initial temperature as 293K and 600K and initial turbulence as 1 and 10 m^2/s^2. Duan, Liu and Sun first calibrated and verified the mesh size and the calculation step length, to reduce calculation deviation.

Decreasing the mesh size and calculation step length saw the fluctuation range of the calculated values become narrower. Once observed fluctuations were below 2%, the mesh size and calculation step length were deemed to have satisfied computing requirements.

Duan, Liu and Sun's simulation results were compared to the intake air mass tests to validate the simulation model. Figure 3.15 demonstrates that the results of the tests and simulations follow each other closely, with less than 5% error, validating the simulation.

Table 3 – Simulation and test results of the air mass intake.

Engine speed (r/min)	Equivalent fuel air ratio	Value of simulation (kg/h)	Value of experiment (kg/h)	Error (%)
1000	1.02	48.58	51.02	4.78
2000	0.83	90.59	93.14	2.74
3000	0.76	140.45	142.92	1.73
4000	0.69	209.35	206.54	1.36
5000	0.65	267.76	271.2	1.27

Figure 3.14: Simulation results (Duan et al., 2013)

4 REQUIREMENTS ANALYSIS

4.1 Customer Requirements Analysis

The customer requirements analysis examines what a hydrogen vehicle would need to accomplish to satisfy what potential customers would require from their hydrogen conversion vehicle. Literature surrounding the expectations of classic vehicle owners for renewable energy conversions is largely absent, thus the customer requirements for a hydrogen fuelled classic vehicle described below relies on **anecdotal evidence** from vehicle enthusiasts. The customer requirements are specified below.

4.1.1 Fuel security for classic/historic vehicles in a post-hydrocarbon economy.

Although it is likely that hydrocarbon fuels will remain available for classic motoring well into the future, the rising cost of motoring may develop appeal for conversion to alternative fuels for classic motoring enthusiasts.

4.1.2 Maximise driving range and adequate cruising power

Inherent to the conversion to alternative fuels is compromise. Conversions of petrol vehicles to dual fuel petrol-LPG systems often lowers power output and smoothness of engine operation in accommodating the combustion of two fuel types. This conversion is still very popular among enthusiasts due to the financial incentive of operating on a cheaper fuel, and increasing the total driving range of the vehicle (SprintGas, 2015). A review of literature suggests that a dual petrol-hydrogen fuel conversion vehicle would have considerably reduced driving range and power under hydrogen operation, while achieving a significant reduction in the emission of harmful pollutants (and possibly in time, cost of operation). To satisfy the needs of a potential hydrogen conversion classic vehicle, adequate cruising power would need to be achieved while maximising driving range.

4.1.3 Maintain originality and preserve aesthetics of the vehicle where possible.

Much of the appeal in classic vehicles is the aesthetics and originality of the vehicles. The desire of the owner to maintain the OEM specification of his/her vehicle can vary greatly, though it is generally accepted that a conversion to any alternative fuel should have a minimal impact on the visual aesthetics of the vehicle. Ideally, the identification of a hydrogen fuelled classic vehicle would not be identifiable from an OEM specification vehicle by visual inspection of the vehicle exterior.

4.1.4 Simplicity and owner-maintainable

Many classic car enthusiasts perform maintenance works on their vehicle rather than employing the use of an automotive tradesperson. Motivations for this can include financial costs, but the owner often enjoys performing these tasks and the simplicity of the vehicles allows the owner to perform these works with confidence. If the installation of a hydrogen fuel system removes the ability to perform maintenance due to safety risks or added complexity, the conversion to hydrogen fuel will lose appeal for many enthusiasts.

4.1.5 Minimize cost where possible

The benefits of alternative fuel vehicles are still out of reach of many due to cost (EERE, 2010). The cost of converting a classic vehicle to hydrogen operation should be minimised where possible to ensure the technology is affordable.

4.1.6 Dual-fuel system

The reduced driving range and power output of a hydrogen conversion vehicle and current infrastructure limitations necessitate a dual-fuel system to ensure adequate driving range and allow for normal petrol operation when greater power output is required (Barbir, undated; Verhelst & Wallner, 2009).

4.1.7 Reliability of system

Adding to the self-maintainability criteria, should the hydrogen system break down it is unlikely that the owner of the vehicle would be qualified or be able to safely perform repair works. Taking this into consideration, the reliability of the system is of great importance, and should not affect the reliability of petroleum operation in a dual-fuel application as can often be the case for LPG-Petroleum conversions (SprintGas, 2015).

4.1.8 Design Specifications

From this, system specifications can be established. They are as follows

- The design must provide adequate power for cruising and mild acceleration
- The design shall provide a driving range of at least 100km.
- The design must not visually impede the outward aesthetics of the car
- The design shall be designed with owner-maintenance in mind.
- The system must be duel fuel.
- The system must be designed with reliability in mind.

5 ENGINE ANALYSIS

An engine analysis was performed to establish performance and fuel consumption characteristics of the Holden Holden 5.0L conversion engine concept. Specifically, the engine analysis:

- Determines the theoretical power and energy requirements of the Holden 5.0L conversion engine concept through urban and extra-urban driving cycle analysis;
- Establishes fuel efficiency of the Holden 5.0L hydrogen conversion engine using a Matlab Engine Simulation Model (ESM);
- Compares ESM and drive cycle energy requirements for the drive cycles;
- Establishes driving range for the Holden 5.0L hydrogen conversion concept; and
- Briefly examines NOx emissions characteristics for the chosen operating conditions.

For the purpose of analysis, where information is required for vehicle specifications are required (ie kerb weight, cross-section, etc), the specifications for a Holden HX GTS sedan have been selected. The vehicle was commonly fitted with the first generation Holden 5.0L engine.

5.1 Drive Cycle Analysis

5.1.1 Introduction

A driving cycle is a data series representing the speed of a vehicle versus time. Driving cycles allow countries and organisations to assess the performance, emission and fuel consumption characteristics of vehicles through standardised testing. Fuel consumption and emission tests are performed on chassis dynamometers. Driving cycles are also used in vehicle propulsion simulations to predict the performance of ICEs (Brundell-Freij & Ericsson, 2005). A drive cycle analysis was performed to establish approximate performance requirements of the Holden 5.0L hydrogen conversion concept engine. The Highway Fuel Economy Test (HWFET) Driving Schedule and Urban Dynamometer Driving Schedule (UDDS) were the drive cycles selected for analysis. The full Matlab calculations and results for the following section can be found in Appendix D1 and Appendix E, respectively.

The HWFET is a dynamometer test representing highway driving conditions for light duty vehicles, developed by the United States Environmental Protection Agency (EPA). The HWFET was selected as the EPA cycle most applicable to Australian highway driving conditions. The HWFET has a duration of 765 seconds with an average speed of 77.6 km/h, covering a distance of 16.5 km with no stops (EPA, 2015). Figure 5.1 depicts the velocity and changes in acceleration over the duration of the HWFET cycle.

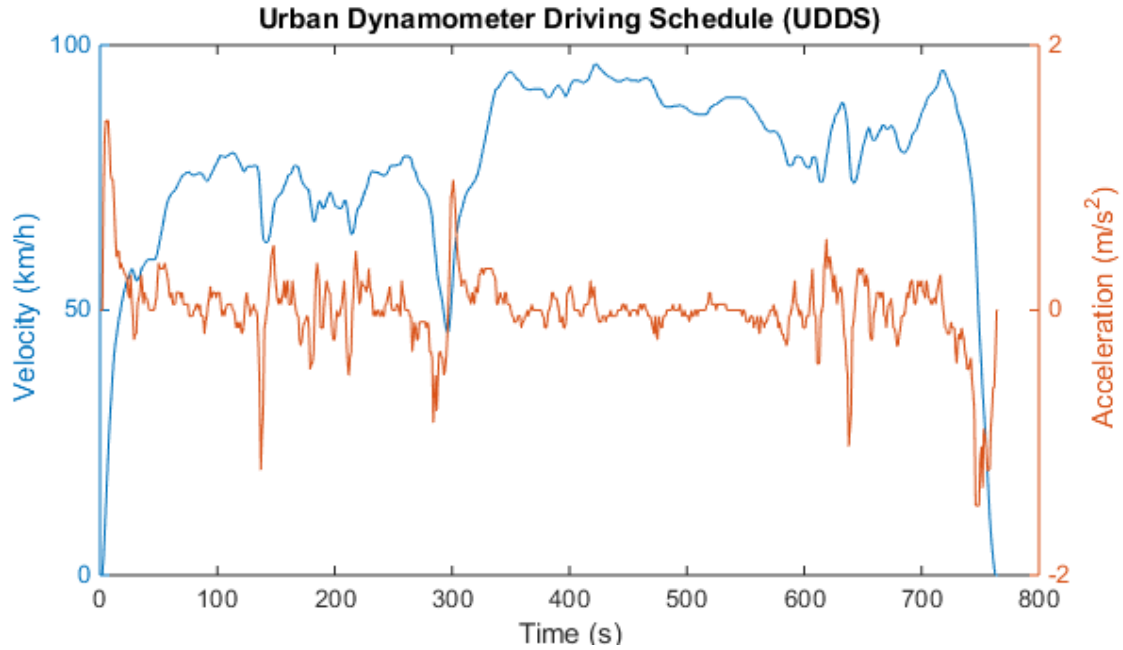

Figure 5.1: EPA Highway Fuel Economy Test Driving Schedule (EPA, 2015).

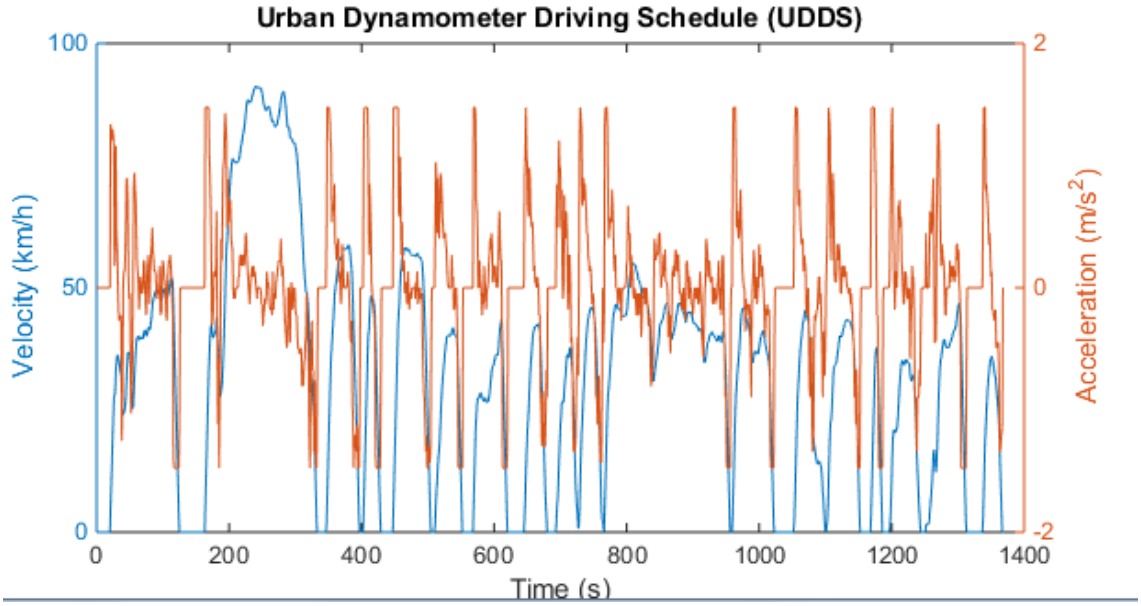

Figure 5.2: Caption: EPA Urban Dynamometer Driving Schedule (EPA, 2015).

The UDDS is a dynamometer test on fuel economy representing city driving conditions for light duty vehicles, mandated by the EPA.

Known in Australia as the ADR 27 cycle, the drive cycle was selected for analysis as it is applicable to Australian road vehicles (dieselnet, 2015). The UDDS has a duration of 1,369 seconds with an average speed of 31.5 km/h, covering a distance of 11.99 km with frequent stops (EPA, 2015). Figure 5.2 depicts the velocity and changes in acceleration over the duration of the UDDS cycle.

5.1.2 Method

Each drive cycle's velocity points were first copied into two-column matrices in separate text files in Matlab, then saved to the working directory. The HWFET.txt and UDDS.txt files were then used individually in the drive_cycle_analysis.m script file using a 'dlmread' function. Using text files saved considerable space in the drive_cycle_analysis.m script file, and allowed quick changing between the drive cycles through the use of an 'If-then' statement. The columns of the matrix were assigned as time and velocity respectively. A 'difference' function was used to obtain the acceleration between each velocity point. Figures 5.1 and 5.2 depict the vehicle speed and changes in acceleration over the duration of the HWFET and UDDS drive cycles, respectively. From this data, it was possible to determine the theoretical power requirement for the vehicle over each driving cycle.

Power (P) is a function of work rate, thus the power requirements can be obtained by dividing the work (W) performed at any point by the time (t). This relationship is shown in Equation 5.1:

$$P = \frac{W}{t} = \frac{F * d}{t} \qquad \text{Equation 5.1}$$

The power required is made up of the rate of work done to overcome rolling resistance and air resistance at speed, as well as the work done to accelerate the vehicle.

The work done due to rolling resistance is a function of the coefficient of rolling resistance (μ_{RR}), the mass of the vehicle (m), gravitational acceleration (g), and the distance the force is applied over (d). This relationship is shown in Equation 5.2.

$$W_{RR} = \mu_{RR} * m * g * d \qquad \text{Equation 5.2}$$

Work performed against air resistance is a function of the density of air (ρ), the front surface area of the vehicle (A_{car}), the vehicle drag coefficient (C_D), and the distance the force is applied over (d). This relationship is shown in Equation 5.3.

$$W_{AR} = \frac{1}{2} * \rho * A_{car} * C_D * d * v^2$$ Equation 5.3

The work performed to accelerate a mass is a function of the object mass (m), the rate of acceleration (a), and the distance (d) the force is applied over. This relationship is shown in Equation 5.4.

$$W_{acceleration} = m * a * d$$ Equation 5.4

The volume of fuel required from to perform this work can determine by dividing the value of total work by the total vehicle efficiency (η), the density of fuel (ρ_{fuel}), and the energy content per litre of fuel. This relationship is shown in Equation 5.5.

$$Fuel\ required = \frac{Work}{\eta * \rho_{fuel} * Energy\ Density}$$ Equation 5.5

Assumptions for the vehicle, fuel, and air properties were made for to perform calculations and are shown in Figure 5.3.

```
% vehicle properties
Urr=0.03;        % coefficient of rolling friction
M=1745;          % vehicle mass (kg)
eta_d=0.85;      % driveline efficiency
eta_v=0.27;      % total vehicle efficiency
Cd=0.46;         % drag coefficient
A=2.1839;        % vehicle cross-section (m^2)

% air and gravitational acceleration assumptions
rho_air=1.27;           % density of air (kg/m^3)
g=9.81;                 % gravitational acceleration (m/s^2)
E_rho_petrol=144e6;     % energy density petrol (J/kg)
E_rho_H2=71e6;         % energy density hydrogen gas @ 350 Bar (J/kg)
```

Figure 5.3: Vehicle, fuel, and air properties assumptions

The Coefficient of Rolling Resistance is dependent on tyre type, the road surface being driven on, as well as other factors including tyre pressure. A coefficient of rolling resistance of 0.03 was selected, representing tyres on asphalt (Engineering Toolbox, 2015).

The energy density of petrol and hydrogen are taken to be 144 MJ/kg and 71 MJ/kg respectively (COD, 2001). The value of hydrogen energy density at 700Bar (142 MJ/kg) was halved, following ideal gas law.

The density of air is taken to be that of air at standard temperature and pressure, 1.27 kg/m^3 (UBC, 2015).

The Holden HX GTS sedan case study vehicle has a factory kerb weight of 1,475 kg (Uniqe Cars & Parts, 2015). The weight of a single driver (70kg), and the estimated weight of the hydrogen system (200 kg) bring the simulation vehicle mass to 1,745 kg.

The total width and height of the vehicle at kerb weight is specified as 1.887m and 1.364m respectively (Uniqe Cars & Parts, 2015). An estimate for the vehicles frontal cross sectional area was made by subtracting the approximate area underneath the vehicle (1.3 m x 0.3 m, measured on vehicle), depicted in Figure 5.4. Leaving a cross sectional area of 2.1839 m^2.

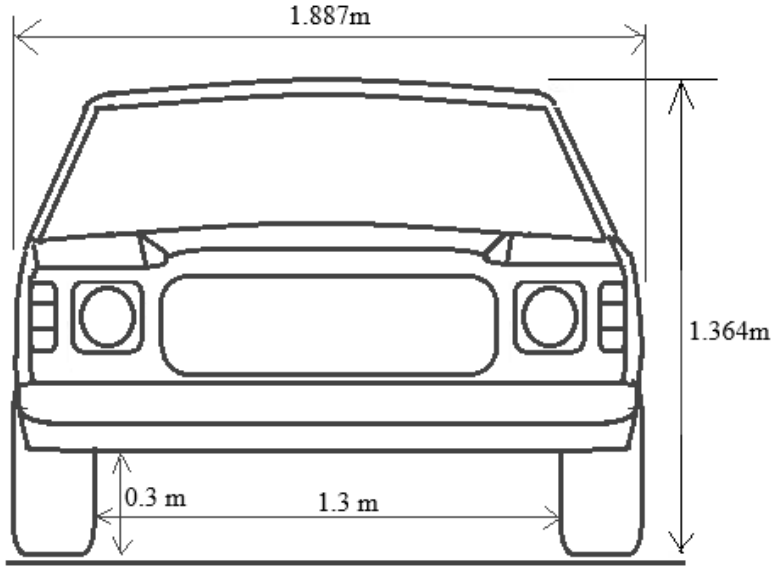

Figure 5.4: HX Holden Monaro GTS sedan exterior dimensions

A drag coefficient of a 1979 Ford mustang (Cd=0.46) was selected due to similarities in shape and style of the two vehicles (Gutenberg, 2015). More accurate drag coefficients for early model Holden vehicles were not available in literature.

5.1.3 Results

The substitution of the vehicle properties and drive cycle data into Equations 5.1 to 5.5 has been performed in Matlab script file title 'drive_cycle_analysis.m' and can be found in Appendix D1. When run for each drive cycle, the script file returns the average wheel power requirement, maximum wheel power requirement, average vehicle speed, total distance travelled, average petrol fuel consumption, average hydrogen fuel consumption, and a gasoline gallon equivalent for hydrogen fuel consumption. Figures 5.5 and 5.6 depict the results of the script file execution that are displayed to the command window for the HWFET and UDDS drive cycles, respectively.

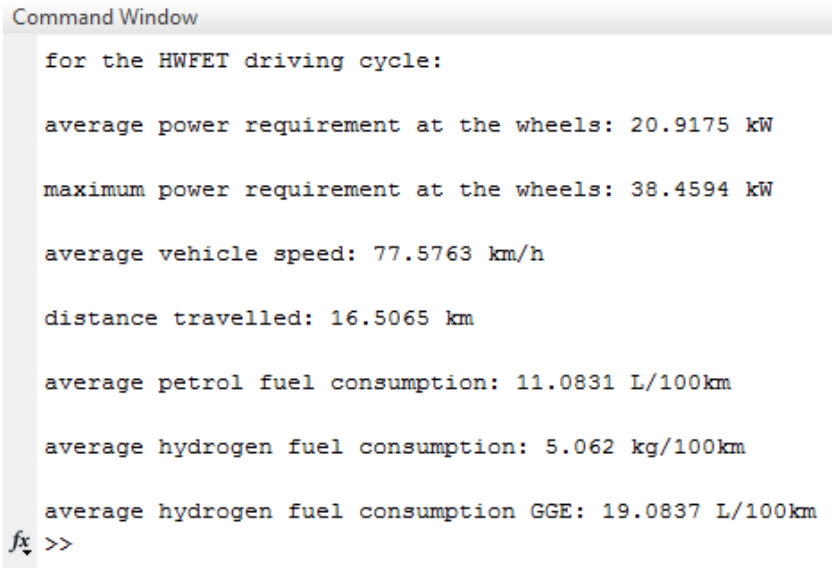

Figure 5.5: Command window results display for HWFET driving cycle

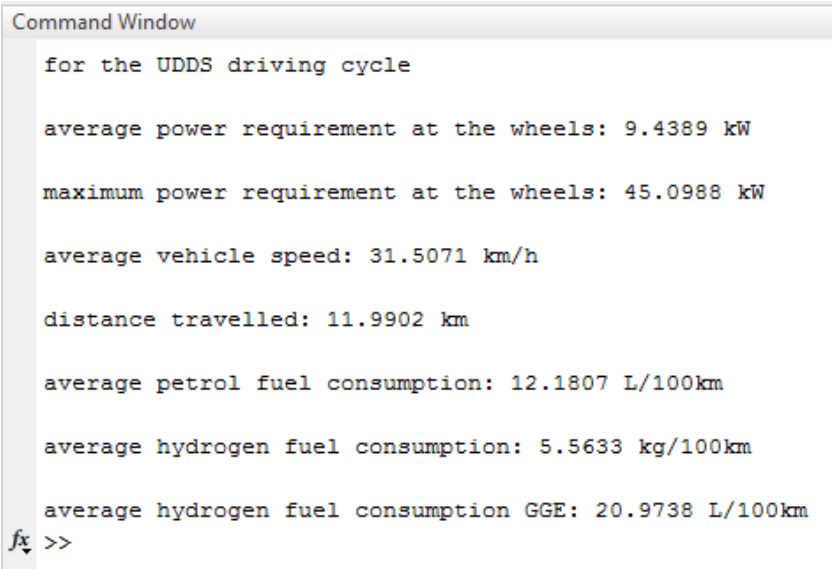

Figure 5.6: Command window results display for UDDS driving cycle

Figure 5.7: Total Power requirement vs time for HWFET cycle

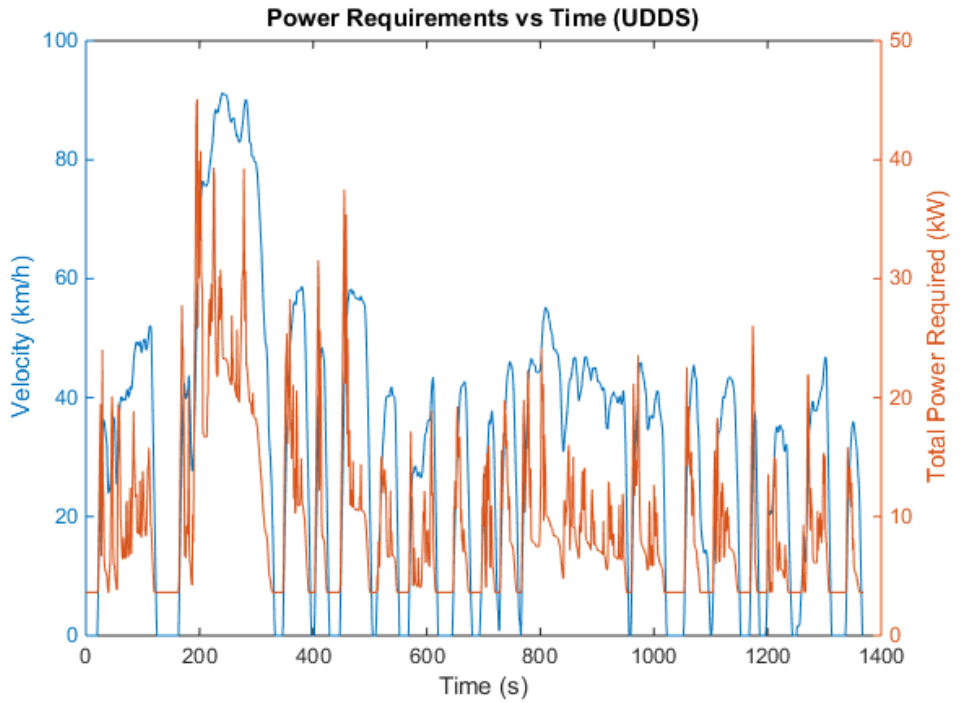

Figure 5.8: Total Power requirement vs time for UDDS cycle

The average wheel power requirements are 20.9175 kW and 9.4389 kW for the HWFET and UDDS drive cycles respectively, the highway cycle requiring approximately twice the power required for the urban cycle. The maximum wheel power requirements are 38.4594 kW and 45.0988 kW for the HWFET and UDDS respectively. The vehicle

averages a speed of 77.5763 km/h over the HWFET drive cycle, over twice the average speed of 33.5071 km/h for the UDDS drive cycle, travelling a distance of 16.5065 km and 11.9902 km in each cycle respectively. For the HWFET cycle, the vehicle achieves a theoretical petrol fuel consumption of 11.0831 L/100km, and 5.062 kg/100km of hydrogen; a gasoline gallon equivalent of 20.9738 L/100km. For the UDDS cycle, the vehicle achieves a theoretical petrol fuel consumption of 12.1807 L/100km, and 5.5633 kg/100km of hydrogen; a gasoline gallon equivalent of 20.0837 L/100km.

Data analysis

In order to significantly reduce the computational time the mean velocity and mean power requirement was obtained from the HWFET and UDDS driving cycles to be used in the ESM. If the ESM was made to iterate for all the velocity and resultant power data points in the drive cycles, the ESM would have to run for 766 and 1370 iterations for the HWFET and UDDS driving cycles respectively, significantly increasing computation time. The assumption to adopt the mean values for velocity and power requirements was analysed to ensure they did not significantly reduced the accuracy of the results.

In order to measure the accuracy of this assumption the percentage of the data within one standard deviation above and below the mean was calculated. Although the drive cycle data were not representative of a normal distribution the standard deviation was considered an appropriate means of representing the variance of the data for the purpose of confirming the accuracy of the assumption.

The HWFET drive cycle distribution for the velocity vs time was negatively skewed (skewed to the right) due to being at higher velocities for longer durations. Similarly the power vs time distribution was slightly negatively skewed but very close to a normal distribution. In contrast the UDDS drive cycle distribution for velocity vs time and power vs time were both positively skewed (skewed to the left) due to frequent zero/low velocities and thus low power due to frequent stopping of vehicles in urban environments.

Figure 5.9 shows the velocity vs time data of the HWFET Driving Cycle which fell within one standard deviation (16.5 km/h) above and below the mean velocity of 77.6 km/h.

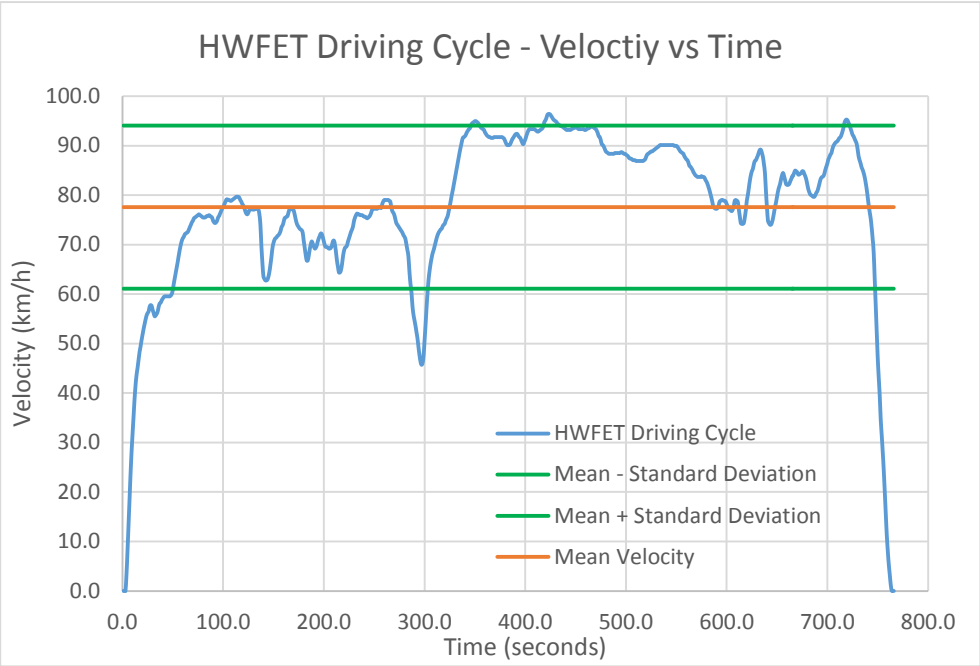

Figure 5.9: Spread of velocity data points for the HWFET driving cycle

It was calculated that 84.9% of the HWFET Driving Cycle velocity vs time data fell within one standard deviation below (61.1 km/h) and one standard deviation above (94.1 km/h) the mean velocity. This was clear to see on Figure 5.9, where the majority of the data points fell between this range.

Similarly Figure 5.10 shows the power vs time values for the HWFET driving cycle that fell between one standard deviation (5.9 kW) above and below the mean power of 20.9kW.

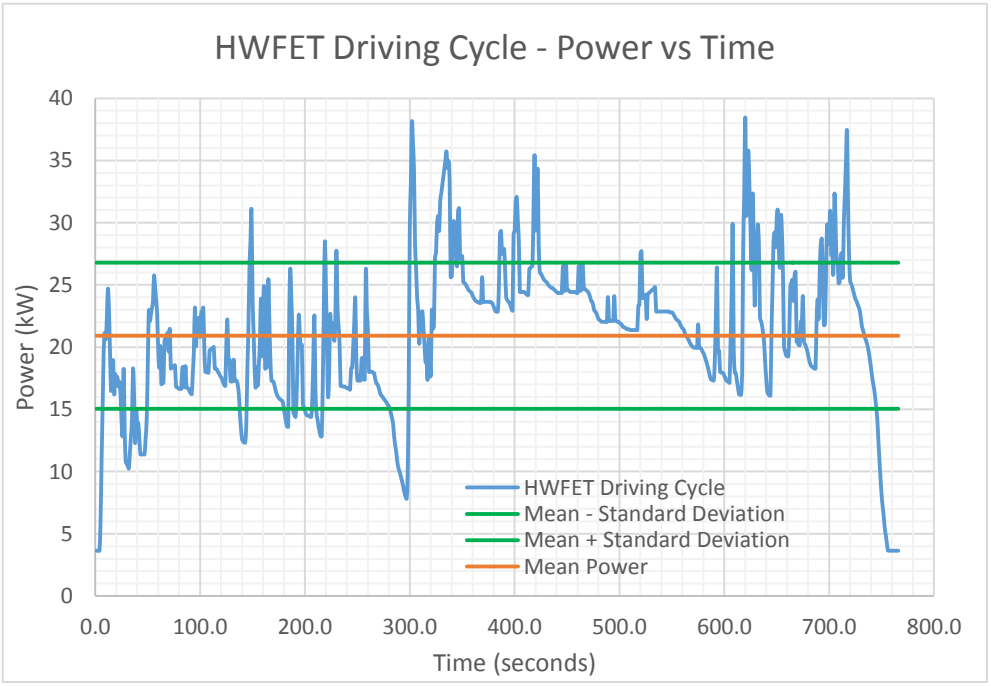

Figure 5.10: Spread of total power data points for the HWFET driving cycle

It was calculated that the percentage of power vs time values that fell between the range of one standard deviation below (15.0 kW) and above (26.8 kW) the mean was 75.2%.

Figure 5.11 shows the velocity vs time data from the UDDS Driving Cycle which fell within one standard deviation (23.7 km/h) above and below the mean velocity of 31.5 km/h. It was clear from this figure that the majority of this data also fell within this range.

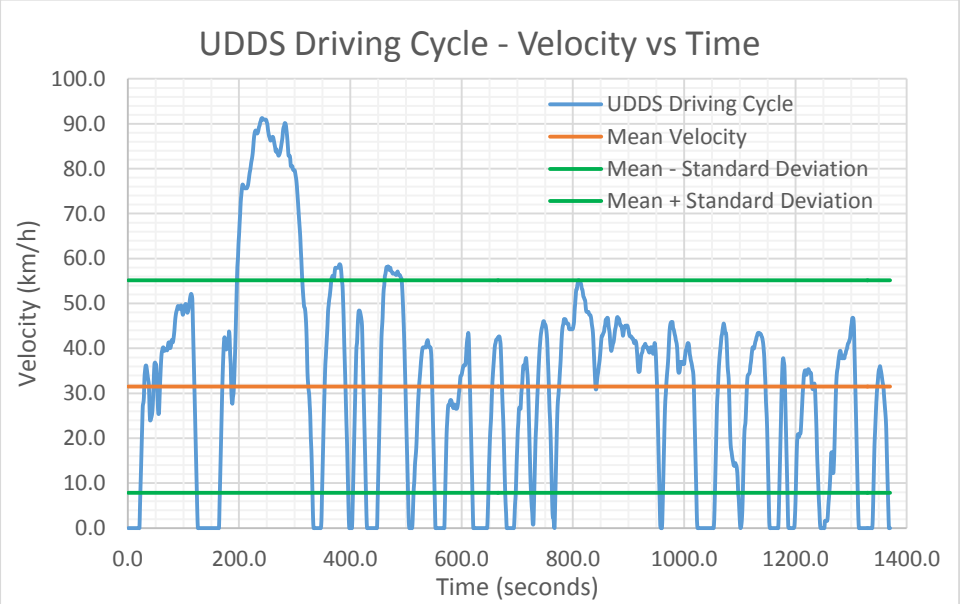

Figure 5.11: Spread of velocity data points for the UDDS driving cycle

It was calculated that 63.5% of the velocity vs time data for the UDDS Driving Cycle fell within one standard deviation below (7.9 km/h) and one standard deviation above (55.2 km/h) the mean velocity. Similarly Figure 5.12 shows the power vs time value for the UDDS driving cycle that fell within the range of one standard deviation (7.0 kW) above and below the mean power of 9.4 KW.

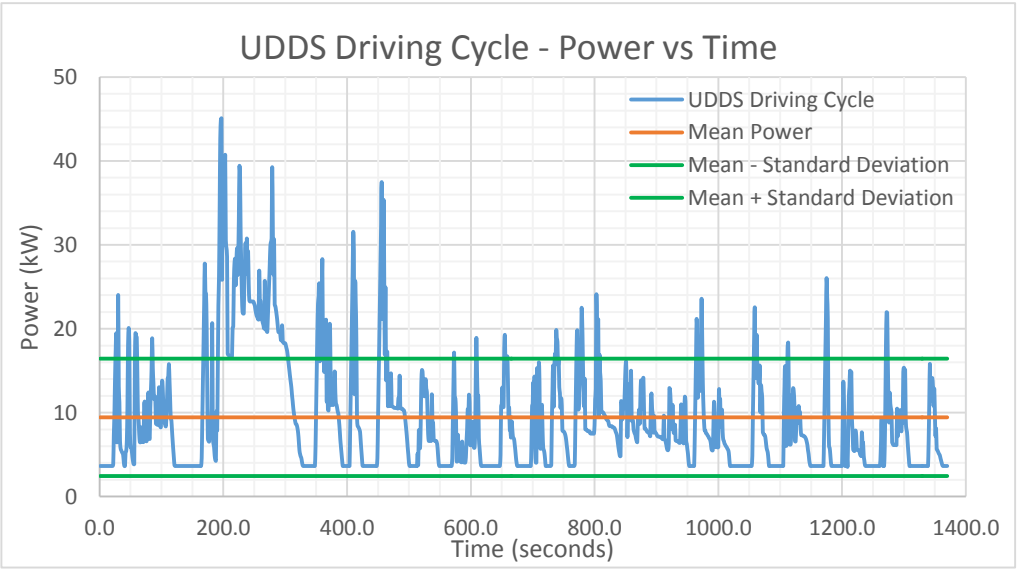

Figure 5.12: Spread of total power data points for the UDDS driving cycle

It was calculated that the percentage of power vs time values that fell within the range of one standard deviation below (2.4 kW) and above (16.4 kW) above the power mean was 85.1%.

From this analysis it was considered that using the mean velocity and power was an appropriate assumption that significantly improved the computational efficiency of the model without significantly reducing the accuracy of the results.

5.2 Ahrind Matlab Engine Simulation Model (AESM)

5.2.1 Introduction

An engine simulation model, ahrind was supplied to aid in the investigation of HICE performance characteristics. The ahrind script file is used to determine performance characteristics of a fuel injected engine based on a user (specified arbitrary) heat release profile as a function of crank angle (Buttsworth, 2007). The model is an evolution of an ESM created by Ferguson (1986). The model performs quasi-dimensional analysis including combustion and heat transfer effects, and includes temperature and pressure dependent combustion products equilibrium. The model integrates the governing differential Equations over the compression and power strokes of the combustion cycle using Matlab ODE solvers (Malpress, 2011).

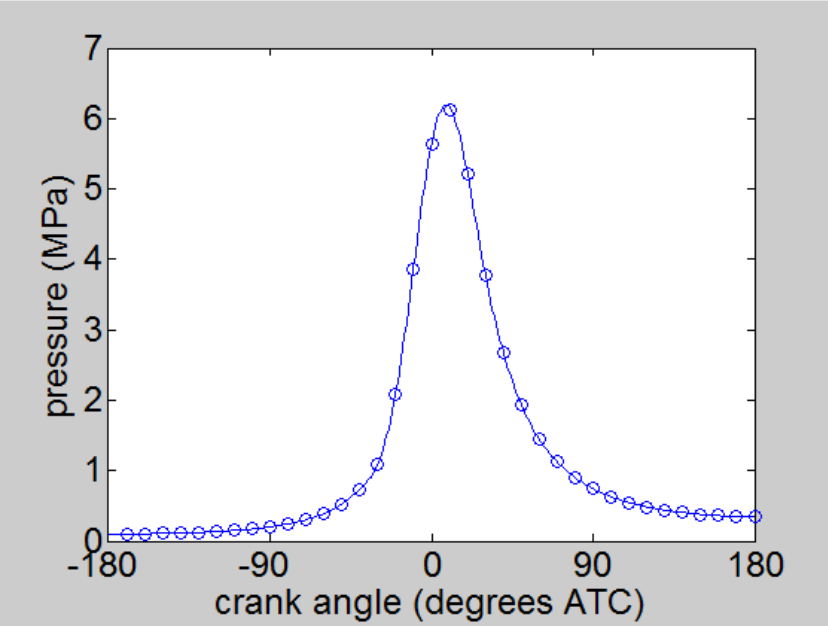

Figure 5.13: The AESM output for in cylinder pressure change over the compression and expansion strokes

Prior to modification, the model output plots of pressure, temperature, heat transfer, work, heat leakage, and heat flux vs crank angle over the compression and expansion strokes.

The in-cylinder pressure vs crank angle output from the original model in shown in Figure 5.13. The solid line and blue circle marker points represent the AESM data and reference data of the experimentally confirmed performance from the original Ferguson (1986) program (Malpress, 2011).

5.2.2 Method

The unmodified AESM provided outputs for fixed input values of engine speed, fuel-air equivalence ratio, and induction pressure. Modifications were made to the AESM to accommodate modelling of hydrogen combustion over a range of fuel-air equivalence ratios (ϕ), induction pressures (p1) and engine speeds (RPM).

Simply changing RPM, p1 and ϕ to arrays was not possible without making significant changes to the complex matrix multiplication throughout the numerous script files that the simulation relies upon to perform analysis. It became apparent that the code needed to iterate for different input values for these variables and a new script file needed to be developed.

The Holden_5L_Engine_analysis.m script file (Appendix D2) was developed to obtain power and fuel consumption characteristics of the concept engine. Based on a review of literature it was decided that the simulation should be iterated for values of hydrogen fuel-air equivalence ratios of $0.35 < \phi < 1.2$ (Sopena et al., 2010; Verhelst & Wallner, 2009), and for induction pressures ranging between 30 kPa < P < 140 kPa (AA1Car Auto Diagnosis, 2015; JEGS Performance, 2015).

```
% set engine speed and fuel ratio range
phi_range = 0.35:0.05:1.2;
Pa_range = 30e3:5e3:140e3;

% length of arrays for zeros matricies
n=length(Pa_range);
m=length(phi_range);

% create power output matrix (kW)
power_out=zeros(n+1,m+1);
power_out(2:end,1)=Pa_range;
power_out(1,2:end)=phi_range;
```

Figure 5.14: Creation of zeros matrix for desired output in Holden_5L_analysis.m

The ranges were transcribed into matlab as vectors of fuel-air ratios and induction pressures. A matrix of zero values the size of the vector lengths was created for each desired output, namely wheel power and fuel consumption outputs. When each output is

calculated, the value is then assigned to its respective place in the zeros matrix, allowing a surface plot to be generated. Figure 5.14 depicts the creation of the power output zeros matrix.

The ahrind.m and enginedata.m script files were then placed within a nested loop, allowing the iteration of ϕ and p1 for the range of range of fuel-air equivalence ratios and induction pressure for a fixed rpm. The developed loop is depicted in Figure 5.11.

The relevant Holden 5.0L engine specifications were then assigned to the variables in the enginedata.m script file (Appendix C1), seen in Figure 5.15.

```
% loop for engine speed and fuel ratios
for k = 1:m
    phi = phi_range(k);
    for l = 1:n
        p1 = Pa_range(l);

% run enginedata and ahrind scriptfiles
enginedata
ahrind
```

Figure 5.15: Creation of nested loop for induction pressure and fuel-air equivalence ratio in Holden_5L_analysis.m

The average engine speed taken from the drive cycle analysis was assigned to the RPM variable and an air intake air temperature of 300K was assumed.

```
case 'hydrogen' % Heywood
   alpha=1e-3; beta=2; gamma=0; delta=0;
   Afuel=[0.30574451E01 0.26765200E-02 -0.58099162E-05 0.55210391E-08...
       -0.18122739E-11 -0.98890474E03 -0.22997056E01];
```

Figure 5.16: Holden 5.0L engine specifications assigned to enginedata.m script file

The AESM model is based on polynomial curve fits to the thermodynamic data for each species in the fuel mixture. The fueldata.m script file (Appendix C9) is used to store the polynomial coefficients for species' thermodynamic properties where they can be called

```
% ***** engine geometry **********************************************
b=0.1016; % engine bore (m)
stroke=0.077724; % engine stroke (m)
r=9.7; % compression ratio
Vtdc=pi/4*b^2*stroke/(r-1); % volume at TDC
Vbdc=pi/4*b^2*stroke+Vtdc; % volume at BDC
RPM=1980; % engine speed at average velocity from drive cycle analysis
```

upon in the enginedata.m script file. To accommodate the simulation of the hydrogen combustion, a vector of the polynomial coefficients for hydrogen gas were added to the fueldata.m script file, using data from Heywood (1988). Figure 5.16 depicts the coefficients vector added to the sript file.

Figure 5.17: Addition of hydrogen polynomial coefficients for species thermodynamic properties to fueldata.m script file to accommodate simulation of hydrogen gas combustion.

Noting that the alpha value, representing the number of carbons in the species is a non-zero value, not reflective of real hydrogen combustion. As the AESM was originally programed for the combustion of hydrocarbons, the use of the ODE solver is dependent on carbon content. Initially, a zero value of carbon was assigned to alpha for hydrogen, and the resulted in fatal run errors in Matlab. Discovering carbon dependency in the Matlab coding resulted in a process of trial and error to find an alpha value that was small enough to not significantly affect results of the model, and large enough to not produce errors in the solving of ODEs.

For greater accuracy of results, the fixed density of air replaced with a variable density, calculated using the ideal gas law and inputs for temperature and the changing induction pressure. Figure 5.18 depicts the code block used to determine the density of air over various induction pressures. For simplicity, it was assumed that the density of hydrogen gas is injected at atmospheric pressure, having a density of 0.089 kg/m^3 (COD, 2001).

```
%% gas properties

% The density of dry air can be calculated using the ideal gas law,
% expressed as a function of temperature and pressure:

% specific gas constant for dry air (J/(kg*K))
R=287.058;

% calculating density
rho_air=p1/(R*T1);
```

Figure 5.18: Determining inducted air density via ideal gas law

A number of vehicle and other properties required for calculations were then assigned to variables; namely the engine capacity, the assumed driveline efficiency (0.95), and the density of petrol (737 kg/m^3).

```
%% Ground speed
% the relationship between RPM and groundspeed is determined by the
% driveline ratios.
gr=[2.54 1.83 1.38 1.0];      % gearbox ratios (x:1)
dr=3.08;                      % differential ratio (x:1)
tw=0.235;                     % tyre width (m)
ar=60;                        % tyre aspect ratio
rim=14;                       % wheel size (inches)

wd=2*tw*(ar/100)+(rim*0.0254);  % wheel diameter

wc=pi*wd; % wheel_circumfrence

dc=((60/1000/dr*wc)/1)/gr(4); % driveline constant

ground_speed=RPM*dc; % speed in top gear
```

Figure 5.19: Ground speed is calculated as a function of the vehicles effective drive ratio and engine speed

To determine the fuel consumption in the form of L/100km, the ground speed of the vehicle needed to be determined. The vehicle is assumed to have a Holden M21 4 speed transmission, commonly used with production vehicles fitted with the Holden 5.0L, with a direct drive ratio in top gear. The 'economy' diff ratio option of 3.08:1 has been selected for simulation, and 235/60/R14 tyres are assumed to be on the standard 14 inch wheels, all commonly fitted to the HX Holden Sedan production model (Uniqe Cars & Parts, 2015). The vehicle ground speed is a function of the vehicle's effective drive ratio, engine speed and the circumference of the driving wheels. Figure 5.19 depicts the calculation used to obtain ground speed as a function of drive ratio and engine speed.

Power

The power output of the vehicle was obtained through Equations 5.6 to 5.9

The relationship between brake power (P_B), wheel power (P_W), and drivetrain efficiency (η_d) is expressed in Equation 5.6.

$$\eta_d = \frac{P_w}{P_B} \qquad \text{Equation 5.6}$$

The relationship between engine mechanical efficiency (η_m), engine indicated power (P_i) and engine brake power (P_B) is shown in Equation 5.7.

$$\eta_m = \frac{P_B}{P_i} \qquad \text{Equation 5.7}$$

The indicated power of the engine is given by the expression in Equation 5.8.

$$Pi = \frac{imep * Ve * N}{z * 60} \qquad \text{Equation 5.8}$$

Where imep is the indicated mean effective pressure, Ve is the engine swept volume, N is the engine speed, and z is the number of revolutions per power stroke (2 for four-stroke engines). Rearranging Equations 5.6, 5.7, and 5.8, we can obtain an expression for wheel power, shown in Equation 5.9.

$$P_w = \eta_d * P_B$$

$$P_w = \eta_d * \eta_m * P_i$$

$$P_w = \frac{\eta_d * \eta_m * imep * Ve * N}{z * 60} \qquad \text{Equation 5.9}$$

Fuel consumption

The idealised stoichiometric combustion of hydrogen in air is given in Equation 5.10

$$H_2 + 0.5(O_2 + 3.76N_2) \rightarrow H_2O + 1.88N_2 \qquad \text{Equation 5.10}$$

The number of moles of each species of the reactants in a stoichiometric combustion of hydrogen and air is shown to be two, one and 1.88 for hydrogen, oxygen and nitrogen respectively. Multiplying the molar weights of each of these species by their respective number yields the molar weights of fuel and oxidiser mixture. This relationship is shown in Equation 5.11.

$$MW_{H2} = N_H * MW_H \qquad \text{Equation 5.11}$$

$$MW_{air} = (N_O * MW_O) + (N_N * MW_N)$$

The ratio of the two mixtures is known as the fuel-air ratio. The fuel-air ratio is shown in Equation 5.12.

$$FAR = \frac{M_{fuel}}{M_{oxidiser}} = \frac{MW_{H2}}{MW_{air}} \qquad \text{Equation 5.12}$$

The stoichiometric fuel air ratio is the ratio of the two mixtures at stoichiometric combustion conditions. Substituting the molar weights for the stoichiometric combustion process (Equation 5.10) into Equation 5.13, we obtain the stoichiometric fuel-air ratio.

$$FAR_{stoi} = \left(\frac{MW_{H2}}{MW_{air}}\right)_{stoi}$$ Equation 5.13

Any instantaneous fuel-air ratio can now be obtained by multiplying the stoichiometric fuel air ratio by the fuel-air equivalence ratio (ϕ). This relationship is shown in Equation 5.14.

$$FAR = FAR_{stoi} * \phi$$ Equation 5.14

Expanding Equation 5.12 and solving for volume we obtain an expression for volume of fuel terms of volume of air, densities and fuel-air ratio, shown in Equations 5.15 and 5.16.

$$FAR = \frac{M_{fuel}}{M_{oxidiser}} = \frac{\rho_{fuel} * V_{fuel}}{\rho_{air} * V_{air}} = \frac{\rho_{fuel}}{\rho_{air}} * \frac{V_{fuel}}{V_{air}}$$ Equation 5.15

$$V_{fuel} - FAR * \frac{\rho_{air}}{\rho_{fuel}} * V_{air} = 0$$ Equation 5.16

Knowing that the sum of the fuel and air in the cylinder prior to compression will be equal the swept cylinder volume (V_{bdc}), we can expression the swept volume of the cylinder in terms of each gasses volume. This relationship is shown in Equation 5.17.

$$V_{fuel} + V_{air} = V_{bdc}$$ Equation 5.17

Arranging Equations 5.16 and 5.17 into matrix form we obtain Equation 5.18.

$$\begin{bmatrix} 1 & 1 \\ -1 & \left(FAR * \frac{\rho_{air}}{\rho_{fuel}}\right) \end{bmatrix} * \begin{bmatrix} V_{fuel} \\ V_{air} \end{bmatrix} = \begin{bmatrix} V_{bdc} \\ 0 \end{bmatrix}$$ Equation 5.18

In this form, the unknowns (V_{fuel} and V_{air}) are expressed in terms of known values.

Solving for the volumes (using ‘linsolve’ function in Matlab) we can obtain the rate of fuel consumption using the expression in Equation 5.19.

$$FC_{Kg\ H2\ per\ hr} = \frac{V_{fuel} * \rho_{H2} * 60 * N * 8}{z}$$ Equation 5.19

Where ρ_{H2} is the density of the inducted hydrogen, $60 * N$ is the engine speed (rev/hr), 8 is refers to the number of cylinders, and z is the number of revolutions per power stroke (2 for a four-stroke engine).

The consumption of hydrogen fuel per 100km is then the hourly consumption rate divided by the groundspeed, multiplied by 100. Equation 5.20 shows this relationship.

$$FC_{Kg\ H2\ per\ 100km} = \left(\frac{FC_{Kg\ H2\ per\ hr}}{groundspeed}\right) * 100 \qquad \text{Equation 5.20}$$

Microsoft Excel

The matrix data outputs of wheel power and fuel consumption were copied from Matlab into Microsoft Excel for further analysis. The average power requirement from the drive cycle analysis was used as a 'target power' to identify all combinations of fuel-air ratio and induction pressure that would produce the required power for the HWFET and UDDS cases. The corresponding fuel consumption for that particular combination is also determined.

Linear interpolation

If two points are assigned the coordinates (x_0, y_0) and (x_1, y_1) along a straight line, the general form of the Equation to find the corresponding coordinate for any one known value along the line between (x_0, y_0 and x_1, y_1) as found in Equation 5.21.

$$y = y_0 + (y_1 - y_0) * \left(\frac{x - x_0}{x_1 - x_0}\right) \qquad \text{Equation 5.21}$$

Using a 'forecast' function, the exact value of induction pressure that corresponds to the target wheel power output (x) for each value of ϕ was obtained. Using an 'mround' function, the value obtained for the induction pressure is rounded to the nearest 5,000 Pa. An 'if-then' statement then adds or subtracts 5,000 Pa to determine the values for induction pressure either side of the exact value obtained (x_0 and x_1). 'Vlookup' functions are then used to obtain the fuel consumption Figures at the rounded pressures and ϕ value (y_0 and y_1). The exact fuel consumption Figure for each equivalence and induction pressure scenario (y) were obtained.

5.2.3 Results

Figure 5.20 and 5.21 depict surface plots of the wheel power produced over the range of fuel-air equivalence ratios and induction pressures for the HWFET and UDDS driving cycles. In both cases the power rises gradually from a fuel-air ratio of 0.35 and peaks at 1.0 before lowing with further increases. Increasing induction pressure is also observed to proportionally increase power output for both cases. Although both plots appear similar it is observed that the UDDS surface plot displays a proportionally lower power output compared to the HWFET cycle. A sharp rise in power is observed at an equivalence of 0.9 in both cases. Peak power outputs of 53kW and 67 kW are for the HWFET and UDDS cycles respectively.

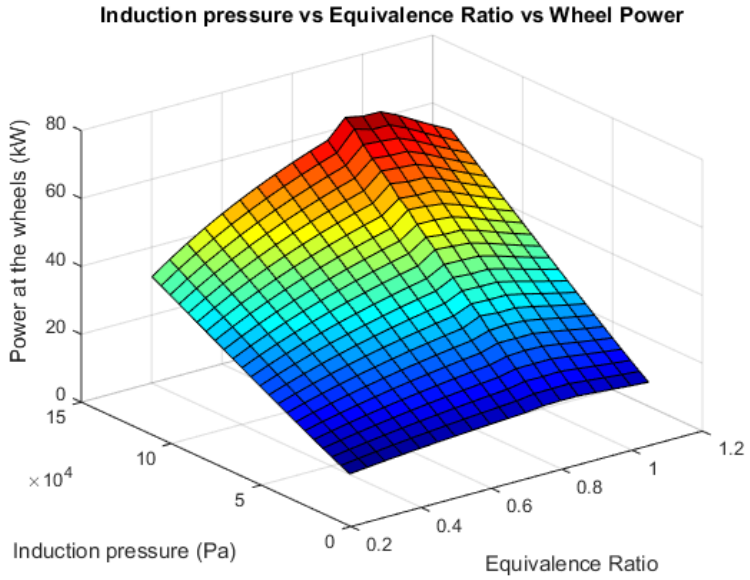

Figure 5.20: Surface plot of power output vs equivalence ratio and induction pressure for the average engine speed of the HWFET driving cycle.

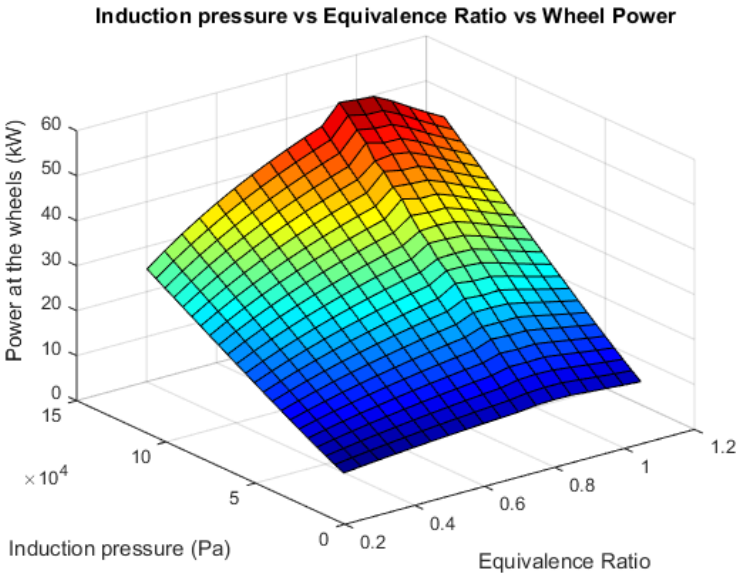

Figure 5.21: Surface plot of power output vs equivalence ratio and induction pressure for the average engine speed of the UDDS driving cycle.

Figure 5.22 and 5.23 depict surface plots of the hydrogen fuel consumption produced over the range of fuel-air equivalence ratios and induction pressures for the HWFET and UDDS driving cycles. In both cases the increase of either induction pressure or the fuel-air equivalence ratio is met with an increase in fuel consumption, peaking at the highest numerical value of induction pressure and fuel-air equivalence at 15 and 27 kg/100km for the HWFET and UDDS cases respectively. The sharp increase in power output observed in Figures 15.18 and 5.19 do not appear to effect the surface plots of fuel consumption at the same point. Although both plots appear similar it is observed that the UDDS surface plot displays a proportionally higher fuel consumption output compared to the HWFET cycle.

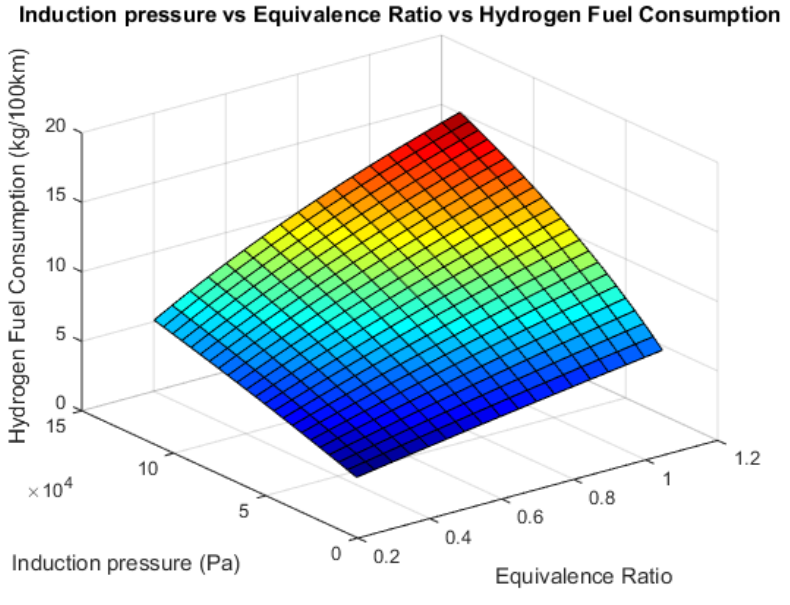

Figure 5.22: Surface plot of hydrogen fuel consumption vs equivalence ratio and induction pressure for the average engine speed of the HWFET driving cycle.

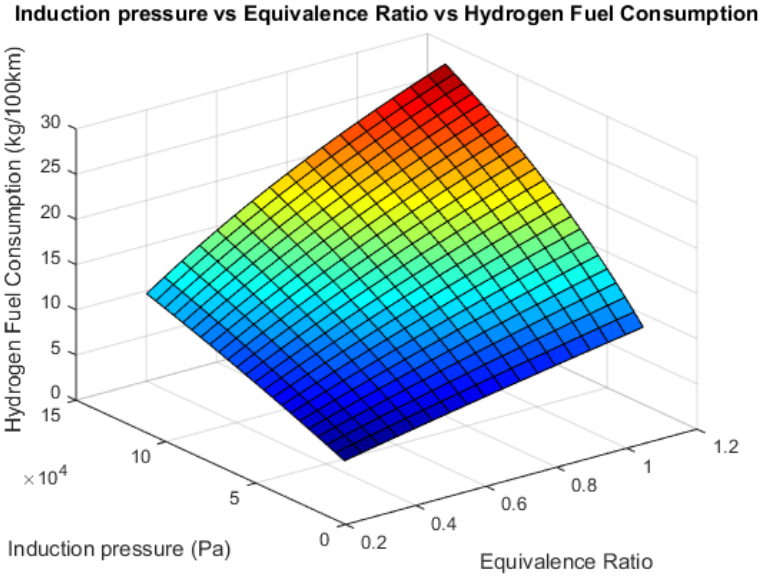

Figure 5.23: Surface plot of hydrogen fuel consumption vs equivalence ratio and induction pressure for the average engine speed of the UDDS driving cycle.

Figures 5.24 and 5.25 depict the numerical outputs for wheel power and fuel consumption over the fuel-air ratio and induction pressure ranges that have been transcribed into Microsoft Excel for the HWFET driving cycle.

Wheel Power (kW)

Induction Pressure (Pa)	Fuel-Air Equivalence Ratio																	
0	0.35	0.4	0.45	0.5	0.55	0.6	0.65	0.7	0.75	0.8	0.85	0.9	0.95	1	1.05	1.1	1.15	1.2
30000	3.97631	4.50687	5.00117	5.46225	5.89226	6.29386	6.66913	7.02012	7.34884	7.65713	7.94658	8.53156	8.67591	8.67464	8.281	7.8575	7.46114	7.09558
35000	5.21406	5.87799	6.49558	7.07022	7.60518	8.10362	8.56841	9.00229	9.4078	9.78727	10.1426	10.8767	10.9613	11.0219	10.5391	10.0105	9.51333	9.05344
40000	6.50574	7.30603	8.04872	8.73867	9.37992	9.97643	10.5318	11.0495	11.5326	11.9839	12.4057	13.3518	13.2982	13.4353	12.8635	12.2283	11.6278	11.071
45000	7.83683	8.77443	9.64378	10.4503	11.1989	11.8944	12.5412	13.1434	13.7046	14.2282	14.7168	15.8237	15.8678	15.8971	15.236	14.4926	13.7866	13.131
50000	9.19592	10.2727	11.2699	12.1937	13.0504	13.8456	14.5844	15.2716	15.9114	16.5078	17.0636	18.2987	18.5324	18.3953	17.6446	16.7905	15.9781	15.2227
55000	10.5769	11.7937	12.9191	13.9611	14.9266	15.822	16.6532	17.4258	18.1447	18.8141	19.4376	20.9467	20.9105	20.9216	20.0815	19.115	18.1951	17.3392
60000	11.9748	13.3319	14.5865	15.7471	16.8218	17.8178	18.7419	19.6002	20.3984	21.1413	21.8327	23.3859	23.7299	23.4702	22.5386	21.461	20.4329	19.4752
65000	13.3854	14.8837	16.268	17.5477	18.7319	19.8289	20.8462	21.7906	22.6683	23.4849	24.2447	26.4816	26.0057	26.0362	25.0139	23.8246	22.6867	21.6259
70000	14.8064	16.4466	17.9608	19.3599	20.654	21.8523	22.963	23.9937	24.9513	25.8419	26.6702	28.8038	28.5964	28.617	27.5036	26.2006	24.9532	23.7889
75000	16.2358	18.0181	19.6626	21.1816	22.5859	23.8856	25.09	26.2072	27.2449	28.2097	29.1069	31.4671	31.2551	31.2102	30.0052	28.5857	27.2298	25.9619
80000	17.6722	19.5968	21.372	23.0109	24.5257	25.9272	27.2254	28.4294	29.5473	30.5866	31.5528	34.1161	33.7641	33.8134	32.517	30.9838	29.5152	28.1433
85000	19.1141	21.1815	23.0875	24.8468	26.4723	27.9756	29.3679	30.6587	31.8571	32.971	34.0066	36.7675	36.6131	36.4245	35.0373	33.3875	31.8079	30.3316
90000	20.5615	22.7715	24.8085	26.6882	28.4244	30.0298	31.5163	32.8941	34.1731	35.3619	36.4669	39.9167	39.498	39.0433	37.565	35.7984	34.1068	32.5259
95000	22.0123	24.3653	26.5338	28.5341	30.3812	32.0889	33.6697	35.1347	36.4945	37.7583	38.9329	42.3392	41.7144	41.6685	40.0991	38.2142	36.4084	34.7254
100000	23.4663	25.9629	28.2628	30.3839	32.3421	34.1522	35.8274	37.3798	38.8204	40.1593	41.4038	44.8813	44.8255	44.2995	42.6376	40.635	38.7201	36.9289
105000	24.9235	27.5636	29.9952	32.2371	34.3065	36.2191	37.9889	39.6286	41.1504	42.5645	43.879	47.9839	47.6074	46.9356	45.181	43.0613	41.033	39.1361
110000	26.3833	29.167	31.7303	34.0932	36.274	38.2891	40.1536	41.8809	43.4838	44.9733	46.358	50.1018	49.6115	49.5763	47.7285	45.4896	43.3476	41.3468
115000	27.8454	30.7727	33.4678	35.9519	38.2441	40.3619	42.3211	44.1361	45.8202	47.3853	48.8404	53.2142	52.3916	52.221	50.2798	47.9229	45.6685	43.5605
120000	29.3093	32.3806	35.2076	37.8129	40.2165	42.4371	44.4912	46.3938	48.1593	49.8001	51.3257	55.7333	55.3109	54.8696	52.8345	50.3595	47.9908	45.7772
125000	30.7749	33.9902	36.9493	39.6758	42.191	44.5145	46.6634	48.6539	50.5009	52.2174	53.8136	58.1875	57.6338	57.5216	55.3922	52.7987	50.3157	47.9964
130000	32.2419	35.6014	38.6925	41.5405	44.1673	46.5937	48.8377	50.9161	52.8445	54.6369	56.3039	61.0695	60.6498	60.1768	57.9525	55.2404	52.6428	50.2177
135000	33.7104	37.214	40.4373	43.4067	46.1453	48.6747	51.0137	53.18	55.1901	57.0584	58.7964	64.4532	62.8634	62.8348	60.5154	57.6844	54.9723	52.4415
140000	35.18	38.8278	42.1835	45.2743	48.1247	50.7571	53.1913	55.4457	57.5375	59.4817	61.2908	66.6153	65.6002	65.4954	63.0806	60.133	57.304	54.6662

Figure 5.24: numerical outputs for wheel power over the fuel-air ratio and induction pressure ranges that have been transcribed into Microsoft Excel for the HWFET driving cycle.

Fuel consumption (kg H2/100km)

Induction Pressure (Pa)	Fuel-Air Equivalence Ratio																	
0	0.35	0.4	0.45	0.5	0.55	0.6	0.65	0.7	0.75	0.8	0.85	0.9	0.95	1	1.05	1.1	1.15	1.2
30000	1.48707	1.69017	1.89105	2.08975	2.28631	2.48075	2.67311	2.86342	3.05172	3.23804	3.42241	3.60485	3.78541	3.96411	4.14097	4.31603	4.48931	4.66084
35000	1.72381	1.95753	2.1883	2.41617	2.64119	2.86342	3.08291	3.29971	3.51387	3.72543	3.93445	4.14097	4.34503	4.54668	4.74596	4.94291	5.13758	5.32999
40000	1.95753	2.22103	2.48075	2.73677	2.98917	3.23804	3.48343	3.72543	3.96411	4.19952	4.43175	4.66084	4.88688	5.1099	5.32999	5.54719	5.76156	5.97316
45000	2.1883	2.48075	2.76852	3.05172	3.33046	3.60485	3.87499	4.14097	4.40289	4.66084	4.91492	5.1652	5.41178	5.65473	5.89413	6.13006	6.3626	6.59182
50000	2.41617	2.73677	3.05172	3.36116	3.66525	3.96411	4.25787	4.54668	4.83065	5.1099	5.38456	5.65473	5.92051	6.18203	6.43938	6.69265	6.94195	7.18737
55000	2.64119	2.98917	3.33046	3.66525	3.99371	4.31603	4.63237	4.94291	5.2478	5.54719	5.84123	6.13006	6.41383	6.69265	6.96666	7.23599	7.50075	7.76106
60000	2.86342	3.23804	3.60485	3.96411	4.31603	4.66084	4.99876	5.32999	5.65473	5.97316	6.28546	6.59182	6.8924	7.18737	7.47687	7.76106	8.04008	8.31408
65000	3.08291	3.48343	3.87499	4.25787	4.63237	4.99876	5.3573	5.70823	6.0518	6.38824	6.71776	7.04058	7.3569	7.66691	7.9708	8.26876	8.56094	8.84753
70000	3.29971	3.72543	4.14097	4.54668	4.94291	5.32999	5.70823	6.07793	6.43938	6.79284	7.13859	7.47687	7.80792	8.13197	8.44923	8.75993	9.06426	9.36242
75000	3.51387	3.96411	4.40289	4.83065	5.2478	5.65473	6.0518	6.43938	6.81779	7.18737	7.54841	7.90121	8.24604	8.58318	8.91288	9.23538	9.55092	9.85972
80000	3.72543	4.19952	4.66084	5.1099	5.54719	5.97316	6.38824	6.79284	7.18737	7.57218	7.94764	8.31408	8.67182	9.02117	9.36242	9.69585	10.0217	10.3403
85000	3.93445	4.43175	4.91492	5.38456	5.84123	6.28546	6.71776	7.13859	7.54841	7.94764	8.33669	8.71594	9.08576	9.4465	9.79849	10.142	10.4774	10.805
90000	4.14097	4.66084	5.1652	5.65473	6.13006	6.59182	7.04058	7.47687	7.90121	8.31408	8.71594	9.10723	9.48836	9.85972	10.2217	10.5746	10.9188	11.2546
95000	4.34503	4.88688	5.41178	5.92051	6.41383	6.8924	7.3569	7.80792	8.24604	8.67182	9.08576	9.48836	9.88007	10.2613	10.6325	10.9941	11.3464	11.6898
100000	4.54668	5.1099	5.65473	6.18203	6.69265	7.18737	7.66691	8.13197	8.58318	9.02117	9.4465	9.85972	10.2613	10.6518	11.0316	11.4012	11.761	12.1113
105000	4.74596	5.32999	5.89413	6.43938	6.96666	7.47687	7.9708	8.44923	8.91288	9.36242	9.79849	10.2217	10.6325	11.0316	11.4194	11.7964	12.163	12.5197
110000	4.94291	5.54719	6.13006	6.69265	7.23599	7.76106	8.26876	8.75993	9.23538	9.69585	10.142	10.5746	10.9941	11.4012	11.7964	12.1802	12.5532	12.9157
115000	5.13758	5.76156	6.3626	6.94195	7.50075	8.04008	8.56094	9.06426	9.55092	10.0217	10.4774	10.9188	11.3464	11.761	12.163	12.5532	12.9319	13.2997
120000	5.32999	5.97316	6.59182	7.18737	7.76106	8.31408	8.84753	9.36242	9.85972	10.3403	10.805	11.2546	11.6898	12.1113	12.5197	12.9157	13.2997	13.6724
125000	5.5202	6.18203	6.81779	7.42899	8.01702	8.58318	9.12867	9.65459	10.162	10.6518	11.125	11.5823	12.0246	12.4525	12.8668	13.2681	13.6571	14.0342
130000	5.70823	6.38824	7.04058	7.66691	8.26876	8.84753	9.40452	9.94095	10.4579	10.9565	11.4376	11.9022	12.3511	12.785	13.2048	13.611	14.0044	14.3856
135000	5.89413	6.59182	7.26025	7.90121	8.51636	9.10723	9.67524	10.2217	10.7477	11.2546	11.7432	12.2146	12.6696	13.1091	13.5339	13.9447	14.3422	14.727
140000	6.07793	6.79284	7.47687	8.13197	8.75993	9.36242	9.94095	10.4969	11.0316	11.5463	12.042	12.5197	12.9805	13.4252	13.8546	14.2696	14.6707	15.0588

Figure 5.25: numerical outputs for fuel consumption over the fuel-air ratio and induction pressure ranges that have been transcribed into Microsoft Excel for the HWFET driving cycle.

Figure 26 shows the use of Microsoft excel functions to determine the fuel consumption at the induction pressure and fuel-air ratios that produce the target power for the HWFET driving cycle. The lowest hydrogen fuel consumption figure for the HWFET driving cycle is 4.18 kg/100km (15.4 GGE), at an induction pressure of 91227 Pa and a fuel air ratio of 0.35.

Target power (kw):	20.9175																	
	Fuel-Air Equivalence Ratio																	
Induction	0.35	0.4	0.45	0.5	0.55	0.6	0.65	0.7	0.75	0.8	0.85	0.9	0.95	1	1.05	1.1	1.15	1.2
Presssur	91226.9	84167.1	78670.6	74275.3	70681.9	67690.1	65168.5	63007	61143.5	59519.2	58089.4	54944.8	55012.5	54991.9	56701.2	58841.6	61075	63353.1

Fuel	2	3	4	5	6	7	8	9	10	11	12	13	14	15	16	17	18	19
(kg/100k	0.35	0.4	0.45	0.5	0.55	0.6	0.65	0.7	0.75	0.8	0.85	0.9	0.95	1	1.05	1.1	1.15	1.2
x	91226.9	84167.1	78670.6	74275.3	70681.9	67690.1	65168.5	63007	61143.5	59519.2	58089.4	54944.8	55012.5	54991.9	56701.2	58841.6	61075	63353.1
x0	90000	85000	80000	75000	70000	70000	65000	65000	60000	60000	60000	55000	55000	55000	55000	60000	60000	65000
x1	95000	80000	75000	70000	75000	65000	70000	60000	65000	55000	55000	50000	60000	50000	60000	55000	65000	60000
y0	4.14097	4.43175	4.66084	4.83065	4.94291	5.32999	5.3573	5.70823	5.65473	5.97316	6.28546	6.13006	6.41383	6.69265	6.96666	7.76106	8.04008	8.84753
y1	4.34503	4.19952	4.40289	4.54668	5.2478	4.99876	5.70823	5.32999	6.0518	5.54719	5.84123	5.65473	6.8924	6.18203	7.47687	7.23599	8.56094	8.31408
Y	4.19104	4.39306	4.59226	4.78949	4.98449	5.17697	5.36912	5.55746	5.74553	5.93219	6.11571	6.12481	6.41502	6.69183	7.14025	7.63941	8.15207	8.67182
GGE	15.8002	16.5618	17.3128	18.0564	18.7915	19.5172	20.2416	20.9516	21.6607	22.3644	23.0562	23.0906	24.1846	25.2282	26.9188	28.8006	30.7333	32.6927

Figure 5.26: Fuel consumption data for combinations of phi and induction pressure to produce the target power of 20.92 kW for the HWFET driving cycle at 1980 rpm

Figures 5.27 and 5.28 depict the numerical outputs for wheel power and fuel consumption over the fuel-air ratio and induction pressure ranges that have been transcribed into Microsoft Excel for the UDDS driving cycle.

Wheel Power (kW)

Induction Pressure (Pa) \ Fuel-Air Equivalence Ratio	0	0.35	0.4	0.45	0.5	0.55	0.6	0.65	0.7	0.75	0.8	0.85	0.9	0.95	1	1.05	1.1	1.15	1.2
30000	2.76308	3.15778	3.52698	3.87256	4.1958	4.4986	4.78234	5.04854	5.29854	5.53382	5.75565	6.18932	6.35814	6.32852	6.02438	5.70704	5.41286	5.14281
35000	3.70843	4.21018	4.67832	5.11517	5.523	5.90398	6.26019	6.59363	6.90611	7.19948	7.47531	8.01937	8.21112	8.17539	7.79836	7.39653	7.02131	6.67553
40000	4.71119	5.32252	5.89179	6.42188	6.91581	7.37641	7.80632	8.20803	8.58386	8.93606	9.2664	9.99762	10.2226	10.0934	9.6425	9.15357	8.69534	8.27249
45000	5.75572	6.47863	7.15076	7.7754	8.35659	8.89785	9.40229	9.87303	10.3129	10.7244	11.1095	11.9859	11.9434	12.0635	11.5379	10.961	10.4181	9.91593
50000	6.83179	7.6679	8.44364	9.16394	9.83334	10.456	11.0356	11.5759	12.0802	12.5514	12.9921	14.0976	13.934	14.0722	13.4728	12.8062	12.1771	11.5942
55000	7.9326	8.8822	9.76265	10.5794	11.3377	12.0422	12.6976	13.3078	13.8769	14.4082	14.9045	16.2972	16.1014	16.1114	15.4374	14.6804	13.9637	13.2988
60000	9.05162	10.1161	11.1022	12.0159	12.8635	13.6504	14.3818	15.0625	15.6967	16.2883	16.8405	18.1538	18.1221	18.1747	17.426	16.5768	15.772	15.0245
65000	10.1858	11.366	12.4577	13.469	14.4063	15.276	16.0838	16.8351	17.5347	18.1869	18.7953	20.3838	20.444	20.2575	19.4328	18.4915	17.5978	16.7671
70000	11.332	12.6281	13.8265	14.9354	15.9629	16.9156	17.8001	18.6223	19.3875	20.1006	20.7654	22.5616	22.2187	22.3564	21.4557	20.4221	19.4384	18.5241
75000	12.4883	13.9004	15.2056	16.4129	17.5306	18.5667	19.5281	20.4214	21.2524	22.0265	22.748	25.0535	24.4935	24.4685	23.4917	22.3657	21.2913	20.2923
80000	13.6524	15.1812	16.5935	17.8992	19.1077	20.2272	21.2658	22.2304	23.1274	23.9627	24.741	26.9534	26.9013	26.5916	25.5387	24.318	23.1539	22.0696
85000	14.8232	16.4692	17.9888	19.3931	20.6924	21.8957	23.0116	24.0476	25.0108	25.9075	26.7428	28.6979	28.8686	28.7243	27.5951	26.2795	25.0248	23.8548
90000	15.9995	17.7628	19.3901	20.8934	22.2837	23.5709	24.7642	25.8718	26.9013	27.8597	28.7521	31.2141	31.0902	30.8654	29.6595	28.2489	26.9027	25.6468
95000	17.1807	19.0615	20.7966	22.399	23.8806	25.2518	26.5227	27.702	28.798	29.818	30.7679	33.019	33.2364	33.013	31.7309	30.2243	28.7865	27.4445
100000	18.3659	20.3645	22.2076	23.9094	25.4822	26.9376	28.2862	29.5374	30.6999	31.7818	32.7891	35.5187	35.1657	35.1664	33.8083	32.2053	30.6754	29.2473
105000	19.5547	21.6711	23.6226	25.4236	27.0879	28.6276	30.054	31.3771	32.6064	33.7502	34.8152	38.3185	37.3335	37.3253	35.8911	34.1914	32.5685	31.0543
110000	20.7471	22.9813	25.0407	26.9413	28.6972	30.3213	31.8256	33.2208	34.5169	35.7228	36.8455	40.0769	39.735	39.4891	37.9787	36.1812	34.4634	32.8652
115000	21.9415	24.2938	26.4618	28.462	30.3096	32.0182	33.6005	35.0679	36.4309	37.6989	38.8795	42.5927	41.8121	41.6571	40.0698	38.1745	36.3676	34.6794
120000	23.1383	25.6089	27.8854	29.9854	31.9247	33.718	35.3784	36.918	38.3479	39.6783	40.9169	43.997	44.4657	43.8291	42.1642	40.1719	38.2688	36.4963
125000	24.3368	26.9262	29.3114	31.5112	33.5423	35.4202	37.1588	38.7707	40.2677	41.6605	42.9572	47.1358	46.0491	46.0045	44.262	42.1708	40.1758	38.3158
130000	25.5376	28.2453	30.7393	33.039	35.1621	37.1247	38.9415	40.6258	42.19	43.6453	45.0002	49.1057	48.3533	48.1831	46.3627	44.174	42.0861	40.1377
135000	26.7399	29.5662	32.169	34.5687	36.7837	38.8312	40.7263	42.4831	44.1145	45.6323	47.0456	51.3893	50.4785	50.3647	48.4661	46.1798	43.998	41.9617
140000	27.9436	30.8886	33.6003	36.1	38.4071	40.5395	42.513	44.3422	46.041	47.6214	49.0932	53.3579	52.9001	52.5489	50.572	48.188	45.9115	43.7877

Figure 5.27: Numerical outputs for wheel power over the fuel-air ratio and induction pressure ranges that have been transcribed into Microsoft Excel for the UDDS driving cycle.

Fuel consumption (kg H2/100km)

Induction Pressure (Pa) \ Fuel-Air Equivalence Ratio	0	0.35	0.4	0.45	0.5	0.55	0.6	0.65	0.7	0.75	0.8	0.85	0.9	0.95	1	1.05	1.1	1.15	1.2
30000	2.72134	3.09301	3.46063	3.82425	4.18394	4.53976	4.89178	5.24006	5.58465	5.92561	6.263	6.59688	6.9273	7.25431	7.57797	7.89833	8.21544	8.52934
35000	3.15456	3.58228	4.00458	4.42158	4.83337	5.24006	5.64172	6.03847	6.43038	6.81754	7.20005	7.57797	7.95141	8.32043	8.68511	9.04553	9.40176	9.75388
40000	3.58228	4.06448	4.53976	5.00829	5.47019	5.92561	6.37468	6.81754	7.25431	7.68512	8.11009	8.52934	8.94298	9.35113	9.75388	10.1514	10.5437	10.9309
45000	4.00458	4.53976	5.06638	5.58465	6.09475	6.59688	7.09123	7.57797	8.05729	8.52934	8.9943	9.45232	9.90355	10.3481	10.7863	11.218	11.6436	12.063
50000	4.42158	5.00829	5.58465	6.15093	6.7074	7.25431	7.79191	8.32043	8.84009	9.35113	9.85374	10.3481	10.8345	11.3131	11.7841	12.2476	12.7038	13.1529
55000	4.83337	5.47019	6.09475	6.7074	7.30849	7.89833	8.47724	9.04553	9.60347	10.1514	10.6895	11.218	11.7373	12.2476	12.749	13.2419	13.7264	14.2027
60000	5.24006	5.92561	6.59688	7.25431	7.89833	8.52934	9.14773	9.75388	10.3481	10.9309	11.5024	12.063	12.6131	13.1529	13.6827	14.2027	14.7133	15.2148
65000	5.64172	6.37468	7.09123	7.79191	8.47724	9.14773	9.80385	10.4461	11.0748	11.6905	12.2935	12.8843	13.4631	14.0304	14.5866	15.1318	15.6665	16.191
70000	6.03847	6.81754	7.57797	8.32043	9.04553	9.75388	10.4461	11.1226	11.7841	12.4309	13.0636	13.6827	14.2885	14.8815	15.4621	16.0307	16.5876	17.1332
75000	6.43038	7.25431	8.05729	8.84009	9.60347	10.3481	11.0748	11.7841	12.4766	13.1529	13.8136	14.4592	15.0903	15.7072	16.3106	16.9008	17.4782	18.0433
80000	6.81754	7.68512	8.52934	9.35113	10.1514	10.9309	11.6905	12.4309	13.1529	13.8571	14.5442	15.2148	15.8694	16.5087	17.1332	17.7434	18.3398	18.9227
85000	7.20005	8.11009	8.9943	9.85374	10.6895	11.5024	12.2935	13.0636	13.8136	14.5442	15.2561	15.9502	16.6269	17.2871	17.9312	18.5599	19.1737	19.7731
90000	7.57797	8.52934	9.45232	10.3481	11.218	12.063	12.8843	13.6827	14.4592	15.2148	15.9502	16.6662	17.3637	18.0433	18.7057	19.3515	19.9814	20.5959
95000	7.95141	8.94298	9.90355	10.8345	11.7373	12.6131	13.4631	14.2885	15.0903	15.8694	16.6269	17.3637	18.0805	18.7782	19.4576	20.1192	20.7639	21.3923
100000	8.32043	9.35113	10.3481	11.3131	12.2476	13.1529	14.0304	14.8815	15.7072	16.5087	17.2871	18.0433	18.7782	19.4928	20.1879	20.8642	21.5226	22.1636
105000	8.68511	9.75388	10.7863	11.7841	12.749	13.6827	14.5866	15.4621	16.3106	17.1332	17.9312	18.7057	19.4576	20.1879	20.8976	21.5874	22.2583	22.9111
110000	9.04553	10.1514	11.218	12.2476	13.2419	14.2027	15.1318	16.0307	16.9008	17.7434	18.5599	19.3515	20.1192	20.8642	21.5874	22.2898	22.9723	23.6357
115000	9.40176	10.5437	11.6436	12.7038	13.7264	14.7133	15.6665	16.5876	17.4782	18.3398	19.1737	19.9814	20.7639	21.5226	22.2583	22.9723	23.6654	24.3385
120000	9.75388	10.9309	12.063	13.1529	14.2027	15.2148	16.191	17.1332	18.0433	18.9227	19.7731	20.5959	21.3923	22.1636	22.9111	23.6357	24.3385	25.0205
125000	10.102	11.3131	12.4766	13.5951	14.6712	15.7072	16.7055	17.6679	18.5964	19.4928	20.3587	21.1956	22.0049	22.7881	23.5463	24.2807	24.9925	25.6825
130000	10.4461	11.6905	12.8843	14.0304	15.1318	16.191	17.2103	18.1919	19.138	20.0504	20.9308	21.781	22.6025	23.3966	24.1648	24.9082	25.6281	26.3256
135000	10.7863	12.063	13.2863	14.4592	15.5849	16.6662	17.7057	18.7057	19.6684	20.5959	21.4901	22.3527	23.1854	23.9897	24.7671	25.5188	26.2462	26.9504
140000	11.1226	12.4309	13.6827	14.8815	16.0307	17.1332	18.1919	19.2094	20.1879	21.1297	22.0368	22.9111	23.7543	24.5681	25.3539	26.1133	26.8475	27.5577

Figure 5.28: Numerical outputs for fuel consumption over the fuel-air ratio and induction pressure ranges that have been transcribed into Microsoft Excel for the UDDS driving cycle.

Figure 5.29 shows the use of Microsoft excel functions to determine the fuel consumption at the induction pressure and fuel-air ratios that produce the target power for the UDDS driving cycle. The lowest hydrogen fuel consumption figure for the UDDS driving cycle is 5.34 kg/100km (20.27 GGE), at an induction pressure of 61707 Pa and a fuel air ratio of 0.35

Target power (kw):	9.4389																	
Fuel-Air Equivalence Ratio																		
Inductio	0.35	0.4	0.45	0.5	0.55	0.6	0.65	0.7	0.75	0.8	0.85	0.9	0.95	1	1.05	1.1	1.15	1.2
n	61707.3	57255.8	53772.8	50971.2	48664.5	46736.2	45112.1	43696.3	42472.6	41405.9	40468	38587.8	38052	38293.8	39448	40789.3	42158	43548.7

Fuel	2	3	4	5	6	7	8	9	10	11	12	13	14	15	16	17	18	19
(kg/100k	0.35	0.4	0.45	0.5	0.55	0.6	0.65	0.7	0.75	0.8	0.85	0.9	0.95	1	1.05	1.1	1.15	1.2
x	61707.3	57255.8	53772.8	50971.2	48664.5	46736.2	45112.1	43696.3	42472.6	41405.9	40468	38587.8	38052	38293.8	39448	40789.3	42158	43548.7
x0	60000	55000	55000	50000	50000	45000	45000	45000	40000	40000	40000	40000	40000	40000	40000	40000	40000	45000
x1	65000	60000	50000	55000	45000	50000	50000	40000	45000	45000	45000	35000	35000	35000	35000	45000	45000	40000
y0	5.24006	5.47019	6.09475	6.15093	6.7074	6.59688	7.09123	7.57797	7.25431	7.68512	8.11009	8.52934	8.94298	9.35113	9.75388	10.1514	10.5437	12.063
y1	5.64172	5.92561	5.58465	6.7074	6.09475	7.25431	7.79191	6.81754	8.05729	8.52934	8.9943	7.57797	7.95141	8.32043	8.68511	11.218	11.6436	10.9309
Y	5.37721	5.67565	5.96954	6.25902	6.54376	6.82517	7.10693	7.3797	7.65141	7.9225	8.19285	8.26065	8.55666	8.9994	9.63588	10.3197	11.0184	11.7344
GGE	20.2721	21.3972	22.5052	23.5965	24.67	25.7309	26.7931	27.8215	28.8458	29.8678	30.887	31.1426	32.2586	33.9277	36.3273	38.9055	41.5393	44.2387

Figure 5.29: Fuel consumption data for combinations of phi and induction pressure to produce the target power of 9.44 kW for the UDDS driving cycle at 1645 rpm.

Figure 5.30 offers a 'sectioned' top view of the wheel power surface plots at 20.92 kW and 9.44 kW respectively. The plot details the combinations of fuel-air equivalence ratio and induction pressure that produce the target power for the HWFET and UDDS driving cycles. It is observed that the curves are of a similar shape. Second order polynomial curve fits have been applied to each dataset, and show a similar fit to the data with R^2 values of 0.9909 and 0.9905 for the HWFET and UDDS cases respectively. In both cases, the induction pressure required for the lowest fuel air ratio ($\phi = 0.35$) is below atmospheric pressure (100 kPa).

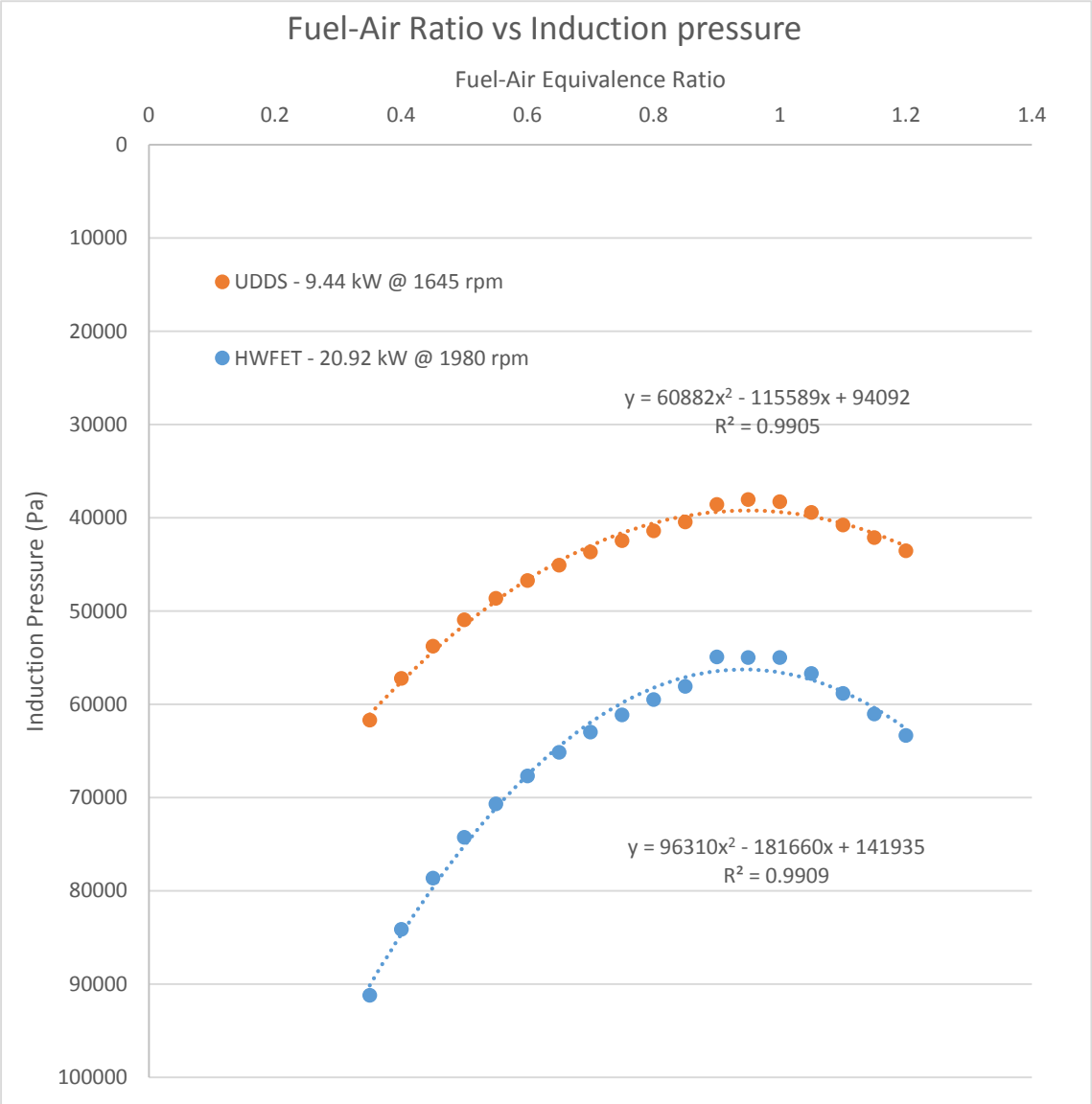

Figure 5.30: a 'sectioned' top view of the wheel power surface plots in Figures 5.18 and 5.19 at 20.92 kW and 9.44 kW.

NOx emissions

The ideal driving strategy for both the HWFET and UDDS driving cycles was identified as fuel-air equivalence ratios of 0.35 and close to WOT conditions. Recalling the review of Verhelst & Wallner in section 3.8.6, it is discussed that The combustion of lean hydrogen-air mixtures with equivalence ratios 0.35 results in extremely low amounts of NOx emissions. Figure 3.10 from section 3.8.6 confirms that increasing the fuel air equivalence ratio up to 0.5 (as could happen under heavy acceleration) would still produce extremely low NOx emissions.

5.3 Discussion

5.3.1 Overview of results

Table 5.1 shows a summary of key results from sections 5.1.3 and 5.2.3

Table 5.1: Summary of key results from sections 5.1.3 and 5.2.3

	Driving Cycle	HWFET	UDDS
Drive cycle analysis	Mean vehicle speed	77.58 km/h	31.51 km/h
	Mean engine speed	1980 rpm (1:1)	1645 rpm (1.83:1)
	Mean power required	20.92 kW	9.44 kW
	Maximum power required	38.46 kW	45.1 kW
	Average consumption (petrol)	11.08 L/100km	12.18 L/100km
	Average consumption (H2)	5.06 kg/100km	5.56 kg/100km
	GGE	19.08 L/100km	20.97 L/100km
	Theoretical endurance from 5.6 kg H2	110.67 km	100.72 km
Engine analysis	Leanest operating strategy (phi)	0.35	0.35
	Induction pressure @ target power	91227 Pa	61707
	Fuel consumption (H2)	4.18 kg/100km	5.34 kg/100km
	GGE	15.4 L/100km	20.27 L/100km
	Theoretical endurance from 5.6 kg H2	133.62 km	104.14 km

The drive cycle analysis returns a hydrogen fuel consumption of 5.06 kg/100km and 5.56 kg/100km for the extra-urban and urban driving cycles respectively, a gasoline gallon equivalent of 19.08 L/100km and 20.97 L/100km. This provides a theoretical endurance of 110.67 km and 100.7 km from vehicles proposed 5.6 kg of useable hydrogen storage for the cycles respectively.

The engine simulation model returns a hydrogen fuel consumption of 4.18 kg/100km and 5.34 kg/100km for the extra-urban and urban driving cycles respectively, a gasoline gallon equivalent of 15.4 L/100km and 20.27 L/100km. This provides a theoretical endurance of 133.62 km and 104.14 km from vehicles proposed 5.6 kg of useable hydrogen storage for the cycles respectively.

5.3.2 Drive cycle analysis

During a highway drive cycle, a vehicle will accelerate through transmission drive ratios to reach a desired speed. Any points where the vehicle then decelerates or accelerates would see another change in transmission drive ratio selected. For the HWFET drive cycle analysis, the assumption was made that the vehicle remained at a constant

transmission drive ratio (1:1), even when accelerating from rest at the start of the drive cycle. The additional code block required to automate the selection of the correct transmission drive ratio for each acceleration or velocity is significant.

The Holden 5.0L will 'comfortably' operate in each gear between engine speeds of 1,200 to 3000 rpm, corresponding to a speed range of 27-64 km/h and 47-117 km/h for second (1.83:1) and fourth (1:1) gears respectively, using the M21 4 speed transmission and a 3.08 final drive ratio specified in section 5.1.2. The analysis of velocity data point spread in section 5.1.3 showed that for the HWFET drive cycle 84.9% of the velocity points were inside one standard deviation (16.5 km/h) either side of the mean velocity of 77.6 km/h. Thus 84.9% of the data points exist between a ground speed of 61.1 to 94.1 km/h, well inside the 'comfortable' operating range of 47-117 km/h for fourth gear. The effect the data points that exist outside this range however cannot be ignored. It is predicted that the assumption of selecting 4th gear for the entire duration of the HWFET will indicate a lower fuel consumption that would be observed in reality. Further, it should be noted that the changes in acceleration across the driving cycle, including those within the 'comfortable' engine operating speeds, would likely require the selecting of a lower gear to perform the acceleration in the time between data points. This will further weaken the quality of results.

Similarly for the UDDS drive cycle, the analysis of velocity data point spread in section 5.1.3 showed that 75.2% of the velocity points were inside one standard deviation (23.7 km/h) either side of the mean velocity of 31.5 km/h, giving a range of 7.9 to 55.2 km/h. A large amount of data points then do not exist within the lower half of the 'comfortable' operating range of 27-64 km/h for second gear, with 114 data points of the 1,370 of the cycle alone are spent at rest (0 km/h). This suggests that 1st gear, which has an operating speed of between 0-38 km would be used in reality where ground speed did not exceed the lower limit of the operating speed for second gear.

Further work on improving the accuracy of the drive cycle analysis would include creating a block of code to automatically select the correct drive ratio required for the acceleration and speed at each data point. A short term method for mildly improving accuracy of results for the UDDS test would be to perform the analysis again using a fictitious transmission drive ratio that is a function of the OEM transmission drive ratios for first and second gear and the percentage of time spent in each gear.

The drive cycle analysis assumes various vehicle property coefficients and static efficiencies. For example, a lack of literature available surrounding the automotive drag coefficients for earlier generations of vehicle meant a ‘similar’ body shape of a 1979 Ford mustang coupe (Cd = 0.46) was selected as being the closest representation of the Holden HX sedan.

The static assumptions of driveline efficiency of 0.95 and fuel mass and energy densities are grounded in literature (COD, 2001; Consumer Energy Center, 2015), however the assumption of a static total vehicle efficiency is not as accurate as the thermal efficiency of the engine does not remain constant.

5.3.3 Engine Analysis

The wheel power surface plots in demonstrate a clear proportionality between induction pressure and power output. It is expect that an increase in induction pressure will increase the volume of the engine resulting in a greater volume of charge inducted, and in turn increasing the power output.

The HWFET wheel power data is proportionally higher than the UDDS data, though not by much (14 kW at max power). This is likely attributed to the similar engine speeds of 1,645 rpm and 1,980 rpm respectively. It seems counterintuitive then that the fuel consumption plot shows significantly higher values for the UDDS driving cycle. We recall however that the assumed transmission drive ratios for the UDDS and HWFET are 1.83:1 and 1:1 respectively. This means for similar power output rates, the distance travelled in the HWFET is 54% further than in the UDDS, increasing the fuel consumption rate per kilometre travelled. A limited change in thermal efficiency is also observed between the two engine speeds.

A sharp spike in power is noted at phi = 0.9, displaying the maximum powers for the HWFET and UDDS cycles at 67 kW and 53 kW respectively. Attempts to shorten the iteration phi step at this point to investigate further were met with the codes inability to resolve the ODE for those conditions. This anomaly should be investigated in further ESM revisions.

Ignition timing needs advancing at higher rpm. 5 x rpm = 1/5 duration of piston in ‘burn zone’. Vacuum advance and centrifugal device in distributor advance ignition timing. This could be accounted for in future ESM revisions.

It is assumed that a throttling event does not change temperature of inducted gas much. The air is inducted at standard temperature, and would significantly increase in temperature upon entry to the combustion chamber, however the time period is extremely small, justifying an assumption of intake temperature close to atmospheric.

6 CONCEPT DESIGN

6.1 Trade Study

Introduce areas for design or modification under storage/refuelling, delivery, Induction, ignition, combustion, exhaust, lubrication and cooling, and safety categories.

6.1.1 Storage and delivery

A review of hydrogen storage technology undertaken in section 3.4.4 found that on-board storage of hydrogen of hydrogen for transportation applications remains as one of the most technically challenging barriers to the widespread commercialization of hydrogen-fuelled vehicles (FCTO, 2015). A review of Verhelst and Walner (section 3.5.5) found that several prototype vehicles have already been produced by manufactures using compressed hydrogen as a fuel stock.

A compressed hydrogen Tank developed by EERE and Quantum Technologies that provides 5.6 kg of usable hydrogen has been selected for the design concept. The tank comes in a 258L, 350Bar or 149L, 700Bar storage options, prices at $ 2727 and $3334 at the time of publication (2010). Assessing the present day value of the storage costs is not straightforward. Changes in the price of composite or other technology since the time of publication may drastically change the actual present cost of the technology. As the retail price of the storage options were not give, it is also difficult to determine added shipping and handling costs as well as retailer mark up. A net present value for each tank arrangement considered, indexed at 2.6% pa has been assumed, and a nominal 25% additional cost for shipping, handling and retail mark up have been assumed. This price adjustment brings the total storage costs to AUD $3,872 and AUD $4,734. These assumptions are purely nominal and must not to be used to accurately predict the current

value of hydrogen storage options, but rather indicate a possible cost scenario for the sake of the investigation. Figure 6.1 provides details of the storage tank.

Figure 6.1: Compressed H2 storage tank details

6.1.2 Throttle control

A review of literature and results from engine simulation have concluded that to achieve

Key Design Assumptions: Compressed Gaseous Tanks

Design Parameter	Base Case Value	Basis/Comment
Nominal pressure	350 and 700 bar	Design assumptions based on DOE and industry input
Number of tanks	Single and dual	Design assumptions based on DOE and industry input – base case results reflect single tank systems
Tank liner	Type III (Aluminum) Type IV (HDPE)	Design assumptions based on DOE and industry input – base case results reflect Type IV tanks
Maximum (filling) pressure[1]	350-bar: 438 bar 700-bar: 875 bar	125% of nominal design pressure is assumed required for fast fills to prevent under-filling
Minimum (empty) pressure	20 bar	Discussions with Quantum, 2008
Usable H_2 storage capacity	5.6 kg	Design assumption based on ANL drive-cycle modeling for FCV 350 mile range for a midsized vehicle
Recoverable hydrogen (fraction of stored H_2)	350 bar: 93% 700 bar: 98%	ANL calculation based on hydrogen storage density at maximum and minimum pressure and temperature conditions
Tank size (water capacity)	350-bar: 258 L 700-bar: 149 L	ANL calculation for 5.6 kg useable H_2 capacity (6.0 and 5.8 kg total H_2 capacity for 350 and 700-bar tanks, respectively)
Safety factor	2.25	Industry standard specification (e.g., ISO/TS 15869)[1]
L/D ratio	3.0	Discussions with Quantum, 2008; based on the outside of the CF wrapped tank

high fuel efficiency and avoid abnormal combustion phenomena, a lean-burn operating strategy at WOT will be employed wherever possible.

This mode of operation is incompatible with the existing mechanical throttle control system and thus must be replaced with electronic throttle, also known as a ‘drive-by-wire’ system. The drive-by-wire system will use a position sensor on the accelerator and control the throttle position for both petrol and hydrogen operation through the ECU or a separate PID controller.

Development of a drive-by-wire throttle control system for the Holden 5.0L hydrogen conversion concept is an area of significant investigation. The system must:

- Use an accelerator position sensor to determine the appropriate throttle position for hydrogen and petrol operation
- Be compatible with either the standard Holden 5.0L carburettor or an aftermarket/redesigned carburettor.
- Easily switch between hydrogen and petrol modes.

It is also possible that an aftermarket cruise control system could be reprogramed to suit the needs of the hydrogen operation while leaving the mechanical acceleration mode intact for petrol operation. If this is not possible, it is worth investigating if a similar geometry or design could be used to render electronic control inactive during petrol

operation such that mechanical throttle control could remain the mode throttle control. This will further increase the independence of the two systems; reducing the likelihood that a failure of one fuel operating mode will affect the other mode.

Literature has shown that complete aftermarket cruise control kits for retro fitment classic vehicles can be purchased for USD $290 at the time of writing (Mustang 360, 2015). It is difficult to price such a control system due to uncertainty of design, and is an ideal topic for further investigation.

6.1.3 Inlet manifold

Harrop Engineering is an Australian engineering specialising in the design and manufacture of performance and racing products and have a prominent place in the history of Australian motorsport.

Harrop sell both a single and a dual plane manifold to suit Holden 5.0L engines with later model (injection) cylinder heads. Both manifolds can be machined to suit the customer's carburettor bolt pattern, and both can be machined to suit fuel injection. The manifolds are both priced at $1,089AUD at the time of writing for the EFI compatible model.

The Single plane manifold is designed for an optimum operating range of 3500-7000 rpm, and suitable for competition purposes. The carburettor bolt face is 180mm above the top plane of the engine block. Figure 6.2 shows the stock list photograph for the single plane manifold.

Figure 6.2: Harrop inlet manifold stock list photograph

Caption: Harrop Engineering Single Plane Manifold to suit Holden 5.0L with late model EFI cylinder heads only.

The dual plane manifold has been designed for low-end torque applications and street stop-and-go driving, with an optimum operating range of 1000-5500 rpm. The carburettor bolt face is 120mm above the top plane of the engine block

The low height of the dual[KPR1] plane manifold would allow for the conversion to take place with no modification to the vehicle bonnet, rendering it as the preferred option against aesthetics criteria. The dual plane manifold has a more desirable optimum engine speed operating range for the concept engine application.

6.1.4 Injectors

A literature review surrounding the selection of injectors in section 3.3.6 concluded that gaseous fuel injectors are necessary for hydrogen fuel injection. It was established that appropriate modification to valve seat material must be made to account for a lack of upper cylinder lubrication from the hydrogen combustion (compared to petroleum combustion and even other gaseous fuels) (Verhelst & Wallner, 2009). Quantum Technologies is provider of hydrogen storage and combustion solutions, and appears frequently in literature, used in the works of Sopena et al. (2010) and supply hydrogen solutions to vehicle manufacturers including Ford and Toyota (Quantum Technologies, 2015).

The Quantum alternative fuel injector is designed for multi-port internal combustion engine applications, and is tested to achieve over 150 million cycles. The Quantum injectors are low impedance devices requiring a peak and hold drive circuit. The system

H_2 and CNG Injectors

Connector:
Injector mates with AMP™ connector
Supply Voltage:
8-16 Volts typical
Resistance:
2.05 +/- 0.25 Ω at 20°C
Inductance:
3.98 +/- 0.3 mH at 1000 Hz typical
Drive Circuit:
Peak and Hold

Quantum Part #	Description
110764	Hydrogen injector
100078	CNG injector

voltage is supplied during the peak current time followed by a hold current for the remainder of the pulse (Quantum Technologies, 2015). Figure 6.3 depicts the Quantum Technologies Hydrogen injector stocklist image.

Figure 6.3: Quantum Technologies Hydrogen and CNG injectors

Quantum hydrogen injectors or similar are recommended for the Holden 5 litre hydrogen conversion concept. As pricing of hydrogen injectors is not redily available in literature, possibly due to the competitive nature of hydrogen vehicle development, it is difficult to estimate the added cost of hydrogen injectors.

A set of eight Xspurt 2000cc CNG injectors retails for about AUD $ 990 (Injectors online, 2015). Though similar in construction, it is expected that a premium would be placed on hydrogen injectors due to a lack of market availability. It is also noted that the manifold selected previously may require machining to suit the hydrogen injectors.

6.1.5 Engine Control Unit (ECU)

A review of literature surrounding strategies employed to mitigate abnormal combustion undertaken in sections 3.6 and 3.8 concluded that electronically timed fuel injection was a prerequisite for reliable combustion. The timed injection of hydrogen allows for pre-cooling of the combustion chamber, and can be used to ensure limited hydrogen remains in the manifold to reduce likelihood of backfire. (Barbir, undated; Sopena et al., 2010; Verhelst & Wallner, 2009). Timed fuel injection necessitates the use of a programmable Engine Control Unit.

In the investigation undertaken by Sopena et al. (2010) a commercial spark ignition engine was converted operate on hydrogen with a high degree of success by replacing the OEM ECU with a programmable MoteC M 400 unit. MoteC produce ECUs for a variety of applications, including performance engines and Vee Eight engines.

The MoteC M84 is suitable for a broad range of high performance engine applications, including engines with up to 8 cylinders, and available in Australia for AUD $1,925 while associated wiring loom and sensors total to $533 (MoteC, 2015). Figure 6.4 shows the MoteC M84 ECU Stocklist photo.

Figure 6.4: MoteC M84 ECU

Alternatively, should a second hand OEM Holden 5 Litre ECU were able to be reprogramed to suit the desired application, the cost would be significantly lower. Second hand, OEM 5 Litre ECUs and associated wiring looms can be obtained for as little as $300 (eBay, 2015).

It is recommended that for the Holden 5 litre hydrogen conversion concept the strategy of reprogramming the OEM ECU be investigated before use of an aftermarket ECU due to obvious price advantage and direct compatibility.

6.1.6 Spark Plugs

As identified in section 3.6.1, cold rated spark plugs are recommended to avoid the temperature of spark plug electrodes exceeding the auto-ignition limit of hydrogen . Platinum electrodes are to be avoided as platinum can act as a catalyst for the oxidation of hydrogen. Figure 6.5 shows the NGK BP6FS Holden 5.0L spark plug stock image.

Figure 6.5: NGK BP6FS Holden 5.0L spark plug stock image.

NGK BP6FS are a standard cold rated replacement plug for the Holden 5.0L. The plugs have a nickel tipped centre electrode and are commonly available from auto parts stores for AUD $6 per unit.

6.1.7 Ignition Coil

A literature review surrounding necessary modifications to ignition systems for hydrogen ICEs concluded that high voltage output, coil on plug ignition system is required (Verhelst & Wallner, 2009). Somewhat counterintuitively, a high voltage ignition is required, in spite of the low ignition energy of hydrogen, as the ignition of mixtures requires an increased secondary ignition voltage. Adopting a coil on plug ignition system satisfies this condition and avoids induction ignition in adjacent ignition cables (Verhelst & Wallner, 2009).

Ignition coils to suit the Holden 5 litre can be purchased at automotive spare parts stockists for approximately AUD $30 per each. Additional ECU programming will be required to account for a coil on plug arrangement.

6.1.8 Engine Modifications

Repower engine reconditioning suggest a typical engine rebuild for a Holden 5 litre would include the acid bathing, crack testing, decking of heads, boring and honing of cylinders

of the engine block. The crank shaft main cap bearings, camshaft bearings, and engine block welsh plugs are replaced. Camshafts and timing gear are replaced regardless of the level of wear. The connecting rods are straightened, new pistons are sourced, and the crankshaft is often ground and polished. The mating surface of the cylinder heads are resurfaced, the valve seats are replaced with harder materials to suit unleaded fuels (or gaseous fuels with low upper cylinder lubrication) (Repower Engine Reconditioning, 2015). Engine rebuilding can often cost in excess of $3,000 and is expected to last a significant percentage of the vehicles service life.

Flat top pistons both increase compression ratio and lower in-cylinder turbulence. Verhelst & Wallner cite Berger et al in suggesting that prior to installation, the top ring groove of the pistons can be applied with a special coating to reduce crevice volume and associated abnormal combustion phenomena. This is recommended for the Holden 5 litre concept design engine, and is predicted to add a very minimal cost to the rebuild of an engine.

6.1.9 Lubrication

As mentioned in section 3.6.7, the increased blowby during hydrogen combustion leads to high concentrations of hydrogen in the crankcase of up to +5% (Verhelst & Wallner, 2009). The increased concentrations of hydrogen have been found to significantly accelerate the loss of lubrication qualities of the engine oil. Verhelst & Wallner suggest that a high water concentration compatible, demulsifying, lubrication oil or synthetic oil that forms a solution with water is necessary, and an ashless oil is recommend to avoid formation of deposits (Verhelst & Wallner, 2009). It is noted that the ideal engine oil for hydrogen ICEs is not yet readily available. While some oils with a number of these qualities are available, the grades are incompatible with older engines that require heavy grade oil to maintain pressure.

For the Holden 5 litre hydrogen concept, it is recommended that the standard 20W-50 grade oil be used and changed more regularly. This is a high maintenance but low cost method to avoid deterioration of the oil lubrication properties due to acid formation from high hydrogen concentrations in the crankcase. It is possible that the installation of a venturi on the air intake to drive crankcase ventilation will significantly reduce hydrogen concentration in the crankcase and lower the frequency of oil changes required. 20W-50

Can be purchased from automotive parts stockist for approximately $25 per service (REPCO, 2015).

6.1.10 Crankcase ventilation

As highlighted in section 5.3, the Holden 5.0L conversion engine will operate at throttled conditions to maximise efficiency. As a result the pressure difference between the inlet manifold and crankcase, such as during throttled petroleum operation, is not present for some hydrogen operating strategies and cannot be used as a driving force for crankcase ventilation. This can be solved by either placing a venturi on the intake, or using other forced ventilation methods.

For simplicity and minimal cost, it is recommended that for the Holden 5 litre design concept that a venturi be placed on the intake as the driving force for crankcase ventilation.

6.1.11 Safety

A review of literature surrounding hydrogen safety conducted in section 3.7 discussed the safety requirements required for vehicles utilising hydrogen as a fuel. This section will investigate the safety implications of the system as they relate to the Holden _____. This will focus on the detection of a hydrogen leaks, emergency shut off systems and collision mitigation.

Control over ignition sources in automotive applications is limited when compared to that of laboratory testing. As investigators (Gentilhomme et al., 2012; Verhelst & Wallner, 2009) have suggested the use hydrogen detection systems combined with diluting hydrogen concentrations (providing lower ignition limits). The literature review surrounding hydrogen safety in automotive applications highlights the need for increased ventilation, hydrogen leak and flame detection, leak detection/flame sensor evaluation and placement.

Typically a number of options exist for the detection of hydrogen in a vehicular setting and these have been discussed in ____. In this instance it is suggested that __ detectors are most applicable because _. In this selection due consideration has been payed to detector response time, detection range, durability/longevity, maintenance and calibration required. These will be placed in all areas where leaks are likely to occur including connectors and intake and exhaust points, this should be confirmed and furthered through the use of CFD analysis of vehicle specific ventilation. This would more explicitly

identify the optimal locations for hydrogen leak detectors. As suggested in the literature review a concentration of 1 Vol% is a commonly used and accepted as an alarm activation threshold for hydrogen in air, which is equivalent to 25% of the lower flammability limit (Verhelst & Wallner, 2009).

Consideration must also be made for the detection of flames as it is well known that hydrogen flame is invisible to the human eye, this will be achieved through the use of __ because __.

The vehicle would also carry a small reservoir of high-pressure helium gas for purging the system of hydrogen when switching between fuel modes, and in the event of vehicle collision.

As discussed in the literature review; compressed hydrogen can build pressure inside storage vessel over time, placement of relief valves is paramount to the overall safety of the system. These would typically be _____

6.2 Cost

Using the prices determined in section 6.1, the following table (Table 6.1) is produced, showing the estimated cost of conversion.

Table 6.1: Minimum component cost estimate

Item	Cost (AUD)
Hydrogen Storage Tank (700 bar)	4,734
Throttle Controller	290
Inlet Manifold	1,089
Injectors	990
ECU	2458
Spark Plugs	48
Coil	30
Rebuild	3,000
Lubrication	25
total Mimimum cost	12664

7 CONCLUISONS

This project has been undertaken to establish the feasibility of the *System Design of a Hydrogen Induction System as a Retrofit Item Compatible with Existing Internal Combustion Engines*, by examining the conversion of a Holden 5.0L V8 to accommodate hydrogen combustion. The for the purpose of analysis, a Holden HX GTS sedan has been chosen as a case study vehicle, commonly optioned with the first generation Holden 5.0L V8.

Analysis of urban and extra-urban drive cycles provided theoretical power requirements for the operation of the vehicle for the duration of the cycles. Outputs from the drive cycle analysis were used in an engine simulation model that was modified to accommodate simulation of hydrogen combustion.

The engine simulation model returns a hydrogen fuel consumption of 4.18 kg/100km and 5.34 kg/100km for the extra-urban and urban driving cycles respectively, a gasoline gallon equivalent of 15.4 L/100km and 20.27 L/100km. This provides a theoretical endurance of 133.62 km and 104.14 km from vehicles proposed 5.6 kg of useable hydrogen storage for the cycles respectively.

An extensive literature review has identified design modifications that are required to accommodate hydrogen combustion in internal combustion engines. A trade study was used to identify the measures specifically required to adapt the Holden 5.0L case study engine to dual hydrogen/petrol operation modes. The modifications and additional components required were costed where possible, resulting in an estimated minimum cost of AUD $12,664 in parts for the conversion.

8 Other Considerations and Further Work

8.1 Ethical considerations

There exists a significant ethical advantage in the adoption of hydrogen internal combustion over conventional hydrocarbon fuels in the reduction of harmful tailpipe emissions. The clean burning properties of hydrogen examined in this investigation can be exploited to produce emissions of NOx in super low emission vehicle category. Greenhouse gasses emission levels are negligible due to no carbon content in the fuel.

However, for the transition to hydrogen fuel to have a net reduction of emission levels, significant increase in the renewable production of hydrogen is required. A well-to-wheel analysis of hydrogen internal combustion energy is an area of significant further work.

Beyond the ethical use of hydrogen from a safety perspective, there is also ethical questions raised about the implementation of hydrogen technology it what is an already obsolete vehicle platform. The vehicles of the past do not have the same level of safety features that are now expected as standard on new vehicles. These include crumple zones, traction control, air bags, reverse parking cameras and ABS, and are likely to soon include forward collision warning, city breaking, radar cruise control, forward collision avoidance. The question of whether a hydrogen conversion classic vehicle is a vehicle of the future is simple to answer, however some questions that will be asked include:

- Is the implementation of hydrogen combustion to existing petrol internal combustion engines as a retrofit item stretching the life of an already obsolete technology?;

- Is such a car compatible with the future of personal transport?; and

- Is the conversion of the vehicles of yesteryear to hydrogen operation an ethical process?

These questions cannot be easily answered and are suitable research questions for further work.

8.2 Further work

This section outlines areas of potential further work outlined in the investigation

Throttle Control: As outlined in section 6.1.2, the development of a throttle control system compatible with carburetted petrol induction and hydrogen fuel injection is a significant area of study.

Refine engine analysis: As outlined in section 5.3, the drive_cycle_analysis.m and Holden_5L_Analysis.m Matlab models can be improved through the automation of appropriate gear selection for the various driving conditions.

Market uptake: An investigation into potential market uptake would be required before further work towards a prototype is undertaken.

Prototyping: the development of a prototype hydrogen conversion engine as performed by Sopena et al. (2010), using a Holden 5.0 Litre to model performance and emission characteristics is a significant and exciting area of further study.

Risk Analysis: Evaluation of risk posed by hydrogen-fuelled vehicles via review of literature and evaluation of a concept design a necessary area of investigation for the furthering of the Holden 5.0L hydrogen conversion concept. This would include the CFD simulation of in-car ventilation systems to identify optimal placement of hydrogen detectors, and design of optimum on-board storage arrangement.

REFERENCES

AA1Car Auto Diagnosis. (2015). Manifold Absolute Pressure MAP Sensors. 2015, from http://www.aa1car.com/library/map_sensors.htm

Bakker, S., van Lente, H., & Meeus, M. T. H. (2012). Dominance in the prototyping phase—The case of hydrogen passenger cars. *Research Policy, 41*(5), 871-883. doi: http://dx.doi.org/10.1016/j.respol.2012.01.007

Barbir, F. (undated). REVIEW OF HYDROGEN CONVERSION TECHNOLOGIES. *Clean Energy Research Institute*.

Brundell-Freij, K., & Ericsson, E. (2005). Influence of street characteristics, driver category and car performance on urban driving patterns. *Transportation Research Part D: Transport and Environment, 10*(3), 213-229. doi: http://dx.doi.org/10.1016/j.trd.2005.01.001

Buttsworth, D. (2007). *Ahrind Engine Simulation Model.* University of Southern Queensland.

Çengel, Y., & Boles, M. (2001). *Thermodynamics: An Engineering Approach* (Vol. 7th). Boston: McGraw-Hill.

COD, C. o. t. D. (2001). Hydrogen Properties. 2015, from http://energy.gov/sites/prod/files/2014/03/f12/fcm01r0.pdf

Comcare. (2015). Officewise A guide to health and safety in the office. Retrieved May 2015, from https://www.comcare.gov.au/__data/assets/pdf_file/0006/39570/Officewise_OHS1_Apr_10.pdf

Consumer Energy Center. (2015). Energy Losses in a Vehicle. 2015, from http://www.consumerenergycenter.org/transportation/consumer_tips/vehicle_energy_losses.html

dieselnet. (2015). Emission Test Cycles FTP-72 (UDDS). 2015, from http://www.dieselnet.com/standards/cycles/ftp72.php

Duan et al., J. D. F. L., Baigang Sun,. (2013). Backfire control and power enhancement of a hydrogen internal combusiton engine. *International Journal of Hydrogen Energy*.

eBay. (2015). product search: 'Holden 5 v8 ECU'.

EERE. (2010). Technical Assessment of Compressed Hydrogen Storage Tank Systems for Automotive Applications from https://www1.eere.energy.gov/hydrogenandfuelcells/pdfs/compressedtank_storage.pdf

Engineering Toolbox. (2015). Rolling Resistance. 2015, from http://www.engineeringtoolbox.com/rolling-friction-resistance-d_1303.html

EPA. (2015). Dynamometer Drive Schedules. 2015, from http://www3.epa.gov/nvfel/testing/dynamometer.htm

FCTO, F. C. T. O.-. (2015). Hydrogen.

Gentilhomme, O., Proust, C., Jamois, D., Tkatschenko, I., Cariteau, B., Studer, E., . . . Anselmet, F. (2012). Data for the evaluation of hydrogen risks onboard vehicles: Outcomes from the French project drive. *International Journal of Hydrogen Energy, 37*(22), 17645-17654. doi: http://dx.doi.org/10.1016/j.ijhydene.2012.04.147

GoAuto. (2009). We drive Mazda's environmentally friendly RX-8 Hydrogen RE sportscar. Retrieved May 2015, 2015, from http://www.goauto.com.au/mellor/mellor.nsf/story2/FC92724E2C2E0971CA25765A008343AB

Gutenberg. (2015). AUTOMOBILE DRAG COEFFICIENTS. 2015, from http://self.gutenberg.org/articles/automobile_drag_coefficients

HSW, H. S. W. (2015a). How Fuel Injection Systems Work. May 2015, from http://auto.howstuffworks.com/fuel-injection.htm

HSW, H. s. W. (2015b). How Rotary Engines Work. Retrieved May 2015, from http://auto.howstuffworks.com/rotary-engine.htm

HSW, H. s. w. (2015c). How Superchargers Work. 2015, from http://auto.howstuffworks.com/supercharger1.htm

Injectors online. (2015). 2000cc Xspurt Injectors x 8. 2015, from https://www.injectorsonline.com.au/2000cc-xspurt-injectors-x-8.html?GST=1&gclid=CLjt7I6X5sgCFQN9vQodaHMM7w

JEGS Performance. (2015). Superchargers. 2015, from http://www.jegs.com/tech-articles/superchargers.html

Judge, A. (1955). *Modern Petrol Engines*. 37 essex street, london: Chapman & Hall LTD.

Malpress, R. (2011). *Spark Ignition Internal Combustion Engine Efficiency Improvement - a Variable Compression Ratio Option.* (Doctor of Philosophy), University of Southern Queensland.

Mazda. (2015). Hydrogen Vehicle. Retrieved May 2015, 2015, from http://www2.mazda.com/en/technology/env/hre/

MoteC. (2015). M84. 2015, from http://www.motec.com.au/m84/m84overview/

Mustang 360. (2015). How to: Add-On Cruise Control For Vintage Ford Mustangs. 2015, from http://www.mustangandfords.com/how-to/interior-electrical/1305-how-to-add-on-cruise-control-for-vintage-ford-mustangs/

Quantum Technologies. (2015). Alternative Fuel Injectors. 2015, from http://www.qtww.com/assets/u/InjectorBrochure2.pdf

REPCO. (2015). Product Catalogue.

Repower Engine Reconditioning. (2015). Holden 5.0L V8 Engine Rebuild.

Sopena, C., Diéguez, P. M., Sáinz, D., Urroz, J. C., Guelbenzu, E., & Gandía, L. M. (2010). Conversion of a commercial spark ignition engine to run on hydrogen: Performance comparison using hydrogen and gasoline. *International Journal of Hydrogen Energy, 35*(3), 1420-1429. doi: http://dx.doi.org/10.1016/j.ijhydene.2009.11.090

SprintGas. (2015). Frequently asked questions. Retrieved March, 2015, from http://www.sprintgas.com.au/faqs_page.html

UBC, U. o. B. C. (2015). Energy Use in Cars 3: Rolling Resistance. 2015, from http://c21.phas.ubc.ca/article/energy-use-cars-3-rolling-resistance

Uniqe Cars & Parts. (2015). Holden HX Technical Specifications. 2015, from http://www.uniquecarsandparts.com.au/holden_HX_technical_specifications.php

Verhelst, S., & Wallner, T. (2009). Hydrogen-fueled internal combustion engines. *Progress in Energy and Combustion Science, 35*(6), 490-527. doi: http://dx.doi.org/10.1016/j.pecs.2009.08.001

Yvon, K., & Lorenzoni, J. L. (2006). Hydrogen-powered lawn mower: 14 years of operation. *International Journal of Hydrogen Energy, 31*(12), 1763-1767. doi: http://dx.doi.org/10.1016/j.ijhydene.2005.12.012

APPENDICIES

Appendix A – Project Specification

University of Southern Queensland

FACULTY OF ENGINEERING AND SURVEYING

ENG4111/4112 Research Project
PROJECT SPECIFICATION

FOR: **Kieran Patrick RICHARDSON**

TOPIC: System design of a hydrogen induction system as a retrofit item compatible with existing internal combustion engines.

SUPERVISOR: Ray Malpress/David Buttsworth

PROJECT AIM: To establish the feasibility of utilising existing internal combustion engines as a platform for a hydrogen fuel conversion, as a bridging technology between petrol internal combustion and hydrogen fuel cell vehicles.

PROGRAMME: (issue A, 25 Feb 2015)

1) Research background information relating to existing hydrogen powered vehicles' internal combustion engines (ICEs), technology hurdles associated with fuel storage, and the challenges associated with the conversion of existing ICE engines to operate on hydrogen fuel.
2) Perform modelling to design a hydrogen induction system for an existing petrol internal combustion engine as a retrofit item through the use of Creo Parametric and Simulate modelling programs. The designs will be informed by other modelling where necessary.
3) Building on some existing rudimentary matlab engine simulation models, by exploring techniques to improve the scope of the models including features such as friction, gas flow losses, heat transfer and other phenomenon that would improve the models ability to accurately predict the performance of the proposed hydrogen ICE.
4) Analyse system efficacy.
5) Perform appropriate materials/component selection to analyse the costs in fabrication and build processes.
6) Submit an academic dissertation on the research.

As time permits

7) Acquire materials to fabricate, assemble and commission one or more sub-systems contributing to the overall engine arrangement, working towards an appropriate scale model for use on a small capacity ICE to obtain empirical data.
8) Analyse empirical data.

AGREED:

_____ (student) _____, _____ (supervisors)

__/__/__ __/__/__ __/__/__

Appendix B – Research Risk Assessment

While hazards in office environments for researchers may not always be as obvious as those in experimental environments, researchers may also face a range of health and safety issues, including prolonged repetitive work, moving heavy loads, inadequate lighting and cramped or unsafe working areas. This section raises the reader's awareness of health and safety issues involving the use of computers that may be experienced in the course of the research, and to offer solutions and advice to these issues (Comcare, 2015).

Working with computers

Good design of computer hardware layout, the environment and furniture, and work practices minimises any negative effects of computer use. This section discusses the health and safety issues associated with computer usage (Comcare, 2015).

Hardware and peripherals.

The desktop or tower holds the hard drive and other hardware needed to run software programs. It is important to consider how often the user needs to access the desktop and position it accordingly. Laptop computers are designed for short term or mobile use. The portability of laptops results in them being used in a variety of situations and settings where there is limited capacity to adjust the desk. This can lead to working at an unsuitable height. Lack of adjustability can result in arms being held too high and neck being too bent. If this position is adopted frequently, or for long periods of time, discomfort may result. Adverse effects of using laptops can be mitigated by docking the laptop into a desktop computer at an adjustable station; connecting into existing more ergonomic equipment ie mouse, or keyboard; transferring work to a desktop where practicable; being aware of posture; and learning to type to avoid time spent looking down. Voice recognition software transfers voice information to electrical format. The use of voice recognition can reduce the reliance on keyboards (Comcare, 2015).

Keyboards

Keyboard types can vary according to the task being performed. Generally, the more a keyboard is used, the greater the risk of discomfort. However, regular breaks, adjustable and ergonomic equipment and furniture are important considerations for people who are required to use keyboards extensively for work (Comcare, 2015). Placement of the keyboard should be aligned with the computer and directly in front of the user such that there is no need to twist or rotate to use it. It should be placed at a comfortable distance from the edge of the desk. Reference documents should not be placed between the

keyboard and the edge of the desk. The feet at the rear of the keyboard should be kept as low as practicable, to minimise the angle and height of the keyboard to reduce unnecessary loading of shoulder muscles and wrists. Split keyboards are split in half and angled so as to better reflect the more natural hand position while keying. Where possible, use of split keyboards are recommended. Separate numerical pads are recommended for any user requiring frequent use of number keys (Comcare, 2015).

Mouse Computer

mice come in a variety of shapes and sizes, with features such as scrolling wheels and auxiliary buttons. The key criteria for a mouse should include the placement of the users hand and upper limb in a neutral position; support weight of the arm by desk and not the user; keeping the wrist as flat as practicable; allowing fingers to rest on buttons rather than elevated; and choosing a mouse to fit the users hand . It is good practice to learn to use a mouse in both hands, and periodically switching hands to reduce repetitive motion. Many users can be reluctant to try this, but the skills are developed quickly in most cases. Sustained hand postures during use of the mouse can be greatly reduced via use of keyboard shortcuts, changing hands, and by moving the mouse towards the middle of the desk (Comcare, 2015).

Monitors

LCD computer screens have become an increasingly popular technology. LCD's offer many advantages including greater posture variety; freedom from flicker and geometric image distortions; uniform screen brightness and reduced glare; thinner and lighter displays that allow for greater room for adjustability of hardware (Comcare 2015). Using computer screens for extended time periods increases pressure on eyes and necks of users. The following precautions can be followed to mitigate these effects: screen should be placed an arm's length away from the employee at eye level; locate monitor directly in front of user; place the screen with a tilt of 15 degrees up from vertical; reducing intervals spent in front of a computer to 30 minutes at a time (Comcare, 2015).

Health effects

Eye strain can be caused by inadequate lighting or small print over long periods of time. It is generally believed that visual fatigue does not deteriorate long-term vision, although it can cause irritation, watering, reddening, blurred vision or even headaches. The risk of eye strain can be reduced by looking away from the computer to a far spot or walking

away from the screen and performing eye exercises. Dry air conditioned environments can also cause eye discomfort (Comcare, 2015).

APPENDIX C - Ahrind Engine Simulation script files – Buttsworth (2007)

Appendix C1 – ahrind.m – Engine Simulation (modified)

```
% ahrind.m
%
% Script file to determine the performance of a fuel inducted engine
% based on a (user-specified) arbitrary heat release profile as a
% function of crank angle.
% Method closely follows that of:
% Ferguson, C.R., 1986, "Internal Combustion Engines", Wiley.
% ********************************************************************
% input:
% enginedata.m - this is another script file that defines all of the
% relevant engine parameters and operating conditions.
% output:
% ahrind.mat - this file contains all of the variables.  For plotting
% the results, see the example script file plotresults.m
% ********************************************************************

timestart=cputime;

global b stroke eps r Cblowby f fueltype airscheme ϕ RPM ...
  thetas thetab omega ...
  heattransferlaw hcu hcb ...
  Tw theta1 Vtdc Vbdc mass1 ...
  p1 T1 V1

% load the engine parameters and initial conditions
enginedata

% integration parameters
dtheta=1*pi/180;
options=odeset('RelTol',1e-3);

% integration during compression phase
[thetacomp,pTuWQlHl]=ode45('RatesComp', ...
  [-pi:dtheta:thetas],[p1 T1 0 0 0],options);

% specification of initial conditions at start of combustion phase
% b - beginning of combustion
pb=interp1(thetacomp,pTuWQlHl(:,1),thetas);
Tub=interp1(thetacomp,pTuWQlHl(:,2),thetas);
Tbb=Tadiabatic(pb,Tub,ϕ,f,fueltype,airscheme);
Wb=interp1(thetacomp,pTuWQlHl(:,3),thetas);
Qlb=interp1(thetacomp,pTuWQlHl(:,4),thetas);
Hlb=interp1(thetacomp,pTuWQlHl(:,5),thetas);

% integration during combustion phase
[thetacomb,pTbTuWQlHl]=ode45('RatesComb', ...
  [thetas:dtheta:thetas+thetab],[pb Tbb Tub Wb Qlb Hlb],options);

% specification of initial conditions at start of expansion phase
% e - end of combustion / start of expansion
pe=interp1(thetacomb,pTbTuWQlHl(:,1),thetas+thetab);
Tbe=interp1(thetacomb,pTbTuWQlHl(:,2),thetas+thetab);
We=interp1(thetacomb,pTbTuWQlHl(:,4),thetas+thetab);
Qle=interp1(thetacomb,pTbTuWQlHl(:,5),thetas+thetab);
```

```
Hle=interp1(thetacomb,pTbTuWQlHl(:,6),thetas+thetab);

% integration during expansion phase
[thetaexp,pTbWQlHl]=ode45('RatesExp', ...
   [thetas+thetab:dtheta:pi],[pe Tbe We Qle Hle],options);

% error checks
mass4=mass1*exp(-Cblowby*2*pi/omega);
p4=interp1(thetaexp,pTbWQlHl(:,1),pi);
T4=interp1(thetaexp,pTbWQlHl(:,2),pi);
W4=interp1(thetaexp,pTbWQlHl(:,3),pi);
Ql4=interp1(thetaexp,pTbWQlHl(:,4),pi);
Hl4=interp1(thetaexp,pTbWQlHl(:,5),pi);
[h4,u4,v4,s4,Y4,cp4,dlvlT4,dlvlp4]= ...
   farg(p4,T4,ϕ,1,fueltype,airscheme);
U4=u4*mass4;
error1=1-v4*mass4/Vbdc;
error2=1+W4/(U4-U1+Ql4+Hl4);

% indicated mean effective pressure and thermal efficiency
imep=W4/(pi*b^2/4*stroke);
eta=W4/mass1*(1+ϕ*0.06548*(1-f))/ϕ/0.06548/(1-f)/47870/1e3;

% calcuate the heat flux in W/m^2
qcomp=calcq(thetacomp,pTuWQlHl,'comp'); % compression
qcombu=calcq(thetacomb,pTbTuWQlHl,'combu'); % combustion-unburned zone
qcombb=calcq(thetacomb,pTbTuWQlHl,'combb'); % combustion-burned zone
qexp=calcq(thetaexp,pTbWQlHl,'exp'); % expansion

timefinish=cputime;
timetaken=timefinish-timestart;

% save all data
save ahrind.mat
```

Appendix C2 – airdata.m – Thermodynamic Properties of Air/combustion Products

```
function A=airdata(scheme);
%
% A=airdata(scheme)
%
% Routine to specify the thermodynamic properties of air and
% combustion products.
% Data taken from:
% 1. Gordon, S., and McBride, B. J., 1971, "Computer Program for
% Calculation of Complex Chemical Equilibrium Composition, Rocket
% Performance, Incident and Reflected Shocks, and Chapman-Jouguet
% Detonations," NASA SP-273.  As reported in Ferguson, C. R., 1986,
% "Internal Combustion Engines", Wiley.
% 2. Kee, R. J., et al., 1991, "The Chemkin Thermodynamic Data Base",
% Sandia Report, SAND87-8215B. As reported in
% Turns, S. R., 1996, "An Introduction to Combustion:
% Concepts and Applications", McGraw-Hill.
% **************************************************************************
% input:
% scheme switch:
% 'GMcB_low' - Gordon and McBride 300 < T < 1000 K
% 'GMcB_hi' - Gordon and McBride 1000 < T < 5000 K
% 'Chemkin_low' - Chemkin 300 < T < 1000 K
```

```
% 'Chemkin_hi' - Chemkin 1000 < T < 5000 K
% output:
% A - matrix of polynomial coefficients for cp/R, h/RT, and s/R
% of the form h/RT=a1+a2*T/2+a3*T^2/3+a4*T^3/4+a5*T^4/5*a6/T (for
% example) where T is expressed in K
% columns 1 to 7 are coefficients a1 to a7, and
% rows 1 to 10 are species CO2 H2O N2 O2 CO H2 H O OH and NO
% ****************************************************************

switch scheme
case 'GMcB_low'
  A=[ 0.24007797E+01  0.87350957E-02 -0.66070878E-05  0.20021861E-08 ...
      0.63274039E-15 -0.48377527E+05  0.96951457E+01
      0.40701275E+01 -0.11084499E-02  0.41521180E-05 -0.29637404E-08 ...
      0.80702103E-12 -0.30279722E+05 -0.32270046E+00
      0.36748261E+01 -0.12081500E-02  0.23240102E-05 -0.63217559E-09 ...
     -0.22577253E-12 -0.10611588E+04  0.23580424E+01
      0.36255985E+01 -0.18782184E-02  0.70554544E-05 -0.67635137E-08 ...
      0.21555993E-11 -0.10475226E+04  0.43052778E+01
      0.37100928E+01 -0.16190964E-02  0.36923594E-05 -0.20319674E-08 ...
      0.23953344E-12 -0.14356310E+05  0.29555350E+01
      0.30574451E+01  0.26765200E-02 -0.58099162E-05  0.55210391E-08 ...
     -0.18122739E-11 -0.98890474E+03 -0.22997056E+01
      0.25000000E+01  0.00000000E+00  0.00000000E+00  0.00000000E+00 ...
      0.00000000E+00  0.25471627E+05 -0.46011762E+00
      0.29464287E+01 -0.16381665E-02  0.24210316E-05 -0.16028432E-08 ...
      0.38906964E-12  0.29147644E+05  0.29639949E+01
      0.38375943E+01 -0.10778858E-02  0.96830378E-06  0.18713972E-09 ...
     -0.22571094E-12  0.36412823E+04  0.49370009E+00
      0.40459521E+01 -0.34181783E-02  0.79819190E-05 -0.61139316E-08  ...
      0.15919076E-11  0.97453934E+04  0.29974988E+01];
case 'GMcB_hi'
  A=[ 0.44608041E+01  0.30981719E-02 -0.12392571E-05  0.22741325E-09 ...
     -0.15525954E-13 -0.48961442E+05 -0.98635982E+00
      0.27167633E+01  0.29451374E-02 -0.80224374E-06  0.10226682E-09 ...
     -0.48472145E-14 -0.29905826E+05  0.66305671E+01
      0.28963194E+01  0.15154866E-02 -0.57235277E-06  0.99807393E-10 ...
     -0.65223555E-14 -0.90586184E+03  0.61615148E+01
      0.36219535E+01  0.73618264E-03 -0.19652228E-06  0.36201558E-10 ...
     -0.28945627E-14 -0.12019825E+04  0.36150960E+01
      0.29840696E+01  0.14891390E-02 -0.57899684E-06  0.10364577E-09 ...
     -0.69353550E-14 -0.14245228E+05  0.63479156E+01
      0.31001901E+01  0.51119464E-03  0.52644210E-07 -0.34909973E-10 ...
      0.36945345E-14 -0.87738042E+03 -0.19629421E+01
      0.25000000E+01  0.00000000E+00  0.00000000E+00  0.00000000E+00 ...
      0.00000000E+00  0.25471627E+05 -0.46011763E+00
      0.25420596E+01 -0.27550619E-04 -0.31028033E-08  0.45510674E-11 ...
     -0.43680515E-15  0.29230803E+05  0.49203080E+01
      0.29106427E+01  0.95931650E-03 -0.19441702E-06  0.13756646E-10 ...
      0.14224542E-15  0.39353815E+04  0.54423445E+01
      0.31890000E+01  0.13382281E-02 -0.52899318E-06  0.95919332E-10 ...
     -0.64847932E-14  0.98283290E+04  0.67458126E+01];
case 'Chemkin_low'
  A=[ 0.02275724E+02  0.09922072E-01 -0.10409113E-04  0.06866686E-07 ...
     -0.02117280E-10 -0.04837314E+06  0.10188488E+02
      0.03386842E+02  0.03474982E-01 -0.06354696E-04  0.06968581E-07 ...
     -0.02506588E-10 -0.03020811E+06  0.02590232E+02
      0.03298677E+02  0.14082404E-02 -0.03963222E-04  0.05641515E-07 ...
     -0.02444854E-10 -0.10208999E+04  0.03950372E+02
      0.03212936E+02  0.11274864E-02 -0.05756150E-05  0.13138773E-08 ...
```

```
    -0.08768554E-11 -0.10052490E+04  0.06034737E+02
     0.03262451E+02  0.15119409E-02 -0.03881755E-04  0.05581944E-07 ...
    -0.02474951E-10 -0.14310539E+05  0.04848897E+02
     0.03298124E+02  0.08249441E-02 -0.08143015E-05 -0.09475434E-09 ...
     0.04134872E-11 -0.10125209E+04 -0.03294094E+02
     0.02500000E+02  0.00000000E+00  0.00000000E+00  0.00000000E+00 ...
     0.00000000E+00  0.02547162E+06 -0.04601176E+01
     0.02946428E+02 -0.16381665E-02  0.02421031E-04 -0.16028431E-08 ...
     0.03890696E-11  0.02914764E+06  0.02963995E+02
     0.03637266E+02  0.01850910E-02 -0.16761646E-05  0.02387202E-07 ...
    -0.08431442E-11  0.03606781E+05  0.13588605E+01
     0.03376541E+02  0.12530634E-02 -0.03302750E-04  0.05217810E-07 ...
    -0.02446262E-10  0.09817961E+05  0.05829590E+02];
case 'Chemkin_hi'
  A=[ 0.04453623E+02  0.03140168E-01 -0.12784105E-05  0.02393996E-08 ...
    -0.16690333E-13 -0.04896696E+06 -0.09553959E+01
     0.02672145E+02  0.03056293E-01 -0.08730260E-05  0.12009964E-09 ...
    -0.06391618E-13 -0.02989921E+06  0.06862817E+02
     0.02926640E+02  0.14879768E-02 -0.05684760E-05  0.10097038E-09 ...
    -0.06753351E-13 -0.09227977E+04  0.05980528E+02
     0.03697578E+02  0.06135197E-02 -0.12588420E-06  0.01775281E-09 ...
    -0.11364354E-14 -0.12339301E+04  0.03189165E+02
     0.03025078E+02  0.14426885E-02 -0.05630827E-05  0.10185813E-09 ...
    -0.06910951E-13 -0.14268350E+05  0.06108217E+02
     0.02991423E+02  0.07000644E-02 -0.05633828E-06 -0.09231578E-10 ...
     0.15827519E-14 -0.08350340E+04 -0.13551101E+01
     0.02500000E+02  0.00000000E+00  0.00000000E+00  0.00000000E+00 ...
     0.00000000E+00  0.02547162E+06 -0.04601176E+01
     0.02542059E+02 -0.02755061E-03 -0.03102803E-07  0.04551067E-10 ...
    -0.04368051E-14  0.02923080E+06  0.04920308E+02
     0.02882730E+02  0.10139743E-02 -0.02276877E-05  0.02174683E-09 ...
    -0.05126305E-14  0.03886888E+05  0.05595712E+02
     0.03245435E+02  0.12691383E-02 -0.05015890E-05  0.09169283E-09 ...
    -0.06275419E-13  0.09800840E+05  0.06417293E+02];
end
```

Appendix C3 – calcq.m – Calculate Heat Flux

```
function q=calcq(theta,pTarray,phase);
%
% calculation of the heat flux (W/m^2) from the data generated
% by ahrind.
% theta is an array of crank angles
% pTarray is the corresponding array of pressure, Temperature,
% Work, etc data as generated by running arhind.m
% phase is a switch indicating the part of the cycle:
% 'comp' - compression phase
% 'combu' - combustion phase, unburned gas zone
% 'combb' - combustion phase, burned gas zone
% 'exp' - expansion phase

global b stroke eps r ...
  omega ...
  heattransferlaw hcu hcb ...
  Tw Vtdc Vbdc ...
  p1 T1 V1

switch phase
```

```
case 'comp'
   p=pTarray(:,1);
   T=pTarray(:,2);
   hc=hcu;
   C2=0;
case 'combu'
   p=pTarray(:,1);
   T=pTarray(:,3);
   hc=hcu;
   C2=3.24e-3;
case 'combb'
   p=pTarray(:,1);
   T=pTarray(:,2);
   hc=hcb;
   C2=3.24e-3;
case 'exp'
   p=pTarray(:,1);
   T=pTarray(:,2);
   hc=hcb;
   C2=3.24e-3;
end

switch heattransferlaw
case 'constant'
   hcoeff=hc;
case 'Woschni'
   V=Vtdc*(1+(r-1)/2*(1-cos(theta)+ ...
     1/eps*(1-(1-eps^2*sin(theta).^2).^0.5)));
   upmean=omega*stroke/pi; % mean piston velocity
   Vs=Vbdc-Vtdc;
   k=1.3;
   C1=2.28;
   pm=p1*(V1./V).^k; % motoring pressure
   hcoeff=hc*130*b^(-0.2)*T.^(-0.53).*(p/100e3).^(0.8).* ...
        (C1*upmean+C2*Vs*T1/p1/V1*(p-pm)).^(0.8);
end

q=hcoeff.*(T-Tw);
```

Appendix C4 – ecp.m – Equilibrium Combustion Products

```
function [h,u,v,s,Y,cp,dlvlT,dlvlp]=ecp(p,T,ϕ,fueltype,airscheme,Yguess);
%
% [h,u,v,s,Y,cp,dlvlT,dlvlp]=ecp(p,T,ϕ,fueltype,airscheme,Yguess)
%
% Routine to determine the equilibrium state of combustion products.
% Method closely follows that of:
% 1. Ferguson, C.R., 1986, "Internal Combustion Engines", Wiley, p122;
% which uses the method described by:
% 2. Olikara, C., and Borman, G.L., 1975, "A Computer Program for
% Calculating Properties of Equilibrium Combustion Products with
% Some Applications to I.C. Engines", SAE Paper 750468.
% ****************************************************************
% input:
% p,T,ϕ - pressure (Pa), temperature (K), and equivalence ratio
% fueltype - 'gasoline', 'diesel', etc - see fueldata.m for full list
% airscheme - 'GMcB' (Gordon and McBride) or 'Chemkin'
% Yguess - (optional) initial estimate for mole fractions of the
% species CO2 H2O N2 O2 CO H2 H O OH and NO
```

```
% output:
% h - enthalpy (J/kg), u - internal energy (J/kg),
% v - specific volume (m^3/kg), s - entropy (J/kgK),
% Y - mole fractions of 10 species, cp - specific heat (J/kgK),
% dlvlT - partial derivative of log(v) wrt log(T)
% dlvlp - partial derivative of log(v) wrt log(p)
% ************************************************************************

[alpha,beta,gamma,delta,Afuel]=fueldata(fueltype);
switch airscheme
case 'GMcB'
   A0=airdata('GMcB_hi');
case 'Chemkin'
   A0=airdata('Chemkin_hi');
end

% Equilibrium constant data from Olikara and Borman via Ferguson
Kp=[ 0.432168E+00 -0.112464E+05  0.267269E+01 -0.745744E-04  0.242484E-08
     0.310805E+00 -0.129540E+05  0.321779E+01 -0.738336E-04  0.344645E-08
    -0.141784E+00 -0.213308E+04  0.853461E+00  0.355015E-04 -0.310227E-08
     0.150879E-01 -0.470959E+04  0.646096E+00  0.272805E-05 -0.154444E-08
    -0.752364E+00  0.124210E+05 -0.260286E+01  0.259556E-03 -0.162687E-07
    -0.415302E-02  0.148627E+05 -0.475746E+01  0.124699E-03 -0.900227E-08];

MinMol=1e-25;
tol=3e-12;

Ru=8314.34; % J/kmol.K
M=[44.01 18.02 28.008 32.000 28.01 2.018 1.009 16 17.009 30.004]'; % kg/kmol

dcdT=zeros(4,1);
dcdp=zeros(4,1);
dfdT=zeros(4,1);
dfdp=zeros(4,1);
dYdT=zeros(10,1);
dYdp=zeros(10,1);
B=zeros(4,1);

% check if solid carbon will form
eps=0.210/(alpha+0.25*beta-0.5*gamma);
if ϕ>(0.210/eps/(0.5*alpha-0.5*gamma))
   error('ϕ too high - c(s) and other species will form');
end

if nargin==5 % no Yguess so estimate the composition using farg
   [h,u,v,s,Y,cp,dlvlT,dlvlp]=farg(p,T,ϕ,1,fueltype,airscheme);
   Y(7:10)=ones(4,1)*MinMol; % since farg only returns first 6 species
else
   Y=Yguess;
end

% evaluate constants
patm=p/101.325e3; % convert Pa to atmospheres
TKp=[log(T/1000) 1/T 1 T T^2]';
K=10.^(Kp*TKp);
c=K.*[1/sqrt(patm) 1/sqrt(patm) 1 1 sqrt(patm) sqrt(patm)]';
d=[beta/alpha (gamma+0.42/eps/ϕ)/alpha (delta+1.58/eps/ϕ)/alpha]';

if abs(ϕ-1)<tol
   ϕ=ϕ*(1+tol*sign(ϕ-1));
```

```
end

i=find(Y<MinMol);
Y(i)=ones(length(i),1)*MinMol;

DY3to6=2*tol*ones(4,1);
MaxIter=500;
MaxVal=max(abs(DY3to6));
Iter=0;
DoneSome=0;

while (Iter<MaxIter)&((MaxVal>tol)|(DoneSome<1))
  Iter=Iter+1;
  if Iter>2,
    DoneSome=1;
  end

  D76=0.5*c(1)/sqrt(Y(6));
  D84=0.5*c(2)/sqrt(Y(4));
  D94=0.5*c(3)*sqrt(Y(6)/Y(4));
  D96=0.5*c(3)*sqrt(Y(4)/Y(6));
  D103=0.5*c(4)*sqrt(Y(4)/Y(3));
  D104=0.5*c(4)*sqrt(Y(3)/Y(4));
  D24=0.5*c(5)*Y(6)/sqrt(Y(4));
  D26=c(5)*sqrt(Y(4));
  D14=0.5*c(6)*Y(5)/sqrt(Y(4));
  D15=c(6)*sqrt(Y(4));
  A(1,1)=1+D103;
  A(1,2)=D14+D24+1+D84+D104+D94;
  A(1,3)=D15+1;
  A(1,4)=D26+1+D76+D96;
  A(2,1)=0;
  A(2,2)=2*D24+D94-d(1)*D14;
  A(2,3)=-d(1)*D15-d(1);
  A(2,4)=2*D26+2+D76+D96;
  A(3,1)=D103;
  A(3,2)=2*D14+D24+2+D84+D94+D104-d(2)*D14;
  A(3,3)=2*D15+1-d(2)*D15-d(2);
  A(3,4)=D26+D96;
  A(4,1)=2+D103;
  A(4,2)=D104-d(3)*D14;
  A(4,3)=-d(3)*D15-d(3);
  A(4,4)=0;
  B(1)=-(sum(Y)-1);
  B(2)=-(2*Y(2)+2*Y(6)+Y(7)+Y(9)-d(1)*Y(1)-d(1)*Y(5));
  B(3)=-(2*Y(1)+Y(2)+2*Y(4)+Y(5)+Y(8)+Y(9)+Y(10)-d(2)*Y(1)-d(2)*Y(5));
  B(4)=-(2*Y(3)+Y(10)-d(3)*Y(1)-d(3)*Y(5));

  invA=inv(A);
  DY3to6=invA*B;
  MaxVal=max(abs(DY3to6));
  Y(3:6)=Y(3:6)+DY3to6/10;
  i=find(Y<MinMol);
  Y(i)=ones(length(i),1)*MinMol;

  Y(7)=c(1)*sqrt(Y(6));
  Y(8)=c(2)*sqrt(Y(4));
  Y(9)=c(3)*sqrt(Y(4)*Y(6));
  Y(10)=c(4)*sqrt(Y(4)*Y(3));
  Y(2)=c(5)*sqrt(Y(4))*Y(6);
```

```
  Y(1)=c(6)*sqrt(Y(4))*Y(5);
end

if Iter>=MaxIter
  warning('convergence failure in composition loop');
end

TdKdT=[1/T -1/T^2 1 2*T]';
dKdT=2.302585*K.*(Kp(:,[1 2 4 5])*TdKdT);
dcdT(1)=dKdT(1)/sqrt(patm);
dcdT(2)=dKdT(2)/sqrt(patm);
dcdT(3)=dKdT(3);
dcdT(4)=dKdT(4);
dcdT(5)=dKdT(5)*sqrt(patm);
dcdT(6)=dKdT(6)*sqrt(patm);
dcdp(1)=-0.5*c(1)/p;
dcdp(2)=-0.5*c(2)/p;
dcdp(5)=0.5*c(5)/p;
dcdp(6)=0.5*c(6)/p;
x1=Y(1)/c(6);
x2=Y(2)/c(5);
x7=Y(7)/c(1);
x8=Y(8)/c(2);
x9=Y(9)/c(3);
x10=Y(10)/c(4);
dfdT(1)=dcdT(6)*x1+dcdT(5)*x2+dcdT(1)*x7+dcdT(2)*x8+ ...
  dcdT(3)*x9+dcdT(4)*x10;
dfdT(2)=2*dcdT(5)*x2+dcdT(1)*x7+dcdT(3)*x9-d(1)*dcdT(6)*x1;
dfdT(3)=2*dcdT(6)*x1+dcdT(5)*x2+dcdT(2)*x8+dcdT(3)*x9+ ...
  dcdT(4)*x10-d(2)*dcdT(6)*x1;
dfdT(4)=dcdT(4)*x10-d(3)*dcdT(6)*x1;
dfdp(1)=dcdp(6)*x1+dcdp(5)*x2+dcdp(1)*x7+dcdp(2)*x8;
dfdp(2)=2*dcdp(5)*x2+dcdp(1)*x7-d(1)*dcdp(6)*x1;
dfdp(3)=2*dcdp(6)*x1+dcdp(5)*x2+dcdp(2)*x8-d(2)*dcdp(6)*x1;
dfdp(4)=-d(3)*dcdp(6)*x1;

B=-dfdT;
dYdT(3:6)=invA*B;
dYdT(1)=sqrt(Y(4))*Y(5)*dcdT(6)+D14*dYdT(4)+D15*dYdT(5);
dYdT(2)=sqrt(Y(4))*Y(6)*dcdT(5)+D24*dYdT(4)+D26*dYdT(6);
dYdT(7)=sqrt(Y(6))*dcdT(1)+D76*dYdT(6);
dYdT(8)=sqrt(Y(4))*dcdT(2)+D84*dYdT(4);
dYdT(9)=sqrt(Y(4)*Y(6))*dcdT(3)+D94*dYdT(4)+D96*dYdT(6);
dYdT(10)=sqrt(Y(4)*Y(3))*dcdT(4)+D104*dYdT(4)+D103*dYdT(3);

B=-dfdp;
dYdp(3:6)=invA*B;
dYdp(1)=sqrt(Y(4))*Y(5)*dcdp(6)+D14*dYdp(4)+D15*dYdp(5);
dYdp(2)=sqrt(Y(4))*Y(6)*dcdp(5)+D24*dYdp(4)+D26*dYdp(6);
dYdp(7)=sqrt(Y(6))*dcdp(1)+D76*dYdp(6);
dYdp(8)=sqrt(Y(4))*dcdp(2)+D84*dYdp(4);
dYdp(9)=D94*dYdp(4)+D96*dYdp(6);
dYdp(10)=D104*dYdp(4)+D103*dYdp(3);

% calculate thermodynamic properties
Tcp0=[1 T T^2 T^3 T^4]';
Th0=[1 T/2 T^2/3 T^3/4 T^4/5 1/T]';
Ts0=[log(T) T T^2/2 T^3/3 T^4/4 1]';
cp0=A0(:,1:5)*Tcp0;
h0=A0(:,1:6)*Th0;
```

```
s0=A0(:,[1:5 7])*Ts0;

% Y(1) and Y(2) reevaluated
Y(1)=(2*Y(3)+Y(10))/d(3)-Y(5);
Y(2)=(d(1)/d(3)*(2*Y(3)+Y(10))-2*Y(6)-Y(7)-Y(9))/2;
i=find(Y<MinMol);
Y(i)=ones(length(i),1)*MinMol;

% properties of mixture
h=sum(h0.*Y);
s=sum((s0-log(Y)).*Y);
cp=sum(Y.*cp0+h0.*dYdT*T);
MW=sum(Y.*M);
MT=sum(dYdT.*M);
Mp=sum(dYdp.*M);

R=Ru/MW;
v=R*T/p;
cp=R*(cp-h*T*MT/MW);
dlvlT=1+max(-T*MT/MW,0);
dlvlp=-1-max(p*Mp/MW,0);
h=R*T*h;
s=R*(-log(patm)+s);
u=h-R*T;
```

Appendix C5 – farg.m – Mixtures of fuel, air, residual combustion products at low temp

```
function [h,u,v,s,Y,cp,dlvlT,dlvlp]=farg(p,T,ϕ,f,fueltype,airscheme);
%
% [h,u,v,s,Y,cp,dlvlT,dlvlp]=farg(p,T,ϕ,f,fueltype,airscheme)
%
% Routine to determine the state of mixtures of fuel, air
% and residual combustion products at low temperatures.
% Method closely follows that of:
% 1. Ferguson, C.R., 1986, "Internal Combustion Engines", Wiley, p108;
% who uses the results of:
% 2. Hires, S.D.,  Ekchian, A., Heywood, J.B., Tabaczynski, R.J., and
% Wall, J.C., 1976, "Performance and NOx Emissions Modeling of a Jet
% Ignition Pre-Chamber Stratified Charge Engine", SAE Trans., Vol 85,
% Paper 760161.
% ************************************************************************
% input:
% p,T,ϕ - pressure (Pa), temperature (K), and equivalence ratio
% f - residual mass fraction; set f=0 if no combustion products
% are present and f=1 if only combustion products are present
% fueltype - 'gasoline', 'diesel', etc - see fueldata.m for full list
% airscheme - 'GMcB' (Gordon and McBride) or 'Chemkin'
% output:
% h - enthalpy (J/kg), u - internal energy (J/kg),
% v - specific volume (m^3/kg), s - entropy (J/kgK),
% Y - mole fractions of 6 species: CO2, H2O, N2, O2, CO, and H2,
% cp - specific heat (J/kgK),
% dlvlT - partial derivative of log(v) wrt log(T)
% dlvlp - partial derivative of log(v) wrt log(p)
% ************************************************************************

[alpha,beta,gamma,delta,Afuel]=fueldata(fueltype);
switch airscheme
case 'GMcB'
```

```
   A=airdata('GMcB_low');
case 'Chemkin'
   A=airdata('Chemkin_low');
end

Ru=8314.34; % J/kmolK
table=[-1 1 0 0 1 -1]';
M=[44.01 18.02 28.008 32.000 28.01 2.018]'; % kg/kmol

MinMol=1e-25;

dlvlT=1; dlvlp=-1;
eps=0.210/(alpha+0.25*beta-0.5*gamma);

if ϕ <= 1.0 % stoichiometric or lean
   nu=[alpha*ϕ*eps beta*ϕ*eps/2 0.79+delta*ϕ*eps/2 ...
       0.21*(1-ϕ) 0 0]';
   dcdT=0;
else % rich
   z=1000/T;
   K=exp(2.743+z*(-1.761+z*(-1.611+z*0.2803)));
   dKdT=-K*(-1.761+z*(-3.222+z*0.8409))/1000;
   a=1-K;
   b=0.42-ϕ*eps*(2*alpha-gamma)+K*(0.42*(ϕ-1)+alpha*ϕ*eps);
   c=-0.42*alpha*ϕ*eps*(ϕ-1)*K;
   nu5=(-b+sqrt(b^2-4*a*c))/2/a;
   dcdT=dKdT*(nu5^2-nu5*(0.42*(ϕ-1)+alpha*ϕ*eps)+ ...
     0.42*alpha*ϕ*eps*(ϕ-1))/(2*nu5*a+b);
   nu=[alpha*ϕ*eps-nu5 0.42-ϕ*eps*(2*alpha-gamma)+nu5 ...
       0.79+delta*ϕ*eps/2 0 nu5 0.42*(ϕ-1)-nu5]';
end

% mole fractions and molecular weight of residual
tmoles=sum(nu);
Y=nu/tmoles;
Mres=sum(Y.*M);

% mole fractions and molecular weight of fuel-air
fuel=eps*ϕ/(1+eps*ϕ);
o2=0.21/(1+eps*ϕ);
n2=0.79/(1+eps*ϕ);
Mfa=fuel*(12.01*alpha+1.008*beta+16*gamma+14.01*delta)+ ...
   32*o2+28.02*n2;

% mole fractions of fuel-air-residual gas
Yres=f/(f+Mres/Mfa*(1-f));
Y=Y*Yres;
Yfuel=fuel*(1-Yres);
Y(3)=Y(3)+n2*(1-Yres);
Y(4)=Y(4)+o2*(1-Yres);

% component properties
Tcp0=[1 T T^2 T^3 T^4]';
Th0=[1 T/2 T^2/3 T^3/4 T^4/5 1/T]';
Ts0=[log(T) T T^2/2 T^3/3 T^4/4 1]';
cp0=A(1:6,1:5)*Tcp0;
h0=A(1:6,1:6)*Th0;
s0=A(1:6,[1:5 7])*Ts0;
Mfuel=12.01*alpha+1.008*beta+16.000*gamma+14.01*delta;
a0=Afuel(1); b0=Afuel(2); c0=Afuel(3); d0=Afuel(6); e0=Afuel(7);
```

```
cpfuel=Afuel(1:5)*[1 T T^2 T^3 1/T^2]';
hfuel=Afuel(1:6)*[1 T/2 T^2/3 T^3/4 -1/T^2 1/T]';
s0fuel=Afuel([1:5 7])*[log(T) T T^2/2 T^3/3 -1/T^2/2 1]';

% set min value of composition so log calculations work
if Yfuel<MinMol
   Yfuel=MinMol;
end
i=find(Y<MinMol);
Y(i)=ones(length(i),1)*MinMol;

% properties of mixture
h=hfuel*Yfuel+sum(h0.*Y);
s=(s0fuel-log(Yfuel))*Yfuel+sum((s0-log(Y)).*Y);
cp=cpfuel*Yfuel+sum(cp0.*Y)+sum(h0.*table*T*dcdT*Yres/tmoles);
MW=Mfuel*Yfuel+sum(Y.*M);

R=Ru/MW;
h=R*T*h;
u=h-R*T;
v=R*T/p;
s=R*(-log(p/101.325e3)+s);
cp=R*cp;
```

Appendix C6 – plotresults.m – Plot ahrind results

```
% plotresults.m
%
% Script file to plot output from ahrind.m and compare results
% with output listed in:
% Ferguson, C.R., 1986, "Internal Combustion Engines", Wiley, p178;

load ahrind.mat; % results from ahrind.m
load ferguson.txt; % tabulated output from ferguson p178-179

% Set some parameters to make Figures look attractive
NLW=1; % normal line width
NFS=18; % normal font size
NMS=1; % normal marker size

close all;

Figure(1);
plot(thetacomp*180/pi,pTuWQlHl(:,1)/1e6); hold on;
plot(thetacomb*180/pi,pTbTuWQlHl(:,1)/1e6);
plot(thetaexp*180/pi,pTbWQlHl(:,1)/1e6);
plot(ferguson(:,1),ferguson(:,4)*1e5/1e6,'o');
axis([-180 180 0 7]);
set(gca,'FontSize',NFS)
set(gca,'LineWidth',NLW)
set(gca,'XTick',[-180 -90 0 90 180]);
set(gca,'XTickLabel',[-180 -90 0 90 180]);
xlabel('crank angle (degrees ATC)')
ylabel('pressure (MPa)')
print -deps p_ahr.eps

Figure(2);
plot(ferguson(:,1),ferguson(:,5),'o'); hold on;
plot(ferguson(:,1),ferguson(:,6),'s');
```

```
plot(thetacomp*180/pi,pTuWQlHl(:,2));
plot(thetacomb*180/pi,pTbTuWQlHl(:,3));
plot(thetacomb*180/pi,pTbTuWQlHl(:,2));
plot(thetaexp*180/pi,pTbWQlHl(:,2));
axis([-180 180 0 3000]);
set(gca,'FontSize',NFS)
set(gca,'LineWidth',NLW)
set(gca,'XTick',[-180 -90 0 90 180]);
set(gca,'XTickLabel',[-180 -90 0 90 180]);
xlabel('crank angle (degrees ATC)')
ylabel('temperature (K)')
legend('burned gas','unburned gas',2);
print -deps T_ahr.eps

Figure(3);
nn=4; % for work plot
plot(thetacomp*180/pi,pTuWQlHl(:,nn-1)); hold on;
plot(thetacomb*180/pi,pTbTuWQlHl(:,nn));
plot(thetaexp*180/pi,pTbWQlHl(:,nn-1));
plot(ferguson(:,1),ferguson(:,7),'o');
axis([-180 180 -300 600]);
set(gca,'FontSize',NFS)
set(gca,'LineWidth',NLW)
set(gca,'XTick',[-180 -90 0 90 180]);
set(gca,'XTickLabel',[-180 -90 0 90 180]);
set(gca,'YTick',[-300 -150 0 150 300 450 600]);
set(gca,'YTickLabel',[-300 -150 0 150 300 450 600]);
xlabel('crank angle (degrees ATC)')
ylabel('work (J)')
print -deps W_ahr.eps

Figure(4);
nn=5; % for heat transfer plot
plot(thetacomp*180/pi,pTuWQlHl(:,nn-1)); hold on;
plot(thetacomb*180/pi,pTbTuWQlHl(:,nn));
plot(thetaexp*180/pi,pTbWQlHl(:,nn-1));
plot(ferguson(:,1),ferguson(:,8),'o');
axis([-180 180 -50 300]);
set(gca,'FontSize',NFS)
set(gca,'LineWidth',NLW)
set(gca,'XTick',[-180 -90 0 90 180]);
set(gca,'XTickLabel',[-180 -90 0 90 180]);
xlabel('crank angle (degrees ATC)')
ylabel('heat transfer (J)')
print -deps Ql_ahr.eps

Figure(5);
nn=6; % for heat leakage plot
plot(thetacomp*180/pi,pTuWQlHl(:,nn-1)); hold on;
plot(thetacomb*180/pi,pTbTuWQlHl(:,nn));
plot(thetaexp*180/pi,pTbWQlHl(:,nn-1));
plot(ferguson(:,1),ferguson(:,10),'o');
axis([-180 180 -8 0]);
set(gca,'FontSize',NFS)
set(gca,'LineWidth',NLW)
set(gca,'XTick',[-180 -90 0 90 180]);
set(gca,'XTickLabel',[-180 -90 0 90 180]);
xlabel('crank angle (degrees ATC)')
ylabel('heat leakage (J)')
print -deps Hl_ahr.eps
```

```
Figure(6);
plot(thetacomp*180/pi,qcomp); hold on;
plot(thetacomb*180/pi,qcombu);
plot(thetacomb*180/pi,qcombb);
plot(thetaexp*180/pi,qexp);
axis([-180 180 -0.2e6 1.2e6]);
set(gca,'FontSize',NFS)
set(gca,'LineWidth',NLW)
set(gca,'XTick',[-180 -90 0 90 180]);
set(gca,'XTickLabel',[-180 -90 0 90 180]);
xlabel('crank angle (degrees ATC)')
ylabel('heat flux (W/m^2)')
print -deps qflux_ahr.eps
```

Appendix C7 – RatesComb.m – Combustion Phase derivatives

```
function yprime=RatesComb(theta,y,flag);
%
% yprime=RatesComb(theta,y,flag)
%
% Function that returns the drivatives of the following 6 variables
% w.r.t. crank angle (theta) for the combustion phase:
% 1) pressure; 2) unburned temperature; 3) burned temperature;
% 4) work; 5) heat transfer; and 6) heat leakage.
% See Ferguson, C.R., 1986, "Internal Combustion Engines", Wiley,
% p174.

global b stroke eps r Cblowby f fueltype airscheme ϕ ...
  thetas thetab RPM omega ...
  heattransferlaw hcu hcb ...
  p1 T1 V1 Tw theta1 Vtdc Vbdc mass1

p=y(1);
Tb=y(2);
Tu=y(3);
yprime=zeros(6,1);

% mass in cylinder accounting for blowby:
mass=mass1*exp(-Cblowby*(theta-theta1)/omega);
% volume of cylinder:
V=Vtdc*(1+(r-1)/2*(1-cos(theta)+ ...
  1/eps*(1-(1-eps^2*sin(theta).^2).^0.5)));
% derivate of volume:
dVdtheta=Vtdc*(r-1)/2*(sin(theta)+ ...
  eps/2*sin(2*theta)./sqrt(1-eps^2*sin(theta).^2));
% mass fraction burned and derivative:
x=0.5*(1-cos(pi*(theta-thetas)/thetab));
dxdtheta=pi/2/thetab*sin(pi*(theta-thetas)/thetab);
if x<0.0001, x=0.0001; end;
if x>0.9999, x=0.9999; end;

switch heattransferlaw
case 'constant'
  hcoeffu=hcu;
  hcoeffb=hcb;
case 'Woschni'
  upmean=omega*stroke/pi; % mean piston velocity
  C1=2.28;
```

```
  C2=3.24e-3;
  Vs=Vbdc-Vtdc;
  k=1.3;
  pm=p1*(V1/V)^k; % motoring pressure
  hcoeffu=hcu*130*b^(-0.2)*Tu^(-0.53)*(p/100e3)^(0.8)* ...
    (C1*upmean+C2*Vs*T1/p1/V1*(p-pm))^(0.8);
  hcoeffb=hcb*130*b^(-0.2)*Tb^(-0.53)*(p/100e3)^(0.8)* ...
    (C1*upmean+C2*Vs*T1/p1/V1*(p-pm))^(0.8);
end

A=1/mass*(dVdtheta+V*Cblowby/omega);
Qconvu=hcoeffu*(pi*b^2/2+4*V/b)*(1-sqrt(x))*(Tu-Tw);
Qconvb=hcoeffb*(pi*b^2/2+4*V/b)*sqrt(x)*(Tb-Tw);
Const1=1/omega/mass;

[hu,uu,vu,s,Y,cpu,dlvlTu,dlvlpu]= ...
  farg(p,Tu,ϕ,f,fueltype,airscheme);
[hb,ub,vb,s,Y,cpb,dlvlTb,dlvlpb]= ...
  ecp(p,Tb,ϕ,fueltype,airscheme);
B=Const1*(vb/cpb*dlvlTb*Qconvb/Tb+ ...
  vu/cpu*dlvlTu*Qconvu/Tu);
C=-(vb-vu)*dxdtheta-vb*dlvlTb*(hu-hb)/cpb/Tb*(dxdtheta- ...
  (x-x^2)*Cblowby/omega);
D=x*(vb^2/cpb/Tb*dlvlTb^2+vb/p*dlvlpb);
E=(1-x)*(vu^2/cpu/Tu*dlvlTu^2+vu/p*dlvlpu);

yprime(1)=(A+B+C)/(D+E);
yprime(2)=-Const1/cpb/x*Qconvb+vb/cpb*dlvlTb*yprime(1)+ ...
  (hu-hb)/cpb*(dxdtheta/x-(1-x)*Cblowby/omega);
yprime(3)=-Const1/cpu/(1-x)*Qconvu+vu/cpu*dlvlTu*yprime(1);
yprime(4)=p*dVdtheta;
yprime(5)=Const1*mass*(Qconvb+Qconvu);
yprime(6)=Cblowby*mass/omega*((1-x^2)*hu+x^2*hb);
```

Appendix ##7 – RatesComp.m – Compression Phase derivatives

```
function yprime=RatesComp(theta,y,flag);
%
% yprime=RatesComp(theta,y,flag)
%
% Function that returns the drivatives of the following 5 variables
% w.r.t. crank angle (theta) for the compression phase:
% 1) pressure; 2) unburned temperature;
% 3) work; 4) heat transfer; and 5) heat leakage.
% See Ferguson, C.R., 1986, "Internal Combustion Engines", Wiley,
% p174.

global b stroke eps r Cblowby f fueltype airscheme ϕ ...
  thetas thetab omega ...
  heattransferlaw hcu ...
  Tw theta1 Vtdc mass1 ...

p=y(1);
Tu=y(2);
yprime=zeros(5,1);

% mass in cylinder accounting for blowby:
mass=mass1*exp(-Cblowby*(theta-theta1)./omega);
% volume of cylinder:
V=Vtdc*(1+(r-1)/2*(1-cos(theta)+ ...
```

```
   1/eps*(1-(1-eps^2*sin(theta).^2).^0.5)));
% derivate of volume:
dVdtheta=Vtdc*(r-1)/2*(sin(theta)+ ...
   eps/2*sin(2*theta)./sqrt(1-eps^2*sin(theta).^2));

switch heattransferlaw
case 'constant'
   hcoeff=hcu;
case 'Woschni'
   upmean=omega*stroke/pi; % mean piston velocity
   C1=2.28;
   hcoeff=hcu*130*b^(-0.2)*Tu^(-0.53)*(p/100e3)^(0.8)*C1*upmean;
end

A=1/mass*(dVdtheta+V*Cblowby/omega);
Qconv=hcoeff*(pi*b^2/2+4*V/b)*(Tu-Tw);
Const1=1/omega/mass;

[h,u,v,s,Y,cp,dlvlT,dlvlp]=farg(p,Tu,ϕ,f,fueltype,airscheme);
B=Const1*v/cp*dlvlT*Qconv/Tu; % note typo on p174, eq. 4.76
C=0;
D=0;
E=v^2/cp/Tu*dlvlT^2+v/p*dlvlp;

yprime(1)=(A+B+C)/(D+E);
yprime(2)=-Const1/cp*Qconv+v/cp*dlvlT*yprime(1);
yprime(3)=p*dVdtheta;
yprime(4)=Qconv/omega;
yprime(5)=Cblowby*mass/omega*h;
```

Appendix ##8 – RatesExp.m – Compression Phase derivatives

```
function yprime=RatesExp(theta,y,flag);
%
% yprime=RatesExp(theta,y,flag)
%
% Function that returns the drivatives of the following 5 variables
% w.r.t. crank angle (theta) for the expansion phase:
% 1) pressure; 2) unburned temperature;
% 3) work; 4) heat transfer; and 5) heat leakage.
% See Ferguson, C.R., 1986, "Internal Combustion Engines", Wiley,
% p174.

global b stroke eps r Cblowby f fueltype airscheme ϕ ...
   thetas thetab RPM omega ...
   heattransferlaw hcb ...
   p1 T1 V1 Tw theta1 Vtdc Vbdc mass1

p=y(1);
Tb=y(2);
yprime=zeros(5,1);

% mass in cylinder accounting for blowby:
mass=mass1*exp(-Cblowby*(theta-theta1)/omega);
% volume of cylinder:
V=Vtdc*(1+(r-1)/2*(1-cos(theta)+ ...
   1/eps*(1-(1-eps^2*sin(theta).^2).^0.5)));
% derivate of volume:
dVdtheta=Vtdc*(r-1)/2*(sin(theta)+ ...
   eps/2*sin(2*theta)./sqrt(1-eps^2*sin(theta).^2));
```

```
switch heattransferlaw
case 'constant'
  hcoeff=hcb;
case 'Woschni'
  upmean=omega*stroke/pi; % mean piston velocity
  C1=2.28;
  C2=3.24e-3;
  Vs=Vbdc-Vtdc;
  k=1.3;
  pm=p1*(V1/V)^k; % motoring pressure
  hcoeff=hcb*130*b^(-0.2)*Tb^(-0.53)*(p/100e3)^(0.8)* ...
    (C1*upmean+C2*Vs*T1/p1/V1*(p-pm))^(0.8);
end

A=1/mass*(dVdtheta+V*Cblowby/omega);
Qconv=hcoeff*(pi*b^2/2+4*V/b)*(Tb-Tw);
Const1=1/omega/mass;

if Tb<1000
  [h,u,v,s,Y,cp,dlvlT,dlvlp]=farg(p,Tb,ϕ,1,fueltype,airscheme);
else
  [h,u,v,s,Y,cp,dlvlT,dlvlp]=ecp(p,Tb,ϕ,fueltype,airscheme);
end
B=Const1*v/cp*dlvlT*Qconv/Tb;
C=0;
D=v^2/cp/Tb*dlvlT^2+v/p*dlvlp;
E=0;

yprime(1)=(A+B+C)/(D+E);
yprime(2)=-Const1/cp*Qconv+v/cp*dlvlT*yprime(1);
yprime(3)=p*dVdtheta;
yprime(4)=Qconv/omega;
yprime(5)=Cblowby*mass/omega*h;
```

Appendix C8 – Tadiabatic.m – Calculate Adiabatic flame temp

```
function Tb=Tadiabatic(p,Tu,ϕ,f,fueltype,airscheme);
%
% Tb=Tadiabatic(p,Tu,ϕ,f,fueltype,airscheme)
%
% Routine for calculating the adiabatic flame temperature.
% Method involves iteratively selecting flame temperatures until
% the enthalpy of the combustion products (in equilibrium) matches
% the enthalpy of the initial gas mixture.
% farg.m is used to determine the enthalpy of the unburned mixture,
% and ecp.m is used to determine the enthalpy of the burned gas.
% ***********************************************************************
% input:
% p - pressure (Pa)
% Tu - temperature of the unburned mixture (K)
% ϕ - equivalence ratio
% f - residual mass fraction; set f=0 if no combustion products
% are present and f=1 if only combustion products are present
% fueltype - 'gasoline', 'diesel', etc - see fueldata.m for full list
% airscheme - 'GMcB' (Gordon and McBride) or 'Chemkin'
% output:
% Tb - temperature of the burned gas (K) - adiabatic flame temperature
```

```
% ************************************************************************

MaxIter=50;
Tol=0.00001; % 0.001% allowable error in temperature calculation
Tb=2000; % initial estimate
DeltaT=2*Tol*Tb; % something big
Iter=0;
[hu,u,v,s,Y,cp,dlvlT,dlvlp]=farg(p,Tu,ϕ,f,fueltype,airscheme);

while (Iter<MaxIter)&(abs(DeltaT/Tb)>Tol)
  Iter=Iter+1;
  [hb,u,v,s,Y,cp,dlvlT,dlvlp]=ecp(p,Tb,ϕ,fueltype,airscheme);
  DeltaT=(hu-hb)/cp;
  Tb=Tb+DeltaT;
end

if Iter>=MaxIter
  warning('convergence failure in adiabatic flame temperature loop');
end
```

Appendix C9 – fueldata.m – Thermodynamic properties of fuel (modified)

```
function [alpha,beta,gamma,delta,Afuel]=fueldata(fuel);
%
% [alpha,beta,gamma,delta,Afuel]=fueldata(fuel)
%
% Routine to specify the thermodynamic properties of a fuel.
% Data taken from:
% 1. Ferguson, C.R., 1986, "Internal Combustion Engines", Wiley;
% 2. Heywood, J.B., 1988, "Internal Combustion Engine Fundamentals",
%    McGraw-Hill; and
% 3. Raine, R. R., 2000, "ISIS_319 User Manual", Oxford Engine Group.
% **********************************************************************
% input:
% fuel switch
% from Ferguson: 'gasoline', 'diesel', 'methane', 'methanol',
% 'nitromethane', 'benzene';
% from Heywood: 'methane_h', 'propane', 'hexane', 'isooctane_h',
% 'methanol_h', 'ethanol', 'gasoline_h1', gasoline_h2', 'diesel_h';
% from Raine: 'toluene', 'isooctane'.
% output:
% alpha, beta, gamma, delta - number of C, H, 0, and N atoms
% Afuel - vector of polynomial coefficients for cp/R, h/RT, and s/R
% of the form h/RT=a1+a2*T/2+a3*T^2/3+a4*T^3/4-a5/T^2+a6/T (for
% example) where T is expressed in K.
% **********************************************************************

% Set values for conversion of Heywood data to nondimensional format
% with T expressed in K
SVal=4.184e3/8.31434;
SVec=SVal*[1e-3 1e-6 1e-9 1e-12 1e3 1 1];

switch fuel
case 'gasoline' % Ferguson
   alpha=7; beta=17; gamma=0; delta=0;
   Afuel=[4.0652 6.0977E-02 -1.8801E-05 0 0 -3.5880E+04 15.45];
case 'diesel' % Ferguson
   alpha=14.4; beta=24.9; gamma=0; delta=0;
   Afuel=[7.9710 1.1954E-01 -3.6858E-05 0 0 -1.9385E+04 -1.7879];
case 'methane' % Ferguson
   alpha=1; beta=4; gamma=0; delta=0;
   Afuel=[1.971324 7.871586E-03 -1.048592E-06 0 0 -9.930422E+03 8.873728];
case 'methanol' % Ferguson
   alpha=1; beta=4; gamma=1; delta=0;
   Afuel=[1.779819 1.262503E-02 -3.624890E-06 0 0 -2.525420E+04 1.50884E+01];
case 'nitromethane' % Ferguson
   alpha=1; beta=3; gamma=2; delta=1;
   Afuel=[1.412633 2.087101E-02 -8.142134E-06 0 0 -1.026351E+04 1.917126E+01];
case 'benzene' % Ferguson
   alpha=6; beta=6; gamma=0; delta=0;
   Afuel=[-2.545087 4.79554E-02 -2.030765E-05 0 0 8.782234E+03 3.348825E+01];
case 'toluene' % Raine
   alpha=7; beta=8; gamma=0; delta=0;
   Afuel=[-2.09053 5.654331e-2 -2.350992e-5 0 0 4331.441411 34.55418257];
case 'isooctane' % Raine
   alpha=8; beta=18; gamma=0; delta=0;
   Afuel=[6.678E-1 8.398E-2 -3.334E-5 0 0 -3.058E+4 2.351E+1];
case 'methane_h' % Heywood
   alpha=1; beta=4; gamma=0; delta=0;
   Afuel=[-0.29149 26.327 -10.610 1.5656 0.16573 -18.331 19.9887/SVal].*SVec;
```

```
case 'propane' % Heywood
   alpha=3; beta=8; gamma=0; delta=0;
   Afuel=[-1.4867 74.339 -39.065 8.0543 0.01219 -27.313 26.4796/SVal].*SVec;
case 'hexane' % Heywood
   alpha=6; beta=14; gamma=0; delta=0;
   Afuel=[-20.777 210.48 -164.125 52.832 0.56635 -39.836 79.5542/SVal].*SVec;
case 'isooctane_h' % Heywood
   alpha=8; beta=18; gamma=0; delta=0;
   Afuel=[-0.55313 181.62 -97.787 20.402 -0.03095 -60.751 27.2162/SVal].*SVec;
case 'methanol_h' % Heywood
   alpha=1; beta=4; gamma=1; delta=0;
   Afuel=[-2.7059 44.168 -27.501 7.2193 0.20299 -48.288 31.1406/SVal].*SVec;
case 'ethanol' % Heywood
   alpha=2; beta=6; gamma=1; delta=0;
   Afuel=[6.990 39.741 -11.926 0 0 -60.214 8.01623/SVal].*SVec;
case 'gasoline_h1' % Heywood
   alpha=8.26; beta=15.5; gamma=0; delta=0;
   Afuel=[-24.078 256.63 -201.68 64.750 0.5808 -27.562 NaN].*SVec;
case 'gasoline_h2' % Heywood
   alpha=7.76; beta=13.1; gamma=0; delta=0;
   Afuel=[-22.501 227.99 -177.26 56.048 0.4845 -17.578 NaN].*SVec;
case 'diesel_h' % Heywood
   alpha=10.8; beta=18.7; gamma=0; delta=0;
   Afuel=[-9.1063 246.97 -143.74 32.329 0.0518 -50.128 NaN].*SVec;
case 'hydrogen' % Heywood
   alpha=1e-3; beta=2; gamma=0; delta=0;
   Afuel=[0.30574451E01 0.26765200E-02 -0.58099162E-05 0.55210391E-08...
      -0.18122739E-11 -0.98890474E03 -0.22997056E01];
end
```

APPENDIX D - Engine Simulation script files – Richardson (2015)

Appendix D1 – Drive_Cycle_Anlysis.m – HWFET & UDDS Drive Cycle Analysis

```
%% Holden 5.0L Engine Analysis
% Kieran Richardson - 0061033301

clc
clear all
close all

tic

global ϕ p1

% set engine speed and fuel ratio range
ϕ_range = 0.3:0.05:1.2;
Pa_range = 30e3:5e3:140e3;

% length of arrays for zeros matrices
n=length(Pa_range);
m=length(ϕ_range);

% create power output matrix (kW)
power_out=zeros(n+1,m+1);
power_out(2:end,1)=Pa_range;
power_out(1,2:end)=ϕ_range;

% fuel consumption output matrix (kg/100km)
FC_kg_100km=zeros(n+1,m+1);
FC_kg_100km(2:end,1)=Pa_range;
FC_kg_100km(1,2:end)=ϕ_range;

% petrol fuel consumption equivalent output matrix (L/100km)
FC_L_100km=zeros(n+1,m+1);
FC_L_100km(2:end,1)=Pa_range;
FC_L_100km(1,2:end)=ϕ_range;

% create specific fuel consumption output matrix
SFC=zeros(n+1,m+1);
SFC(2:end,1)=Pa_range;
SFC(1,2:end)=ϕ_range;

% loop for engine speed and fuel ratios
for k = 1:m
    ϕ = ϕ_range(k);
    for l = 1:n
        p1 = Pa_range(l);

% run enginedata and ahrind scriptfiles
enginedata
ahrind

load ahrind.mat; % results from ahrind.m
load ferguson.txt; % tabulated output from ferguson p178-179

% Set some parameters to make Figures look attractive
NLW=1; % normal line width
NFS=18; % normal font size
```

```
NMS=1; % normal marker size


%% additional data

% HQ 5.0L V8
cc_vol=Vbdc*8;      % total engine capacity (m3)
dl_eta=0.9;         % Vehicle driveline efficiency
rho_petrol=737;     % density of petrol (kg/m^3)

% The density of dry air can be calculated using the ideal gas law,
% expressed as a function of temperature and pressure:

R=287.058; % specific gas constant for dry air (J/(kg*K))

% calculating density
rho_air=p1/(R*T1);

% The injection pressure of hydrogen is assumed to be constant
rho_H2=0.089;

%% Ground speed
% the relationship between RPM and groundspeed is determined by the
% driveline ratios.
gr=[2.54 1.83 1.38 1.0];      % gearbox ratios (x:1)
dr=3.08;                      % differential ratio (x:1)
tw=0.235;                     % tyre width (m)
ar=60;                        % tyre aspect ratio
rim=14;                       % wheel size (inches)

wd=2*tw*(ar/100)+(rim*0.0254);  % wheel diameter

wc=pi*wd; % wheel_circumfrence

dc=((60/1000/dr*wc)/1)/gr(4); % driveline constant

ground_speed=RPM*dc; % speed in top gear

%% stoichiometry
% number of moles per species
N_H2=1;N_O2=0.5;N_N2=1.88;

% mole fractions
X_H2=N_H2/(N_H2+N_O2+N_N2);
X_O2=N_O2/(N_H2+N_O2+N_N2);
X_N2=N_N2/(N_H2+N_O2+N_N2);

% molar weights
MW_H2=1.008;MW_N2=28.013;MW_O2=31.999;
MW_air=0.5*(MW_O2+3.76*MW_N2);

% stoichiometric fuel-oxidiser ratio
FAR_stoich=MW_H2/MW_air;

% fuel-air ratio
FAR=ϕ*FAR_stoich;

% matrix operations
```

```
A=[1,1;-1,(FAR*(rho_air/rho_H2))];
C=[Vbdc;0];
B=linsolve(A,C);

% matrix outputs
vol_H2=B(1);        % volume of hydrogen gas in combustion chamber
vol_air=B(2);       % volume of air in combustion chamber

%% Fuel consumption

% calculate power output at the flywheel (kW)
power_out(l+1,k+1)=((eta*imep)*(RPM/60)*(cc_vol))/(2*1000);

% mean effective pressure and thermal efficiency
MEP=(power_out(2:end,2:end))/(((RPM/60)*(cc_vol/2))/1000);

% thermal efficiency
ETA=MEP.*(1/imep);

% mass of hydrogen consumed per cylinder per cycle
mass_H2=vol_H2*rho_H2;

% calculate fuel consumption (kg/hr)
FCH_H2=mass_H2*8*RPM*60;

% calculate consumption (km/kg)
FC_km_per_kg=ground_speed.*(1/FCH_H2);

% calculate consumption (kg/100km)
FC_kg_100km(l+1,k+1)=FCH_H2./(ground_speed/100);

% calculate petroleum litre quivalent (1kg H2 = 3.77L petrol)
FC_L_100km(l+1,k+1)=FC_kg_100km(l+1,k+1).*3.77;

% calculate specific fuel consumption petrol equivalent
SFC(l+1,k+1)=(FCH_H2*3.77)/power_out(l+1,k+1);

    end
end

%% plot results

hold on

Figure(1)
set(gcf, 'Color', [1,1,1])% set plot background colour to white
surf(ϕ_range,Pa_range,power_out(2:end,2:end))
title('Induction pressure vs Equivalence Ratio vs Flywheel Power')
xlabel('Equivalence Ratio')
ylabel('Induction pressure (Pa)')
zlabel('Power at the flywheel (kW)')
colormap(jet)    % change color map

Figure(2)
set(gcf, 'Color', [1,1,1])% set plot background colour to white
surf(ϕ_range,Pa_range,power_out(2:end,2:end)*dl_eta)
title('Induction pressure vs Equivalence Ratio vs Wheel Power')
xlabel('Equivalence Ratio')
```

```
ylabel('Induction pressure (Pa)')
zlabel('Power at the wheels (kW)')
colormap(jet)    % change color map

Figure(3)
colormap(pink)    % change color map
set(gcf, 'Color', [1,1,1])% set plot background colour to white
surf(ϕ_range,Pa_range,FC_kg_100km(2:end,2:end))
title('Induction pressure vs Equivalence Ratio vs Hydrogen Fuel
Consumption')
xlabel('Equivalence Ratio')
ylabel('Induction pressure (Pa)')
zlabel('Hydrogen Fuel Consumption (kg/100km)')
colormap(jet)    % change color map

Figure(4)
colormap(pink)    % change color map
set(gcf, 'Color', [1,1,1])% set plot background colour to white
surf(ϕ_range,Pa_range,FC_L_100km(2:end,2:end))
title('Induction pressure vs Equivalence Ratio vs Fuel Consumption
Petrol Equivalent')
xlabel('Equivalence Ratio')
ylabel('Induction pressure (Pa)')
zlabel('Petrol Fuel Consumption Equivalent (L/100)')
colormap(jet)    % change color map

Figure(5)
set(gcf, 'Color', [1,1,1])% set plot background colour to white
surf(ϕ_range,Pa_range,SFC(2:end,2:end))
title('Induction pressure vs Equivalence Ratio vs Specific Fuel
Consumption Petrol Equivalent')
xlabel('Equivalence Ratio')
ylabel('Induction pressure (Pa)')
zlabel('Specific Fuel Consumption Petrol Equivalent (kW/L)')
colormap(jet)    % change color map

Figure(6)
set(gcf, 'Color', [1,1,1])% set plot background colour to white
surf(ϕ_range,Pa_range,MEP)
title('Induction pressure vs Equivalence Ratio vs Mean Effective
Pressure')
xlabel('Equivalence Ratio')
ylabel('Induction pressure (Pa)')
zlabel('MEP (Pa)')
colormap(jet)    % change color map

Figure(7)
set(gcf, 'Color', [1,1,1])% set plot background colour to white
surf(ϕ_range,Pa_range,ETA)
title('Induction pressure vs Equivalence Ratio vs Thermal efficiency')
xlabel('Equivalence Ratio')
ylabel('Induction pressure (Pa)')
zlabel('Thermal efficiency')
colormap(jet)    % change color map
toc
```

Appendix D2 – Holden_5L_Engine_Anlysis.m

```
%% Holden 5.0L Engine Analysis
% Kieran Richardson - 0061033301

clc
clear all
close all

tic

global ϕ p1 RPM

% set engine speed and fuel ratio range
ϕ_range = 0.35:0.05:1.2;
Pa_range = 30e3:5e3:140e3;

% length of arrays for zeros matricies
n=length(Pa_range);
m=length(ϕ_range);

% create power output matrix (kW)
power_out=zeros(n+1,m+1);
power_out(2:end,1)=Pa_range;
power_out(1,2:end)=ϕ_range;

% fuel consumption output matrix (kg/100km)
FC_kg_100km=zeros(n+1,m+1);
FC_kg_100km(2:end,1)=Pa_range;
FC_kg_100km(1,2:end)=ϕ_range;

% petrol fuel consumption equivalent output matrix (L/100km)
FC_L_100km=zeros(n+1,m+1);
FC_L_100km(2:end,1)=Pa_range;
FC_L_100km(1,2:end)=ϕ_range;

% create specific fuel consumption output matrix
SFC=zeros(n+1,m+1);
SFC(2:end,1)=Pa_range;
SFC(1,2:end)=ϕ_range;

% loop for engine speed and fuel ratios
for k = 1:m
    ϕ = ϕ_range(k);
    for l = 1:n
        p1 = Pa_range(l);

% run enginedata and ahrind scriptfiles
enginedata
ahrind

load ahrind.mat; % results from ahrind.m
load ferguson.txt; % tabulated output from ferguson p178-179

% Set some parameters to make Figures look attractive
NLW=1; % normal line width
NFS=18; % normal font size
NMS=1; % normal marker size
```

```
%% additional data

% HQ 5.0L V8
cc_vol=Vbdc*8;      % total engine capacity (m3)
eta_d=0.95;         % Vehicle driveline efficiency
rho_petrol=737;     % density of petrol (kg/m^3)

% The density of dry air can be calculated using the ideal gas law,
% expressed as a function of temperature and pressure:

R=287.058; % specific gas constant for dry air (J/(kg*K))

% calculating density
rho_air=p1/(R*T1);

% The injection pressure of hydrogen is assumed to be constant
rho_H2=0.089;

%% Ground speed
% the relationship between RPM and groundspeed is determined by the
% driveline ratios.
gr=[2.54 1.83 1.38 1.0];      % gearbox ratios (x:1)
dr=3.08;                      % differential ratio (x:1)
tw=0.235;                     % tyre width (m)
ar=60;                        % tyre aspect ratio
rim=14;                       % wheel size (inches)

wd=2*tw*(ar/100)+(rim*0.0254);  % wheel diameter

wc=pi*wd; % wheel_circumfrence

dc=((60/1000/dr*wc)/1)/gr(2); % driveline constant

ground_speed=RPM*dc; % speed in top gear

%% stoichiometry
% number of moles per species
N_H2=1;N_O2=0.5;N_N2=1.88;

% molar weights
MW_H2=2*1.008;MW_N2=28.013;MW_O2=31.999;
MW_air=0.5*(MW_O2+3.76*MW_N2);

% stoichiometric fuel-oxidiser ratio
FAR_stoich=MW_H2/MW_air;

% fuel-air ratio
FAR=ϕ*FAR_stoich;

% matrix operations
A=[1,1;-1,(FAR*(rho_air/rho_H2))];
C=[Vbdc;0];
B=linsolve(A,C);

% matrix outputs
vol_H2=B(1);        % volume of hydrogen gas in combustion chamber
```

```
vol_air=B(2);       % volume of air in combustion chamber

%% Fuel consumption

% power output at the wheels (kW)
power_out(l+1,k+1)=((cc_vol*imep*RPM*eta*eta_d)/(60*2))/1000;

% mass of hydrogen consumed per cylinder per cycle
mass_H2=vol_H2*rho_H2;

% calculate fuel consumption (kg/hr)
FCH_H2=(mass_H2*8*RPM*60)/2;

% calculate consumption (km/kg)
FC_km_per_kg=ground_speed.*(1/FCH_H2);

% calculate consumption (kg/100km)
FC_kg_100km(l+1,k+1)=FCH_H2./(ground_speed/100);

% calculate petroleum litre quivalent (1kg H2 = 3.77L petrol)
FC_L_100km(l+1,k+1)=FC_kg_100km(l+1,k+1).*3.77;

% calculate specific fuel consumption petrol equivalent
SFC(l+1,k+1)=(FCH_H2*3.77)/power_out(l+1,k+1);

    end
end

%% plot results

hold on

Figure(1)
set(gcf, 'Color', [1,1,1])% set plot background colour to white
surf(ϕ_range,Pa_range,power_out(2:end,2:end)/eta_d)
title('Induction pressure vs Equivalence Ratio vs Flywheel Power')
xlabel('Equivalence Ratio')
ylabel('Induction pressure (Pa)')
zlabel('Power at the flywheel (kW)')
colormap(jet)    % change color map

Figure(2)
set(gcf, 'Color', [1,1,1])% set plot background colour to white
surf(ϕ_range,Pa_range,power_out(2:end,2:end))
title('Induction pressure vs Equivalence Ratio vs Wheel Power')
xlabel('Equivalence Ratio')
ylabel('Induction pressure (Pa)')
zlabel('Power at the wheels (kW)')
colormap(jet)    % change color map

Figure(3)
colormap(pink)    % change color map
set(gcf, 'Color', [1,1,1])% set plot background colour to white
surf(ϕ_range,Pa_range,FC_kg_100km(2:end,2:end))
title('Induction pressure vs Equivalence Ratio vs Hydrogen Fuel
Consumption')
xlabel('Equivalence Ratio')
ylabel('Induction pressure (Pa)')
```

```
zlabel('Hydrogen Fuel Consumption (kg/100km)')
colormap(jet)    % change color map

Figure(4)
colormap(pink)    % change color map
set(gcf, 'Color', [1,1,1])% set plot background colour to white
surf(ϕ_range,Pa_range,FC_L_100km(2:end,2:end))
title('Induction pressure vs Equivalence Ratio vs Fuel Consumption
Petrol Equivalent')
xlabel('Equivalence Ratio')
ylabel('Induction pressure (Pa)')
zlabel('Petrol Fuel Consumption Equivalent (L/100)')
colormap(jet)    % change color map

Figure(5)
set(gcf, 'Color', [1,1,1])% set plot background colour to white
surf(ϕ_range,Pa_range,SFC(2:end,2:end))
title('Induction pressure vs Equivalence Ratio vs Specific Fuel
Consumption Petrol Equivalent')
xlabel('Equivalence Ratio')
ylabel('Induction pressure (Pa)')
zlabel('Specific Fuel Consumption Petrol Equivalent (kW/L)')
colormap(jet)    % change color map

toc
```

Appendix E – Drive cycle analysis plots

Appendix E1 - Power to maintain speed and power to accelerate over HWFET driving cycle

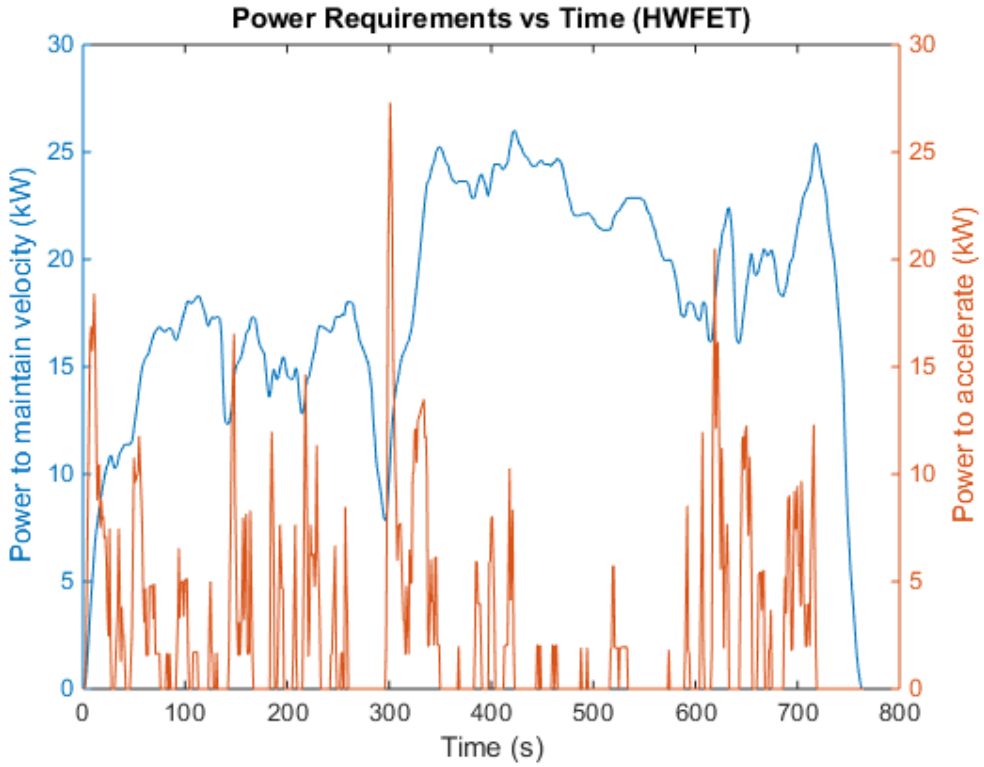

Appendix E2 - Total power required vs time for the HWFET driving cycle

Appendix E3 - Cumulative fuel consumption vs time for the HWFET driving cycle

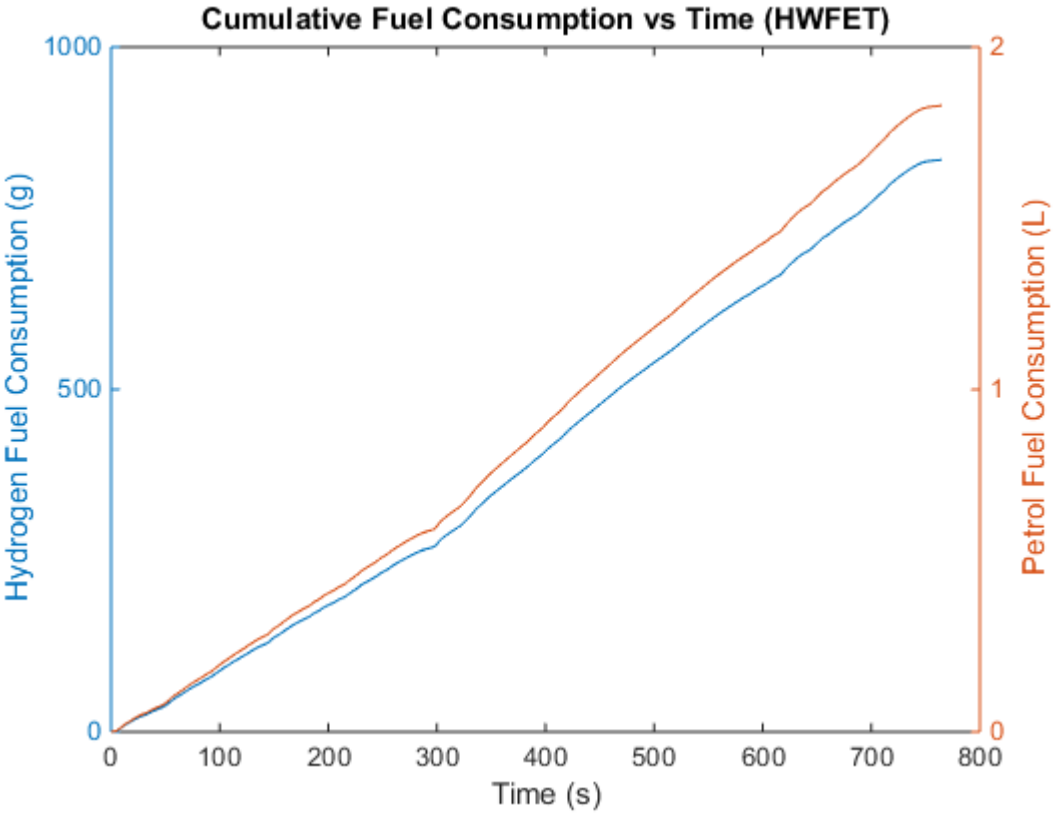

Appendix E4 - Power to maintain speed and power to accelerate over the UDDS driving cycle.

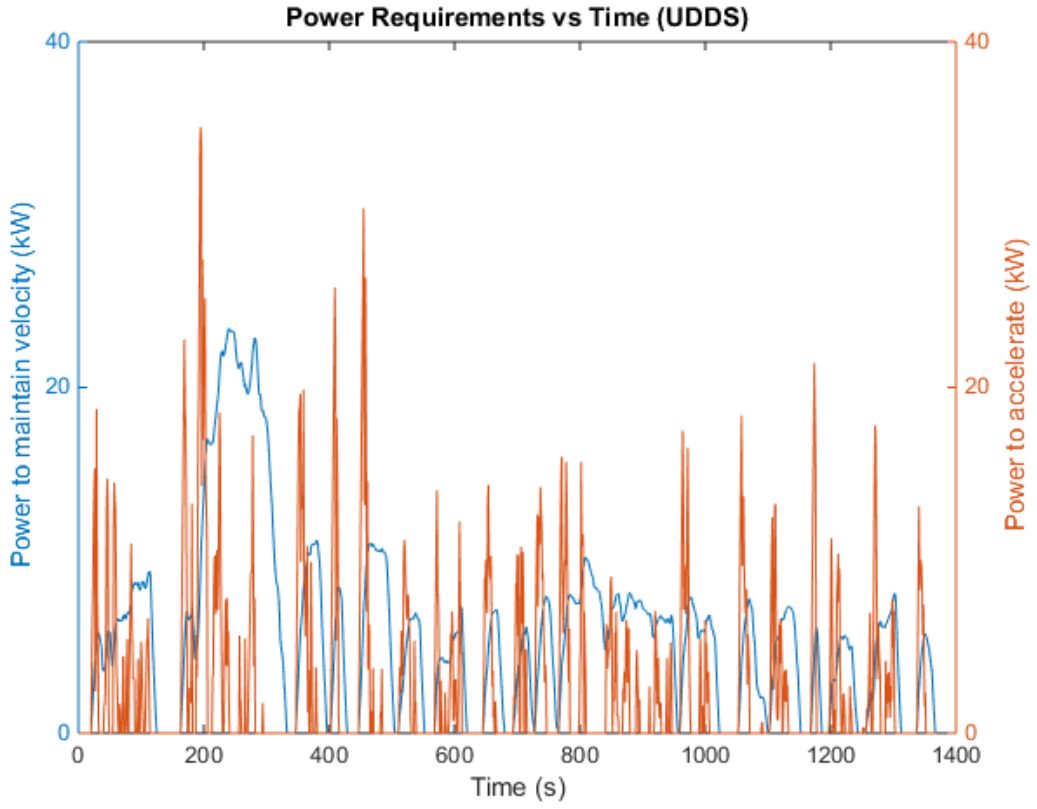

Appendix E5 - Total power required vs time for the UDDS driving cycle

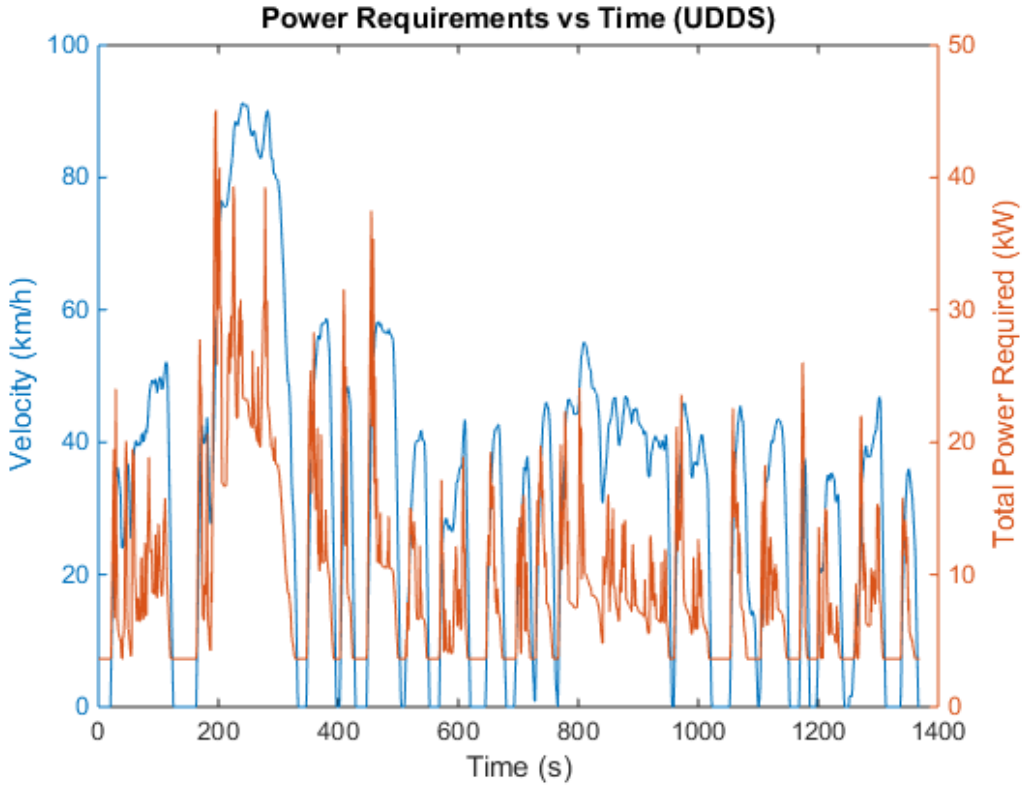

Appendix E6 – Cumulative fuel consumption vs time for the UDDS driving cycle

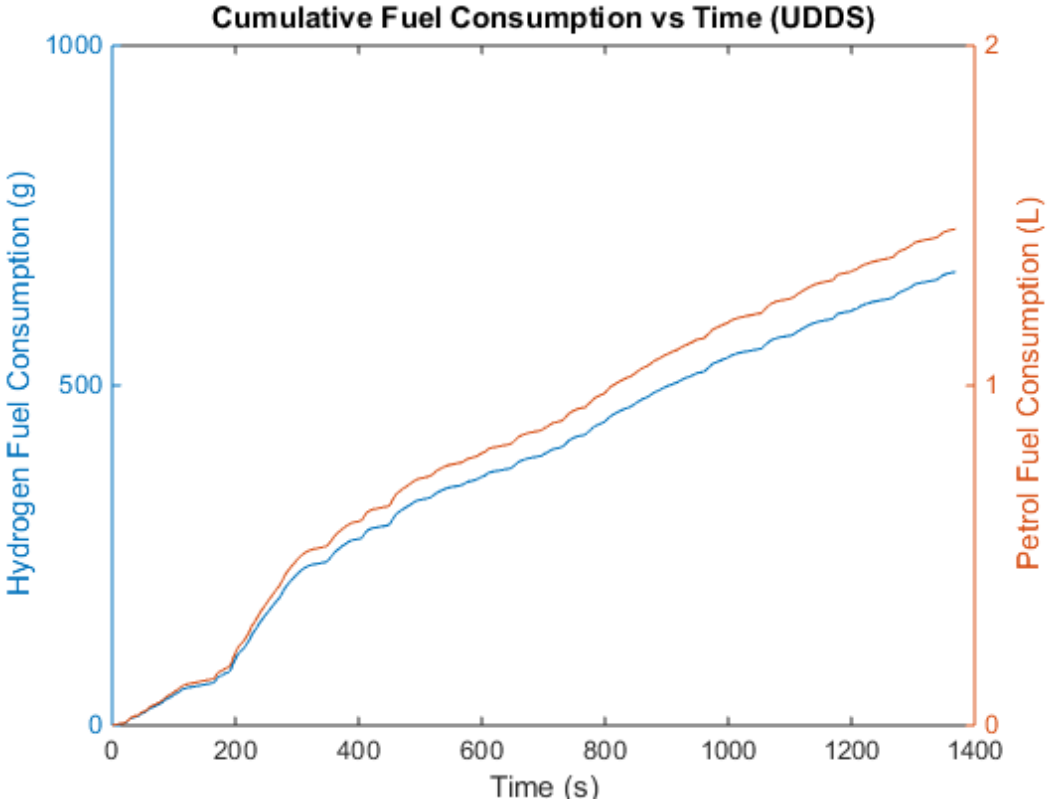

Appendix F - HWFET AESM Power and Fuel consumption plots

Appendix F1 – GGE Surface plot for HWFET driving cycle

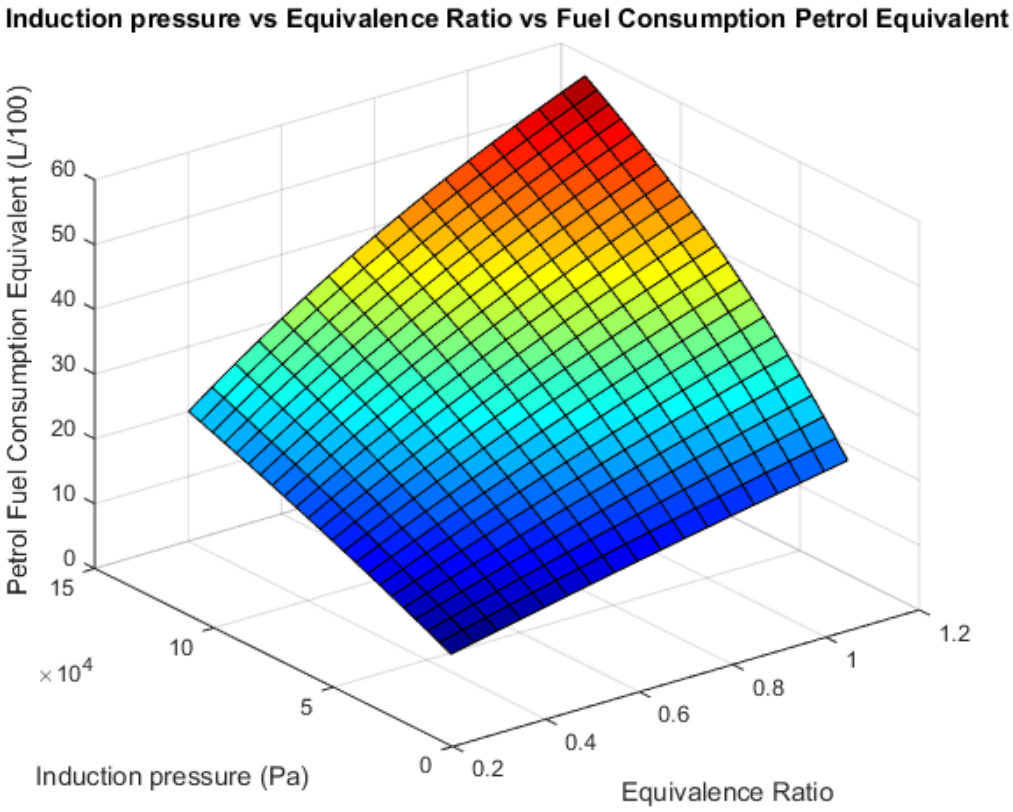

Appendix F2 – Specific Fuel consumption surface plot for HWFET driving cycle

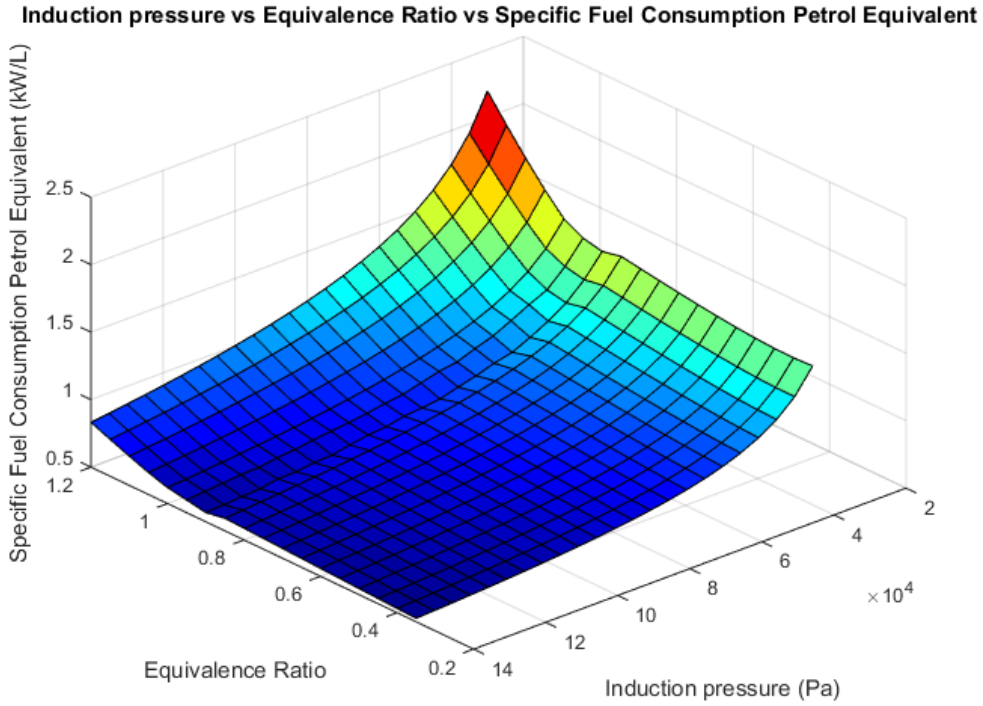

Appendix G - UDDS AESM Power and Fuel consumption plots

Appendix G1 – GGE Surface plot for UDDS driving cycle

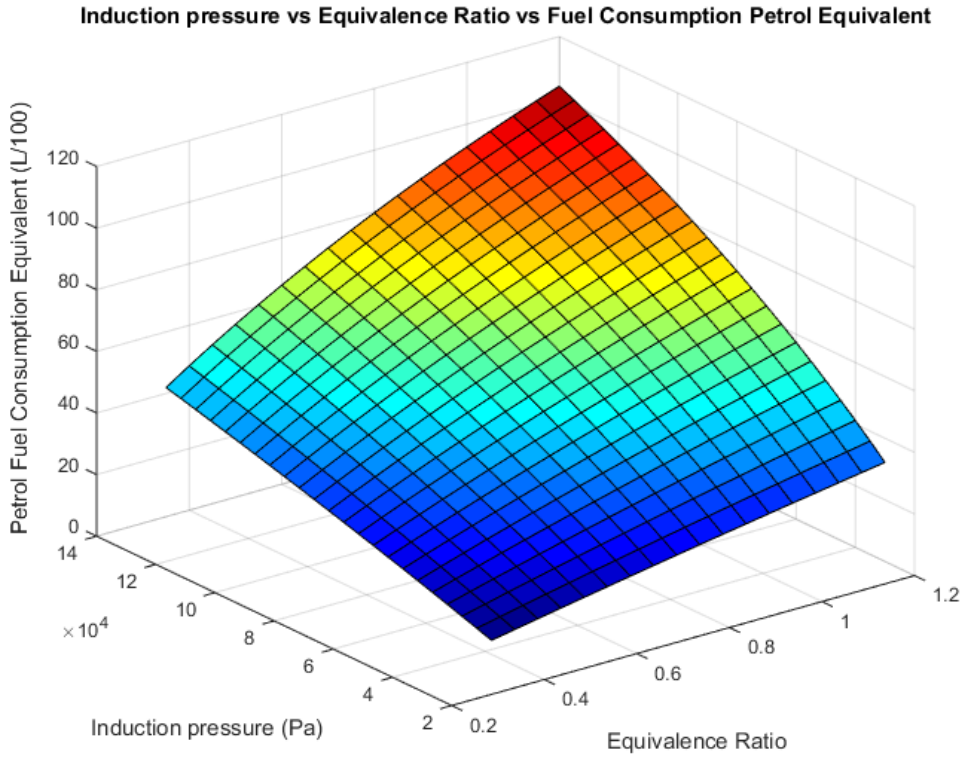

Appendix G2 – Specific Fuel consumption surface plot for UDDS driving cycle